Veðurstofa Íslands

Influence of Iceland's changing climate on extreme precipitation and snow-fraction

Andréa-Giorgio R. Massad
Halldór Björnsson

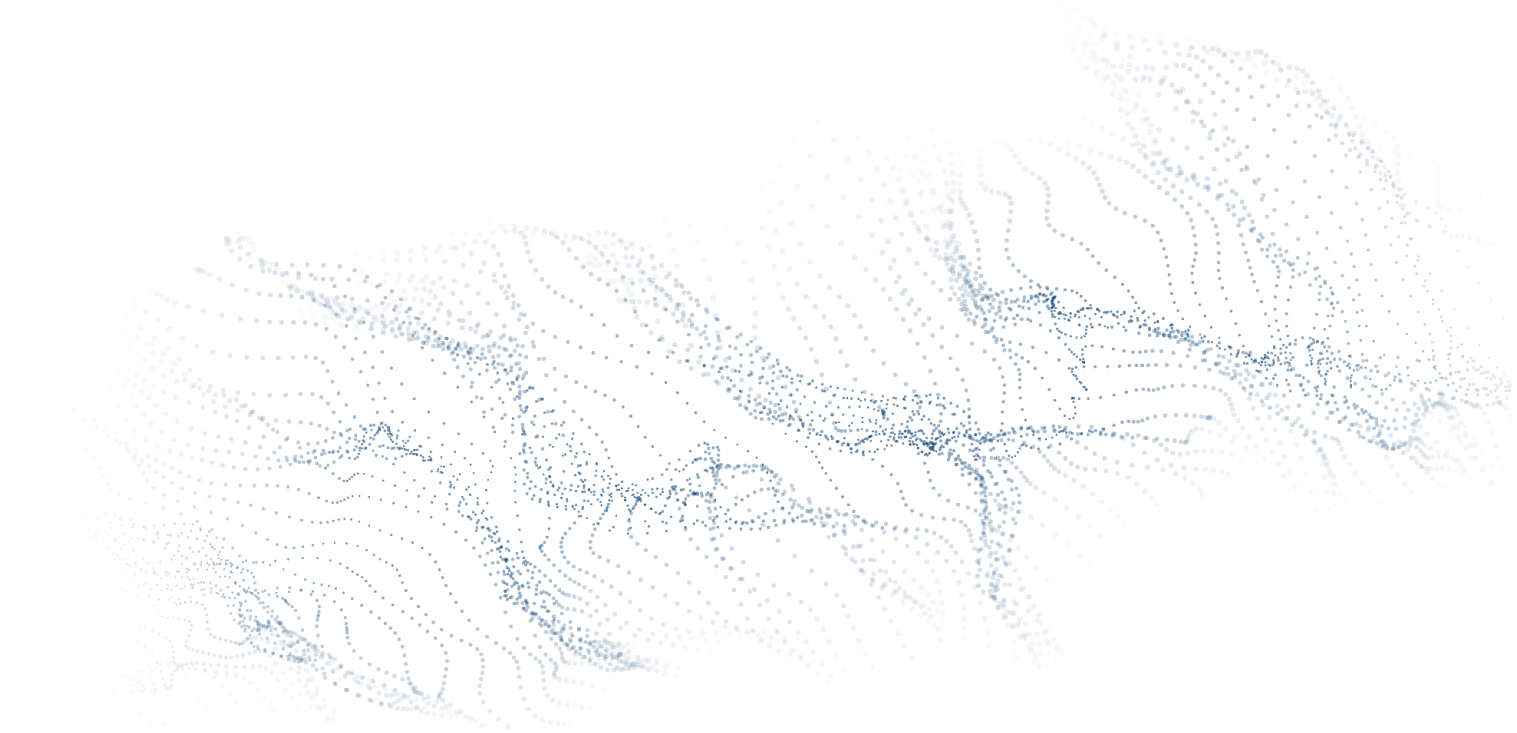

Skýrsla
VÍ 2025-009

Bústaðavegi 7-9 | IS-105 Reykjavík | Iceland | Tel +354 522 6000 | vedur@vedur.is

Veðurstofa Íslands

Influence of Iceland‘s changing climate on extreme precipitation and snow-fraction

Höfundar	Andréa-Giorgio R. Massad, Halldór Björnsson
Unnið fyrir	Orkurannsóknasjóð Landsvirkjunar
Verkefnisstjóri	Tinna Þórarinsdóttir
Yfirfarið af	Guðrún Nína Petersen
Samþykkt af	Tinna Þórarinsdóttir, deildarstjóri loftlag, veður, vatn, jöklar og

Veðurstofa Íslands / Icelandic Meteorological Office

Númer	VÍ 2025-009
ISSN	1670-8261
Dagsetning	Nóvember 2025
Dreifing	Opin
Fjöldi síðna	35 + viðaukar
Upplag	Rafræn útgáfa
Verknúmer	4314-0-0001
Málsnúmer	2023-0026
DOI númer	10.33112/YMHB9604

Bústaðavegi 7-9 | IS-105 Reykjavík | Iceland | Tel +354 522 6000 | vedur@vedur.is

Abstract

Over the last few years, various research have been carried at IMO to assess precipitation extremes, based on observations as well as simulations from the Icelandic Reanalysis (ICRA) and climate projection from the CMIP5 dataset (Coupled Model Intercomparison Project 5). In this study, CMIP6 projections are used to assess how climate change is expected to affect precipitation extremes as well as snow-fraction in Iceland. Daily and 5-day annual maximum precipitation amounts (RX1D and RX5D) are extracted from an ensemble of 19 GCMs (Global Climate Model) and four SSPs (Shared Socioeconomic Pathways) and regridded over a box that covers Iceland with a horizontal resolution of 1°. Overall, percentage changes show a gradual increase as the projection scenarios imply an increased radiative forcing by the end of the century. Depending on the quadrant, percentile, and scenario considered, most results show an increase of the RX1D and RX5D values at the end of the century, up to 25 and 23%, respectively. Snow-fraction is also calculated based on snowfall and precipitation fluxes from 12 GCMs, and data are regridded with a resolution of 0.5°. Results show a snow-fraction decrease overall in Iceland, with a mean value over the whole country for winter months of 44% for the period 1986 – 2014, lowering to 17% with the SSP585 scenario.

Key words: precipitation extremes, return levels, snow-fraction, CMIP6 projections

Ágrip

Á síðustu árum hafa ýmsar rannsóknir verið gerða hjá Veðurstofu Íslands til að meta aftakaúrkomu, byggðar á athugunum sem og líkanagögnum úr íslensku endurgreiningunni (ICRA) og niðurstöðum loftslagsspáa úr CMIP5 (Coupled Model Intercomparison Project 5) gagnasafninu. Í þessari rannsókn eru CMIP6 spár notaðar til að meta möguleg áhrif loftslagsbreytinga á aftakaúrkomu og hlutfall snjós af úrkomu á Íslandi. Mesta úrkoma yfir einn og fimm daga fyrir hvert ár (RX1D og RX5D) eru unnin úr safni 19 veðurfarslíkana (GCM, Global Climate Model) og fjórum sviðsmyndum (SSP, Shared Socioeconomic Pathways). Gögnin eru reiknuð yfir í net sem nær yfir Ísland með 1° láréttri upplausn. Almennt séð sýna hlutfallslegar breytingar hæga aukningu í aftakaúrkomu þar sem spárnar benda til aukins geislunarálags í lok aldarinnar. Ef litið er til landsfjórðuna, úrkomuhlutfalla og sviðsmynda þá sýna flestar niðurstöður aukningu á RX1D og RX5D gildum í lok aldarinnar, allt að 25% fyrir RX1D og 23% fyrir RX5D. Hlutfall snjós af úrkomu er einnig reiknaður út frá snjókomu- og úrkomu í 12 GCM líkönum og gögnin reiknuð yfir í 0,5° reikninet. Niðurstöðurnar sýna að snjóhlutfall lækkar almennt á Íslandi, fyrir allt landið að vetri á tímabilinu 1986–2014 var það 44%, en lækkar í 17% með SSP585 spánni.

Lykilorð: aftakaúrkoma, endurkomutími, hlutfall snjóhula, CMIP6 spár

Table of contents

1 Introduction

In Iceland, periods of intense rainfall have led to localised damage on numerous occasions. In December 2020, a record-breaking rainfall amounting to almost 570 mm over five days, caused landslides and major damages in Seyðisfjörður. More recently, in September 2023, a heavy precipitation episode hit Neskaupstaður with measurements exceeding 250 mm in 48 hours. These events are a reminder of the importance of having reliable data in order to issue accurate flood warnings and help in the design of infrastructure able to handle large surface runoff.

These estimates of precipitation extremes have recently been the subject of several studies in Iceland, using Extreme Value Analysis (EVA) to predict the occurrence of rare events by assessing their frequency from the most extreme values of a dataset. In 2020, a study by Massad *et al*. (2020) reassessed precipitation return levels in Iceland, resulting in a new national map of 24-hour precipitation thresholds for a 5-year event (Figure 1, top), in agreement with the general precipitation pattern in Iceland documented in Björnsson *et al*. (2018) and Crochet *et al.* (2007). But the impact of extreme rainfall in Iceland in recent years also underlines the importance of understanding the occurrence of precipitation extremes, and how they will be affected by the ongoing warming climate. As arctic and subarctic regions warm rapidly, precipitation extremes are expected to broadly increase in the coming decades (Bintanja, 2018), and in 2022, a study partially funded by Orkurannsóknasjóður Landsvirkjurnar examined changes in extreme precipitation towards the end of the century, using CMIP5 projections to calculate future precipitation return levels under two emission scenarios (Massad *et al*. 2022). The analysis of the CMIP5 projections showed that 24-hour precipitation return levels with a 5-year return period will increase by the end of the century with a mean change in the hydropower catchments operated by Landsvirkjun ranging from 3.2 to 5.7%, depending on the emission scenario (Figure 1, bottom).

Another aspect of the 2022 study aimed at assessing changes in precipitation type, over the historical period covered by the Icelandic reanalysis (1979 – 2017). Results were presented for eleven catchments and showed systematic changes in the seasonality of precipitation during winter months, coinciding with periods of enhanced warming in Iceland. In 9 cases out of 11, the onset of the melt season shifted to an earlier date, while the snow fraction (i.e. the snow amount as a fraction of total precipitation) decreased in all catchments, especially for the ones lying at lower altitudes. An important aspect of climate change in cold regions is how the snow fraction will change with warming (O'Gorman, 2014), and studies have shown that snow changes are ongoing and tend to be more pronounced at lower altitudes (Li *et al.*, 2020). Future changes in snow fraction have been the subject of several studies (Li *et al.*, 2022; Krasting *et al.*, 2013), but in combination with other precipitation changes (such as higher extremes), changes in this quantity may have a significant impact. Indeed, if extreme precipitation events occur as rain, it may lead to slope failure, rather than being leading to high accumulation. Furthermore, the future evolution of glaciers may depend sensitively on the fraction of precipitation that falls as

snow during the cold season, and if snow-fraction declines more slowly at higher altitude then this may enhance resilience of glaciers to warming.

Recently, new data from the CMIP6 projections have been released by the Copernicus Climate Service. Available in the new dataset are the daily and 5-day annual maximum precipitation amounts (respectively RX1D and RX5D) as well as snowfall and precipitation fluxes, from which the snow-fraction can be estimated until 2100. Therefore, the aim of this study is twofold: Firstly, CMIP6 projections will be used to improve estimates of return levels of precipitation for different return periods. Secondly, the snow-fraction change analysis will be extended to the end of the century using CMIP6 models both for the whole country, and for the eleven hydropower catchments operated by Landsvirkjun.

This research was funded in 2023 by Landsvirkjun, under the Orkurannsóknasjóður grant.

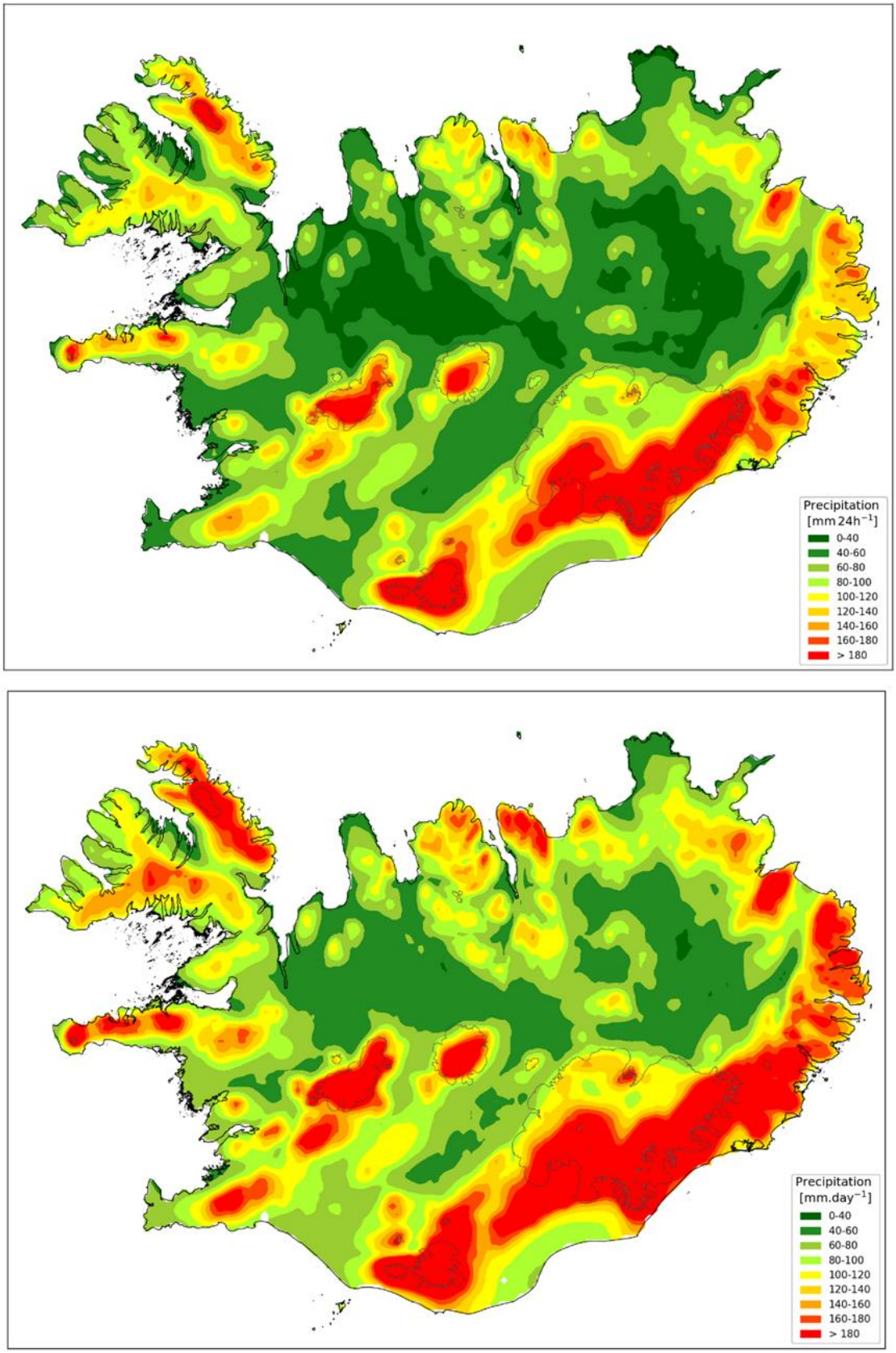

Figure 1 — 1M5 maps based on 24-hour accumulated precipitation from the ICRA dataset (top, from Massad et al. 2020) and with CMIP5 projections from the RCP 8.5 for the interval 2080 – 2100, using the 90th percentile from the climate model ensemble (bottom, from Massad et al. 2022). Results obtained using the Peak-over-Threshold method with Maximum Likelihood Estimation.

2 Data

2.1 Icelandic Reanalysis: the ICRA dataset

The operational Numerical Weather Prediction (NWP) system used by the Icelandic Meteorological Office (IMO) is the non-hydrostatic HARMONIE–AROME model, with a horizontal resolution of 2.5 km and 65 vertical levels (Bengtsson *et al.*, 2017). The fine-scale gridding gives 66,181 terrestrial points over Iceland. The model has been used to reanalyse atmospheric conditions in Iceland at hourly time-steps between September 1979 and August 2017, resulting in the Icelandic Reanalysis (ICRA) dataset (Nawri *et al.*, 2017).

In this study, the ICRA dataset is used to reassess precipitation return levels that will serve as the basis to apply climate projections and create a new set of maps. Total precipitation is not a direct output from the dataset and is calculated as the sum from the rate of fall of rain, snow, and graupel.

2.2 The CMIP6 projections

The Coupled Model Intercomparison Project (CMIP) is a large framework that collects the outputs from global coupled ocean-atmosphere general circulation models (GCMs) to project future climatic changes due to anthropogenic activity.

For this project, results from the sixth phase of the project are used, commonly referred to as CMIP6 (see Eyring *et al.* (2016) for details) and featured in the IPCC Sixth Assessment Report (2021). This time, the climate projections are based on a set of Shared Socioeconomic Pathway (SSP) (Figure 2). These SSPs describe various narratives of global societal developments for the end of the century, into which are derived the Representative Carbon Pathways (RCP) used in the fifth phase of the project (CMIP5). In CMIP6, five SSPs named SSP1 to SSP5 are considered, with the more sustainable scenario being SSP1, and the worst, SSP5, being the continuing development of fossil fuels (see Figure 2, from O'Neill *et al.,* 2017).

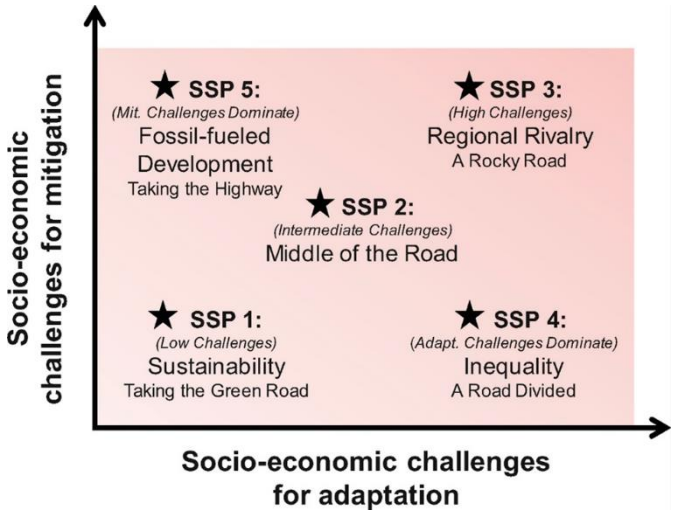

Figure 2 — Five shared socioeconomic pathways (SSPs) representing different combinations of challenges to mitigation and to adaptation. (O'Neill et al., 2017)

Climate models are then run for a specific SSP, coupled with various radiative forcings. In this analysis, the results from four scenarios are used:

- ***SSP126.*** Represents the CMIP6 counterpart of the RCP2.6 scenario that is the most optimistic, with a radiative forcing of 2.6 $W.m^{-2}$ by 2100, compatible with a global temperature raise of 2°C. In this scenario, strict climate protection measures are being taken.
- ***SSP245.*** "Middle of the road" pathway in terms of future greenhouse gas emissions, with an additional forcing of 4.5 W m^{-2}. In this scenario, climate protection measures are also being taken.
- ***SSP370.*** Upper-middle part of the full range of scenarios, with a forcing of 7 $W.m^{-2}$ by 2100.
- ***SSP585.*** Represents the upper boundary range of scenarios, with a radiative forcing of 8.5 W m^{-2} by the end of the century. It represents an update of the RCP8.5 scenarios from the CMIP5 but now combined with socioeconomic considerations.

The global mean temperature change for three of those scenarios are shown in Figure 3. According to the Copernicus Climate Change service, temperature projections under SSP126, SSP245, and SSP585 suggest an increase that range between under 2°C (SSP126) to over 5°C (SSP585) for the period 2071 – 2100 when compared to the historical period 1985 – 2014.

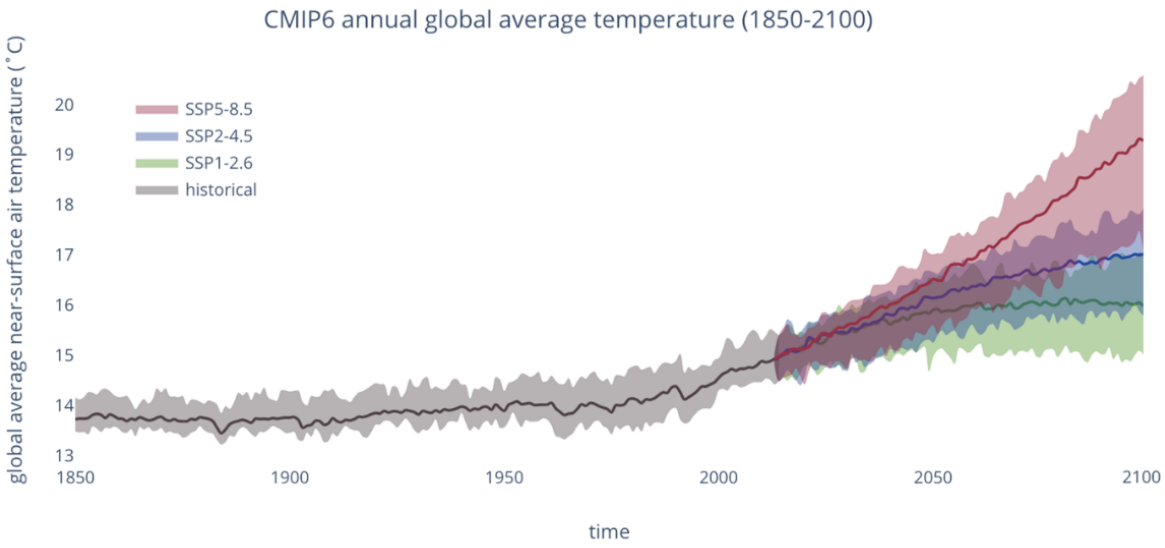

Figure 3 — Global mean temperature between 1850 and 2100 for selected CMIP6 models. The grey shaded area shows the range of historical simulations while the coloured areas show potential future temperature change based on different greenhouse gas emission scenarios (from Copernicus Climate Change Service, ECMWF).

The CMIP6 projections provide a global dataset that include a large range of variables, calculated both monthly and yearly. Depending on the variable, a different number of GCMs is available, both for a historical period spanning from 1850 to 2014, and for a projection period that runs throughout the end of the century. In this study, four variables were extracted from the CMIP6 dataset, as described in the following paragraphs.

2.2.1 Precipitation data: RX1D and RX5D

The CMIP6 dataset provides annual maximum series both for daily and 5-day precipitation data. These variables, respectively referred to as RX1D and RX5D, can be used as the basis for an Extreme Value Analysis (EVA) carried with a Block Maxima method as only annual maximum values are needed to calculate return levels with this method. In the previous studies, the Peak-over-Threshold method had been privileged, because the dataset available had an hourly temporal resolution. However, here to match the resolution of the projections, the Block Maxima method is used, as explained in Section 3 of the report.

Because all the GCMs used to make the projections did not run necessarily for the same scenarios, it was decided to keep in this study only the models that simulated RX1D and RX5D for both the historical period and the four SSPs scenarios selected. This led to the selection of 19 GCMs, all listed in Table 1.

In the first place, the variables were extracted globally, both for the historical period (1850 – 2014) and the projection period (2015 – 2100). Because the initial spatial resolution differs in all models, the data were regridded over a box that covers Iceland between longitudes -13 and -19°, and latitudes 63 and 67°, with a horizontal resolution of 1°. In most cases, this consisted in downscaling the initial data, which was done using a bilinear interpolation between the gridpoint values.

Table 1 — Model name, realisation and initial resolution used for RX1D and RX5D

	Model name	Initial resolution	Variant
1	*ACCESS-CM2*	1.9°x 1.3°	r1i1p1f1
2	*ACCESS-ESM1-5*	1.9°x 1.2°	r1i1p1f1
3	*BCC-CSM2-MR*	1.1°x 1.1°	r1i1p1f1
4	*CNRM-CM6-1*	1.4°x 1.4°	r1i1p1f2
5	*CNRM-ESM2-1*	1.4°x 1.4°	r1i1p1f2
6	*EC-Earth3*	0.7°x 0.7°	r1i1p1f1
7	*EC-Earth3-Veg*	0.7°x 0.7°	r1i1p1f1
8	*GFDL-ESM4*	1.3°x 1.0°	r1i1p1f1
9	*INM-CM4-8*	2.0°x 1.5°	r1i1p1f1
10	*INM-CM5-0*	2.0°x 1.5°	r1i1p1f1
11	*KACE-1-0-G*	1.9°x 1.3°	r1i1p1f1
12	*MIROC6*	1.4°x 1.4°	r1i1p1f1
13	*MIROC-ES2L*	2.8°x 2.8°	r1i1p1f2
14	*MPI-ESM1-2-HR*	0.9°x 0.9°	r1i1p1f1
15	*MPI-ESM1-2-LR*	1.9°x 1.9°	r1i1p1f1
16	*MRI-ESM2-0*	1.1°x 1.1°	r1i1p1f1
17	*NorESM2-LM*	2.5°x 1.9°	r1i1p1f1
18	*NorESM2-MM*	1.3°x 0.9°	r1i1p1f1
19	*UKESM1-0-LL*	1.9°x 1.3°	r1i1p1f2

2.2.2 Snowfall and precipitation fluxes

In the second half of the study, the focus is on the evolution of snow-fraction at the end of the century. Because snow-fraction is not a direct output from the GCMs, it needs to be calculated by dividing the snowfall fluxes by the total precipitation fluxes (both available in kg m^{-2} s^{-1}).

Similarly to the RX1D and RX5D data, only models that run for both variables over the historical and the four SSP scenarios were kept, which led to the 12 models listed in Table 2. The regridding was done over the same box around Iceland, but this time with a 0.5° resolution, with the goal to be able to use those data at catchment-scale, as described in Section 4.

Table 2 — Model name, realisation and initial resolution used for snowfall and precipitation fluxes.

	Model name	Initial resolution	Main realisation
1	*BCC-CSM2-MR*	1.1°x 1.1°	r1i1p1f1
2	*CanESM5-CanOE*	2.8°x 2.8°	r1i1p1f1
3	*CMCC-CM2-SR5*	1.0°x 1.0°	r1i1p1f1
4	*CNRM-CM6-1*	1.4°x 1.4°	r1i1p1f2
5	*CNRM-ESM2-1*	1.4°x 1.4°	r1i1p1f2
6	*FGOALS-f3-L*	1.3°x 1.0°	r1i1p1f1
7	*GFDL-ESM4*	1.3°x 1.0°	r1i1p1f1
8	*INM-CM4-8*	2.0°x 1.5°	r1i1p1f1
9	*IPSL-CM6A-LR*	2.5°x 1.3°	r1i1p1f1
10	*MIROC-ES2L*	2.8°x 2.8°	r1i1p1f1
11	*MRI-ESM2-0*	1.1°x 1.1°	r1i1p1f1
12	*TaiESM1*	1.3°x 0.9°	r1i1p1f1

3 Extreme precipitation analysis and climate projections from the CMIP6 dataset

3.1 Spatial distribution of RX1D and RX5D

As explained in Section 2.2.1 and shown in Table 1, 19 models were used in this EVA, all of them ran over a historical period (1850 – 2014), and four SSP projections (2015 – 2100).

In order to analyse the spatial distribution of the precipitation maxima, a control period was defined between 1986 and 2014. The same control period has recently been used in the fourth assessment report from the Scientific Committee on Climate Change (2023). For each model, RX1D and RX5D values were averaged over the control period for each gridpoint, and then the ensemble median values were calculated as shown in Figure 4. The model grid is plotted on top of the maps to account for the resolution of the data used in this analysis. Despite the data coarseness, precipitation patterns are well respected when compared to previous studies (Björnsson *et al.,* 2018; Massad *et al*., 2020). On both maps, maximum values are obtained in the southeastern region (S.E. quadrant), with maximum values of 37 mm for RX1D, and 80 mm for RX5D. Overall, more precipitation is found in the southern half of Iceland, with values above 28 mm for RX1D, and above 65 mm for RX5D. Minimum values are found in the northeastern part of Iceland (N.E. quadrant), with a minimum median RX1D of 25 mm, and a minimum median RX5D of 53 mm. It should be noted that both values are found over gridpoints covered by sea.

This spatial distribution of extreme precipitation is further illustrated by Figure 5 and Table 3. On Figure 5, ensemble median RX1D and RX5D values were calculated for each quadrant by taking the mean value over all gridpoints within the region and plotted over time from 1850 to 2100 for each SSP projection. The annual maximum series for the SSP585 scenario are shown in the figure, other SSPs are available in Appendix I. In all scenarios, spatial trends shown on Figure 4 with higher precipitation in the S.E. quadrant and lower precipitation in the N.E. quadrant translate from the historical period to the end of the century. Indeed, in the case of the SSP585, higher values are found for RX1D and RX5D in the S.E. quadrant with median values of 33 and 76 mm respectively for the control period (1986 – 2014), and median values of 37 and 77 mm at the end of the century (2091 – 2100). From Figure 5, the increase appears to be more pronounced for RX1D than RX5D for SSP585, and this trend is also present for the other scenarios as shown in the table.

Therefore, despite the coarseness of the climate model resolution, GCMs are still able to represent the main features of the Icelandic precipitation patterns: enhanced precipitation in the southern half, with maximum values over the Vatnajökull region, and less precipitation in the N.E. quadrant, in the lowlands. In regions of complex orography such as the East- and Westfjords, values are higher than in areas of similar latitudes but more inland. This project will therefore consider geographical changes in precipitation patterns and use them as part of the analysis when calculating new return levels for the end of the century.

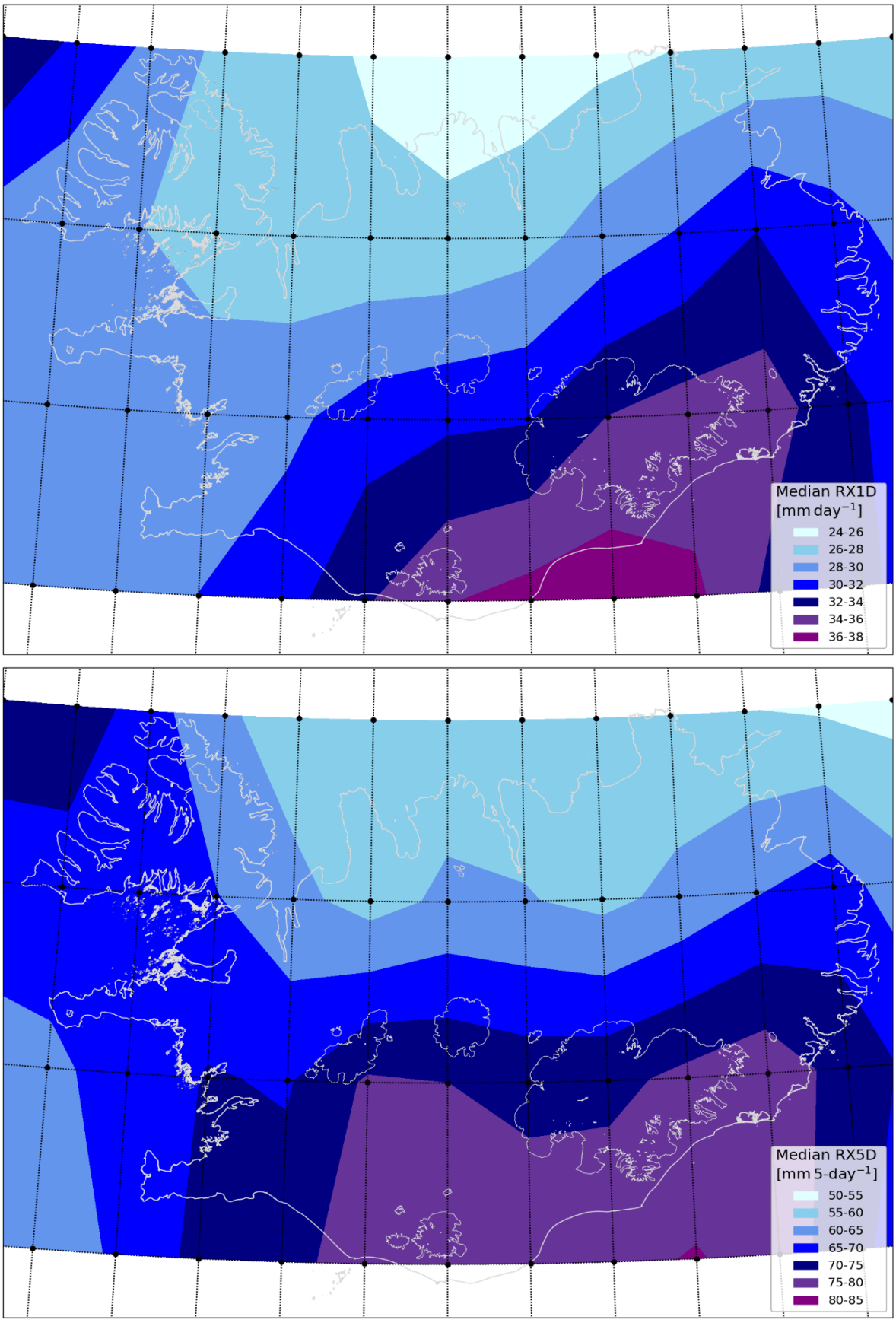

Figure 4 — Median RX1D (top) and RX5D (bottom) values for each gridpoint averaged over the control period 1986 – 2014 for the ensemble of climate models. Note that the colour scale differs for each map.

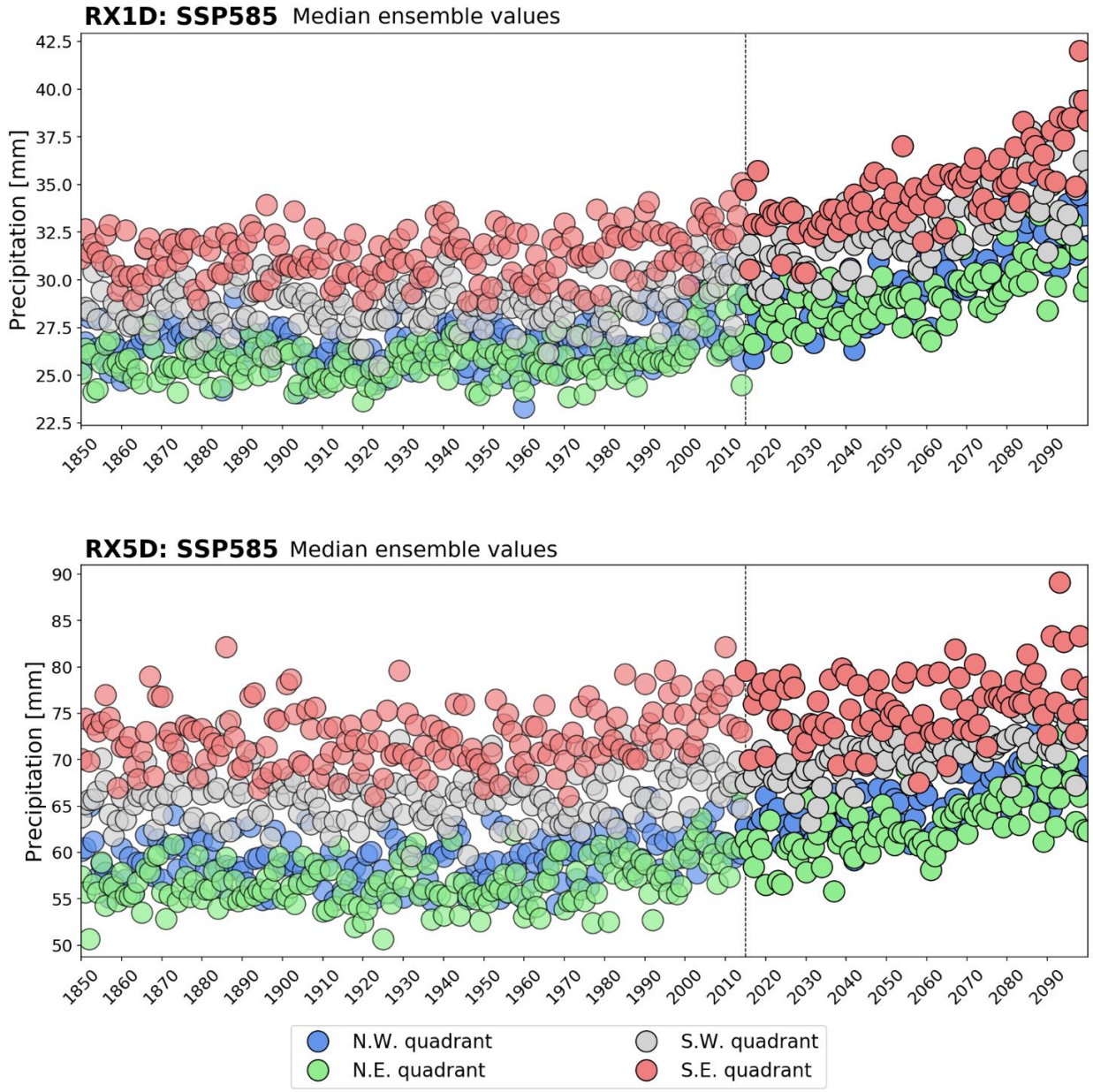

Figure 5 — Median RX1D (top) and RX5D (bottom) values for each quadrant calculated from the ensemble of climate models for a historical period (1985 – 2014, transparent dots) and the SSP585 period (2015 – 2100, opaque dots).

Table 3 – Median RX1D and RX5D values as calculated for each quadrant for a control period (Hist., 1986 – 2014) and four SSP scenarios (2091 – 2100).

Quadrant	Median RX1D values (mm)					Median RX5D values (mm)				
	Hist.	*SSP (2091 – 2100)*				*Hist.*	*SSP (2091 – 2100)*			
		126	*245*	*370*	*585*		*126*	*245*	*370*	*585*
N.W.	27	27	30	31	32	62	62	63	65	67
N.E.	26	28	28	30	31	58	58	63	65	65
S.W.	30	29	31	33	34	69	67	69	71	72
S.E.	33	33	32	35	37	76	76	73	77	77

3.2 Percentage changes of precipitation maximum by quadrant and SSP

In order to take into account the geographical distribution of precipitation from the ensemble of climate models, it was decided to calculate the percentage changes between a control period (1986 – 2014) and an end-of-the-century period (2091 – 2100) for each scenario by quadrant.

Results are shown for scenario SSP585 in Figure 6 and 7, respectively for RX1D and RX5D. Other scenarios are shown in Appendix II. Instead of working directly with the median values as on Figure 5, the range of values for each one of the 19 models is shown on the figures for each year, and precipitation values were normalised by dividing each one of them by the median values over the control period. Each subplot shows the results for a different quadrant, with the ensemble values represented as green dots, and the yearly median and 10th-90th percentile range with a different colour for each quadrant. While the values are shown continuously for the entire period from 1986 to 2100, only the two periods used to calculate the percentage changes are shown with opaque colours. Percentage changes are indicated on the figures. They were calculated based on median values, as well as 10th and 90th percentiles from all data for each period. Another method was tested where statistics based on the yearly quantiles shown on the figure were compared for the two periods, which gave very similar results, although slightly lower. In the end, the first method was chosen as it gets rid of possible trends within the two periods. Those results are also compiled for every scenario in Table 4 and 5, respectively for RX1D and RX5D.

Overall, precipitation percentage changes show a gradual increase as the projection scenarios imply an increased radiative forcing by the end of the century. With the SSP126 scenario, values in the 10th percentile show a decrease both for RX1D and RX5D in all quadrants indicating lower annual maximum precipitation values. However, in the case of RX1D, besides two negative percentages calculated with the median values of the SSP126 scenario, and one negative value calculated with the 10th percentile of the SSP245

scenario, all percentage changes in Table 4 are positive, indicating an increase of precipitation, ranging from 0 to 25%, depending on the quadrant, percentile, and scenario. For RX5D (Table 5), some negative values are found for other percentiles and scenarios, but most trends also indicate an increase in precipitation, up to 23% for the SSP585 scenario, based on the 90th percentile and for the N.W. quadrant. However, percentage changes are overall lower for the RX5D data, which is especially notable with the SSP370 scenario where the mean percentage change in all quadrants with the 90th percentile is 18% for RX1D and 10% for RX5D.

Table 4 – Percentage change for RX1D between the control period 1986 – 2014 and 2091 – 2100 for all quadrants, percentiles, and SSP.

	RX1D – Percentage changes (%)											
	SSP126			*SSP245*			*SSP370*			*SSP585*		
Quadrant	10th	50th	90th	10th	50th	90th	10th	50th	90th	10th	50th	90th
N.W.	-3.2	1.9	8.8	2.2	9.0	12.3	6.1	14.4	19.9	12.3	17.3	24.6
N.E.	-2.2	-1.6	4.6	3.2	7.8	12.4	7.4	10.4	14.8	8.7	14.9	22.0
S.W.	-6.0	-0.6	1.3	-0.9	3.8	10.0	7.7	9.1	21.4	12.1	14.1	21.9
S.E.	-1.4	0.5	7.4	0.3	3.5	5.4	3.3	8.8	15.7	6.6	12.2	20.7

Table 5 – Percentage change for RX1D between the control period 1986 – 2014 and 2091 – 2100 for all quadrants, percentiles, and SSP.

	RX5D – Percentage changes (%)											
	SSP126			*SSP245*			*SSP370*			*SSP585*		
Quadrant	10th	50th	90th	10th	50th	90th	10th	50th	90th	10th	50th	90th
N.W.	-1.3	-0.2	4.2	0.2	3.2	1.7	5.5	5.9	12.8	5.5	8.0	15.3
N.E.	0.0	2.0	7.7	3.7	5.8	11.8	6.8	10.0	10.6	5.6	11.1	23.2
S.W.	-3.6	-2.4	1.8	-3.2	0.5	3.2	0.7	3.6	7.6	2.3	5.6	7.7
S.E.	-3.2	-1.8	4.0	-0.9	-1.7	4.6	-1.7	2.2	9.7	0.6	4.3	12.3

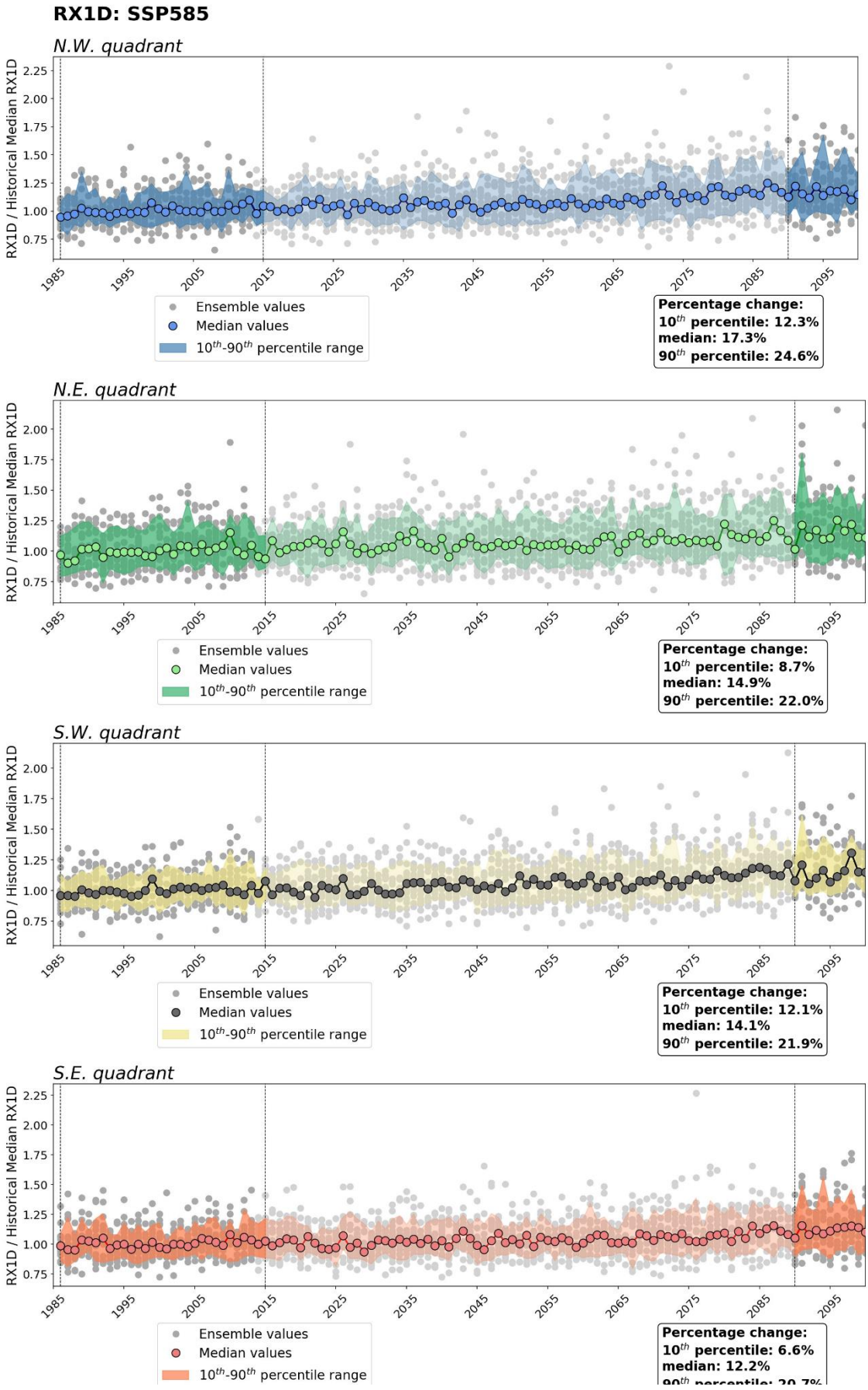

Figure 6 — RX1D percentage changes by quadrant calculated from median, 10th and 90th percentile values of the ensemble of climate models.

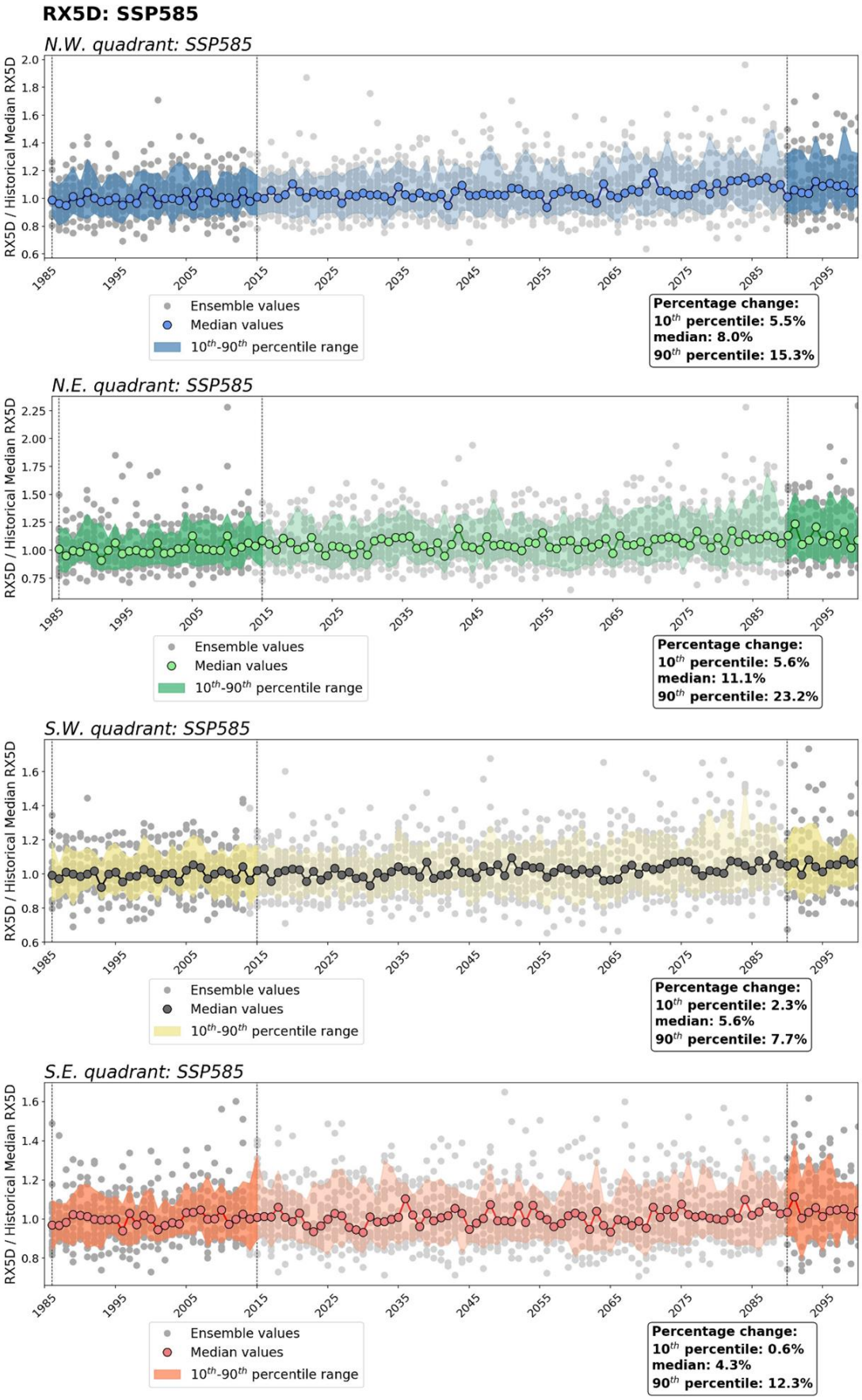

Figure 7 — RX5D percentage changes by quadrant calculated from median, 10th and 90th percentile values of the ensemble of climate models.

3.3 Updated precipitation return levels in regard to CMIP6 climate projections

3.3.1 1M5 and 5M5 maps

3.3.1.1 Results for the whole country

One of the main results presented in Massad *et al.* (2020) was a new map showing 24-hour precipitation return levels with a 5-year return period (also known as 1M5 map). In the subsequent study (Massad *et al.*, 2022), this map was reassessed by applying precipitation percentage change for various CMIP5 climate scenarios into the EVA. These percentage changes were calculated seasonally and later integrated into the analysis before calculating the 5-year return levels in each ICRA gridpoint using the Peak-over-Threshold method with Maximum Likelihood Estimation. For further details, a summary was written in Section 3 of the 2020 report, adapted from Coles (2001).

In this present case, because of the temporal resolution of the dataset, the Peak-over-Threshold method is not suited. Indeed, RX1D gives annual maximum series, for which a Block Maxima method is more adequate. Therefore, before applying the climate projections, a new 1M5 map for daily precipitation with a 5-year return period was calculated by the Block Maxima method with Maximum Likelihood Estimation (MLE) (Figure 8, top). Overall, precipitation extreme patterns are the same as in the 2020 study (Figure 1, top), with maximum precipitation (over 180 mm) in the S.E. quadrant over Vatnajökull as well as in regions of complex orography. However, region with lower values (as shown by the dark green shaded area in the lowlands) are more spread on this map obtained with Block Maxima than in the previous version. This can be justified by two reasons. Firstly, it was shown in the 2020 study that 1M5 values for selected weather stations based on Block Maxima give slightly lower values than based on the Peak-over-Threshold, although still in the same range. Secondly, the 1M5 map presented in 2020 was based on 24-hour precipitation, which is not the case in Figure 8. Indeed, here the annual series calculated for each gridpoint was based on daily precipitation in order to fit the RX1D variable better. Although it is very likely that the difference between RX1D and annual maximum series based on 24-hour precipitation would give about the same difference than comparing daily to 24-hour precipitation values, it cannot be verified in our case and therefore the Block Maxima analysis was carried on daily rather than 24-hour accumulated precipitation. As a reminder, it should be noted that the difference for the whole country between daily and 24-hour precipitation on the 5-year return level was 14% when calculated with the Peak-over-Threshold method.

Since the precipitation data only give access to annual values, reproducing the method used for the 2022 project by applying seasonal percentage changes is not an option in this study. Instead, the percentage changes calculated for each quadrant are used to create the new set of maps. Precipitation return levels with a 5-year return period calculated on Figure 8 were therefore obtained by applying the percentage changes according to the location of the gridpoint.

Eventually, 12 new 1M5 maps were created: one for each quantile (10th percentile, median, and 90th percentile), and each scenario (SSP126, SSP245, SSP370, SSP585). For practical reasons, only one new map is shown within this report: the 1M5 map for the end of the century, based on percentile changes calculated from the 90th percentile, and in the case of a SSP585 scenario (Figure 8, bottom). From the range of percentage changes in Table 4, this map can be seen as the most extreme 1M5 map which can be calculated from the climate dataset available.

Comparing both maps on Figure 8, the main differences lie in the presence of precipitation values above 160 mm in the Eastfjords and south-Westfjords as well as the narrowing of the area with values under 40 mm in the lowlands. Compared to results from the 2022 map (Figure 1, bottom), newer results lead to a map with overall lower values. This is expected as the seasonal percentage changes applied in 2022 ranged from 23 to 30%, while the values in this case vary between 20 and 25% depending on the quadrant.

With the availability of RX5D data, it was also decided to create maps for 5-day precipitation with a 5-year return period, that will be referred to as 5M5 maps. Figure 9 shows such maps both based on the ICRA dataset without projection (top figure), and with percentage changes based on the 90th percentile of the ensemble of climate models for SSP585 (bottom figure). Most of the S.E. quadrant now appears in red tones both with and without projections, indicating values above 180 mm. Minimum, median and maximum 5M5 values for the whole country are 42, 122, and 1153 mm on the current map, and 48, 139, and 1421 mm for the SSP585 scenario. In the map that includes the SSP585 projections, it appears that only small, localised patches are coloured in dark green (indicating values under 60 mm), and a continuous area with values above 180 mm now covers the southern half of Iceland from Mýrdalsjökull to the north of the Eastfjords, the whole northern part of the Westfjords, and the mountainous regions of Tröllaskagi and Flateyjarskagi.

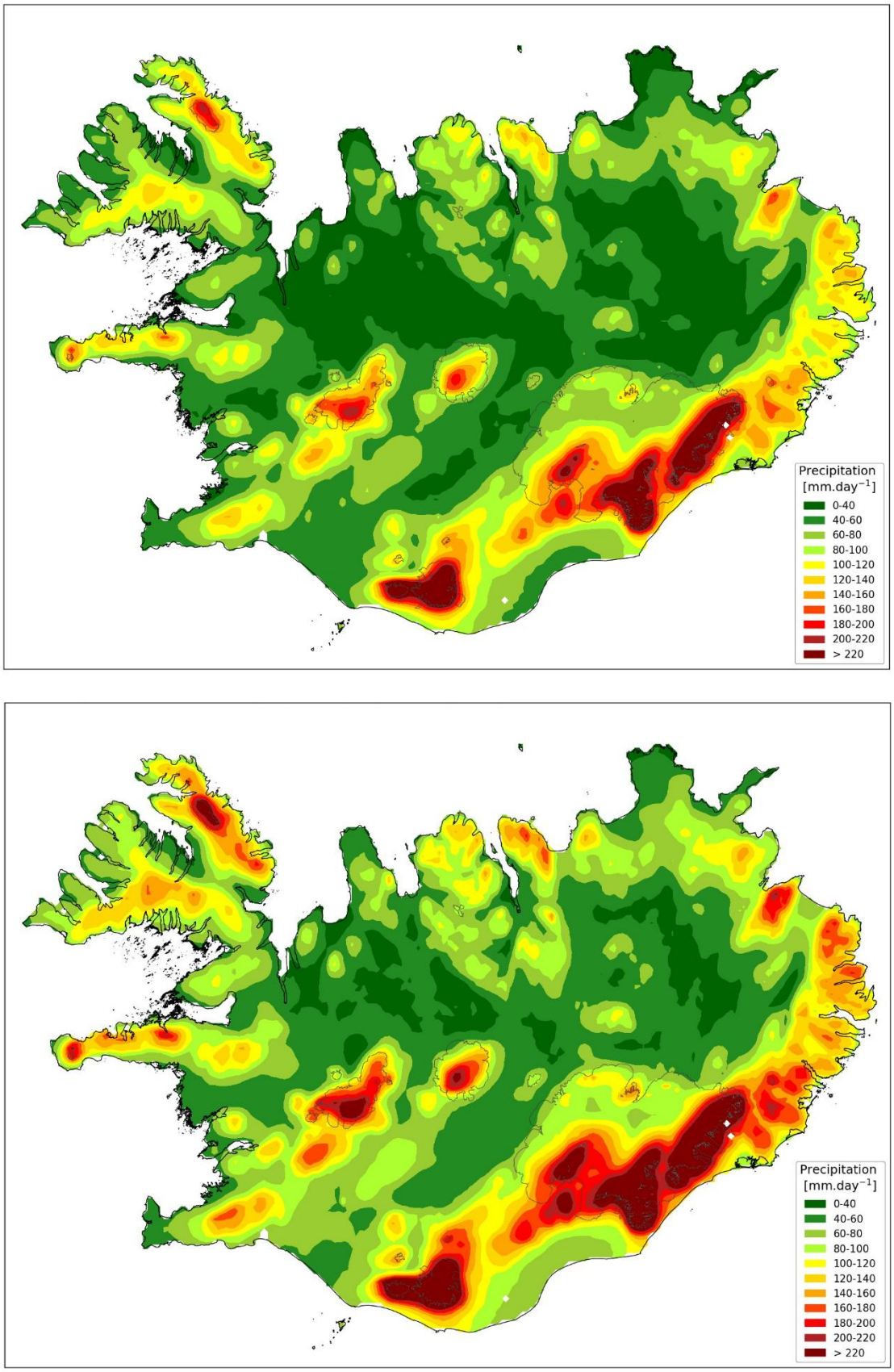

Figure 8 — 1M5 maps for daily precipitation with a 5-year return period, based on the ICRA dataset and obtained with Block Maxima with MLE. Top figure shows current results, without climate projection. Bottom figure shows results based on 90th percentile percentage changes for SSP585 at the end of the century.

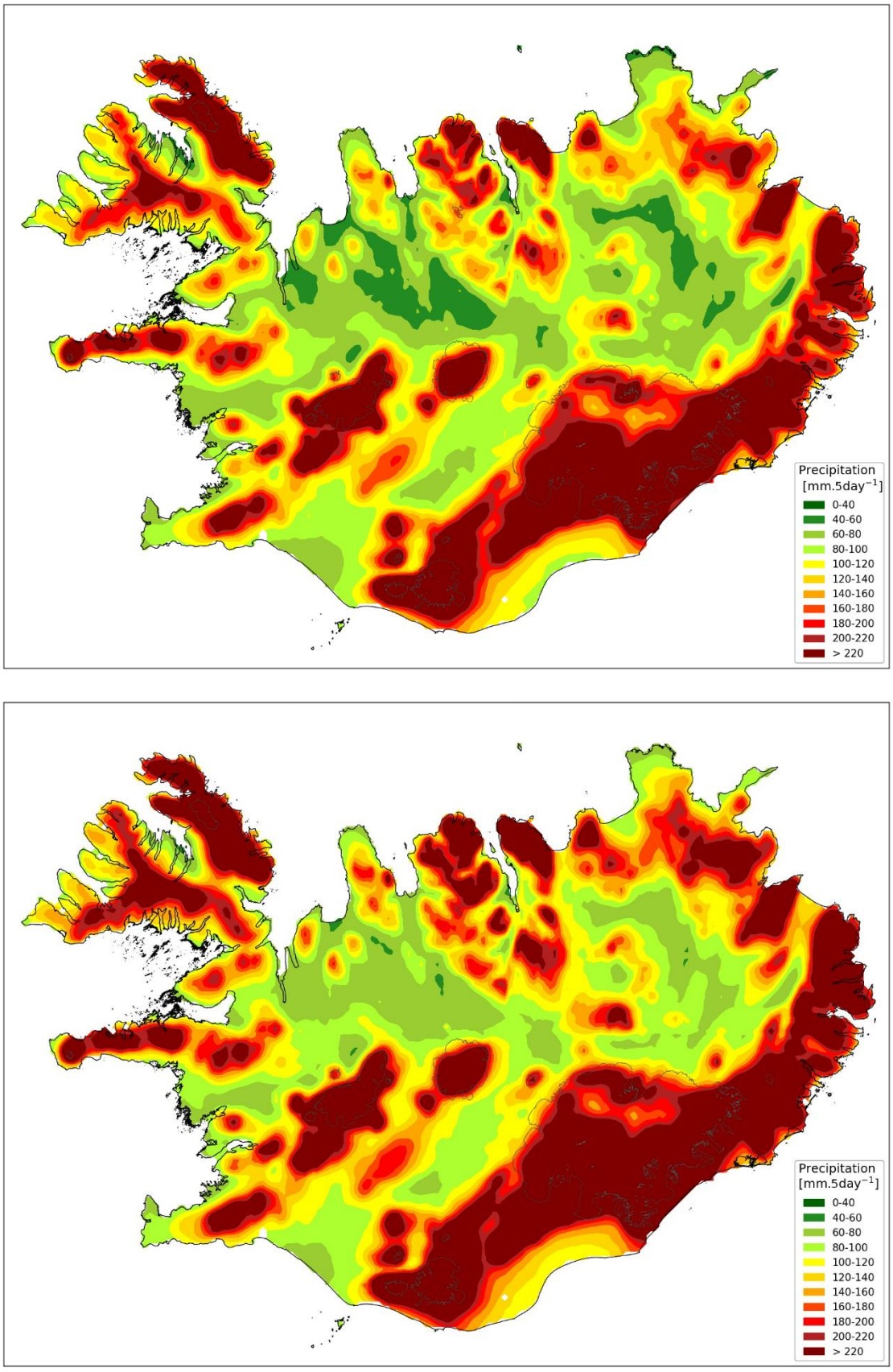

Figure 9 — 5M5 maps for 5-day precipitation with a 5-year return period, based on the ICRA dataset and obtained with Block Maxima with MLE. Top figure shows current results, without climate projection. Bottom figure shows results based on 90th percentile percentage changes for SSP585 at the end of the century.

3.3.1.2 *Results for individual catchments*

Individual 1M5 maps were also created for each hydropower catchment operated by Landsvirkjun. An example is given for Hálslón on Figure 10, that can be directly compared to Figure 19 of the 2022 study. Indeed, with the Peak-over-Threshold method on 24-hour precipitation, the median value for catchment Hálslón as calculated in 2022 was 85 mm, against 72 mm on Figure 10, obtained with Block Maxima over daily values. With percentage changes from Table 3 applied, the new median value with SSP858 based on 90th percentile percentage change is 88 mm, while it was 109 mm with RCP8.5. This is explained by the lower current 1M5 value compared to results obtained with the Peak-over-Threshold method over 24-hour precipitation, and by the lower percentage change applied (21% for this quadrant with CMIP6, 27% with CMIP5). Figures for other catchments are shown in Appendix III.

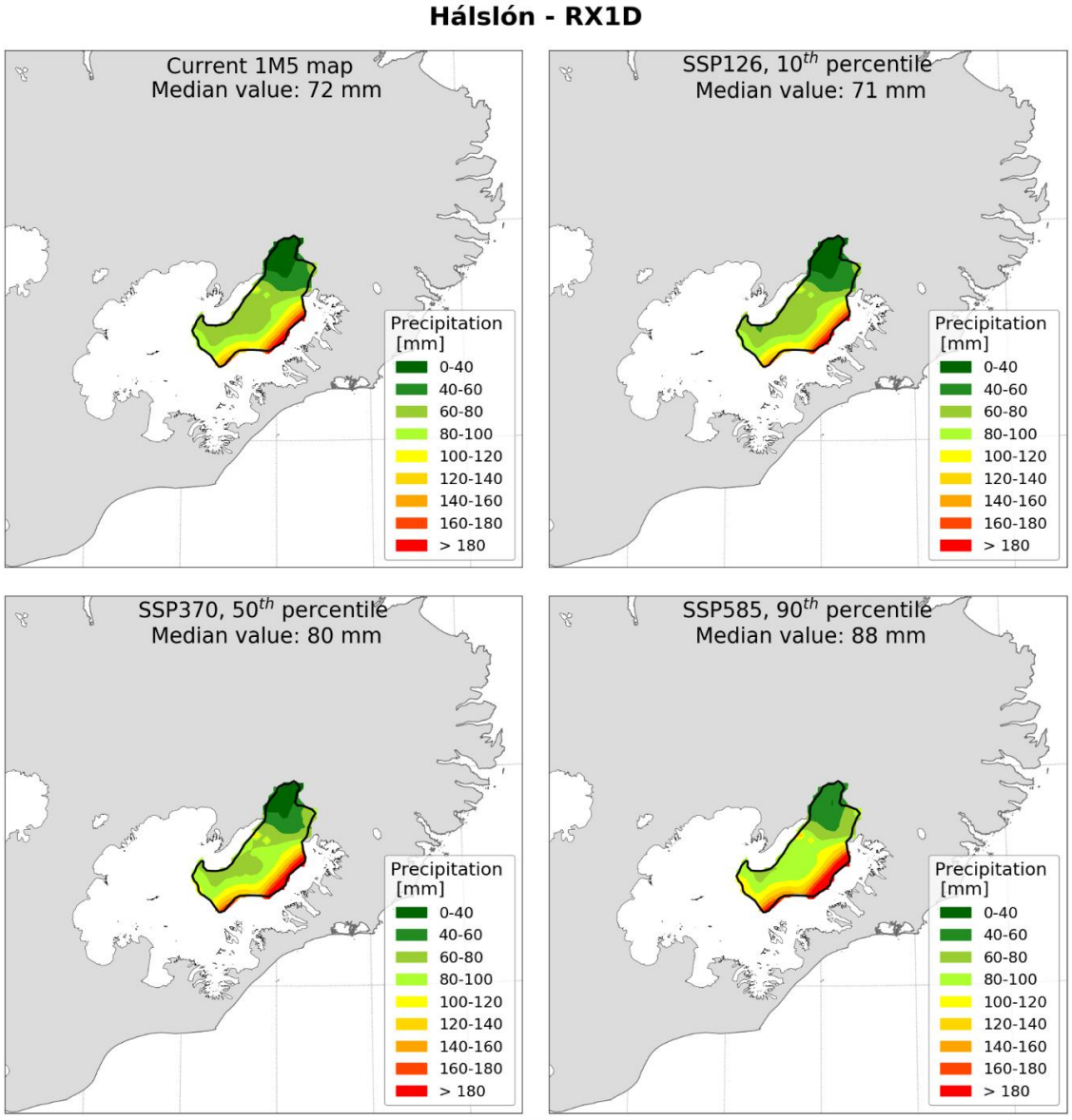

Figure 10 — 1M5 maps for catchment Hálslón based on the ICRA dataset without projection (top left), with SSP126 and 10th percentile percentage changes (top right), with SSP370 and median percentage changes (bottom left) and with SSP585 and 90th percentile percentage changes (bottom right).

3.3.2 Other return-level maps

While the focus in the 2020 and 2022 studies was mostly on the 5-year return levels, other return periods have been compiled in tables and Intensity-Duration-Frequency curves (IDF curves) for a selection of weather stations as well as for the hydropower catchments. Based on the ICRA dataset, return level maps with a 2-, 5-, 10-, 25-, 50- and 100-year return periods have been created using the Block Maxima method with MLE. Thus, using the percentage changes as calculated from the different percentiles under the various climate projection scenarios, a large set of maps have been created.

Figure 11 shows two of these maps: the daily and 5-day precipitation maps with a 100-year return period based on the 90th percentile percentage changes for SSP585. On the daily precipitation map, it appears that the dark green shaded areas (0 – 40 mm) have almost completely disappeared and can only be found in the northern half of the country. Minimum, median, and maximum values are 37, 125, and 1138 mm respectively, which are extremely close to the range of values presented for the original 5M5 map and presented on Figure 9 (42, 122, and 1153 mm). However, when comparing more closely those two maps (Figure 11, top, and Figure 9, top), it appears that on the daily precipitation map, lower values can be found in the southern part of Iceland, even for the 100-year return period, while values in that part of the country always exceeded 60 mm on the 5M5 map. Figure 11 also presents a map for 5-day precipitation with a 100-year return period (bottom), and most of the country appears in red, indicating values above 160 mm. Values range from 69 to 1916 mm, with a median value of 230 mm.

In the Appendix IV, maps based on the median percentage changes from Table 4 are shown for other for daily and 5-day precipitation with a 2-, 5-, 10-, 25-, 50- and 100-year return period. Maps are based on percentage changes calculated from the median values.

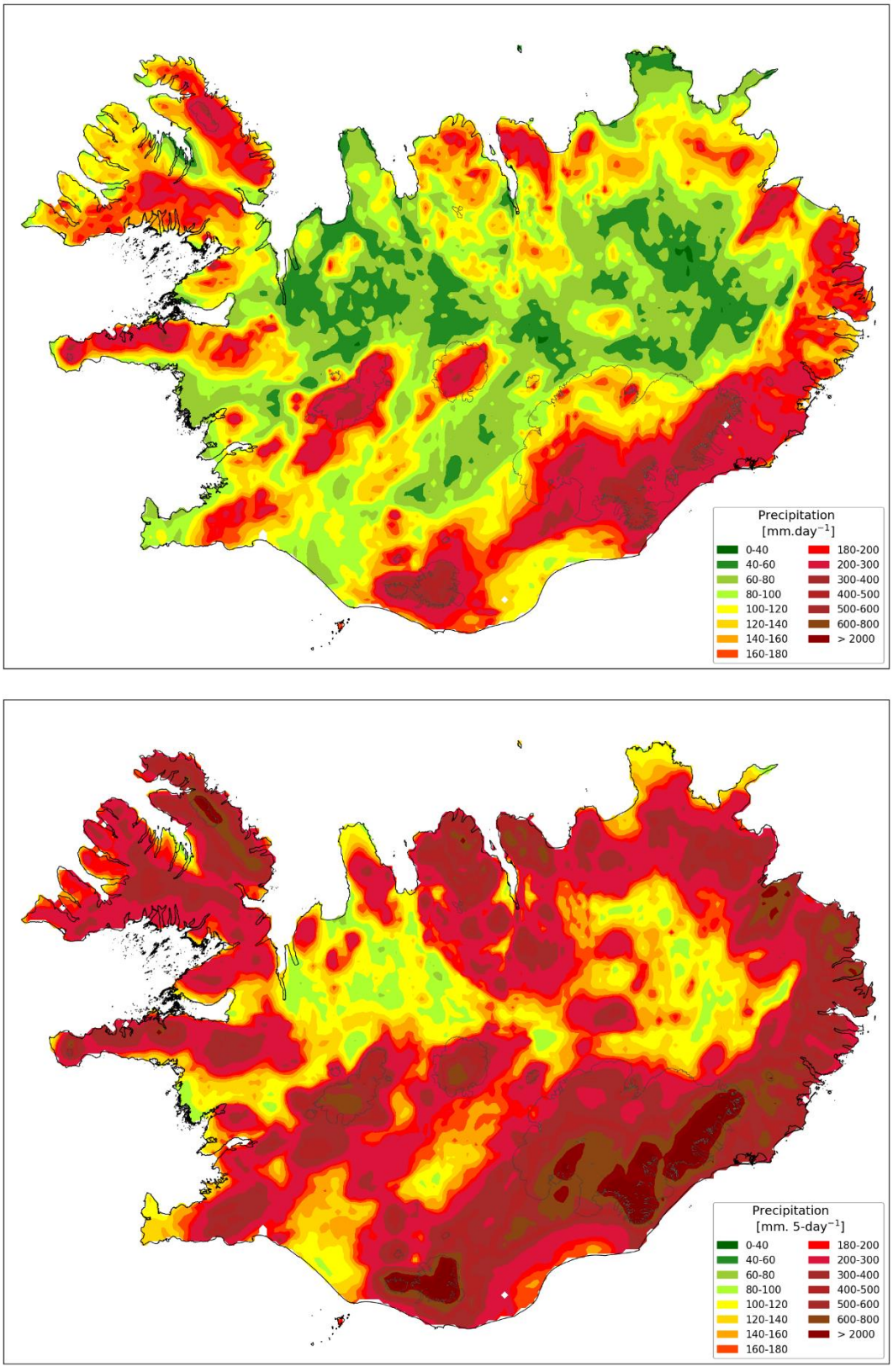

Figure 11 — Maps for daily (top) and 5-day (bottom) precipitation with a 100-year return period. Results were obtained using Block Maxima on the ICRA dataset with added projections for SSP585 based on 90th-percentile percentage changes.

4 Snow-fraction change in the hydropower catchments

4.1 Calculation of gridded snow-fraction for the whole country

As explained in Section 2.2.2, snow-fraction is not a direct output of the climate models and is therefore calculated as the ratio between the snowfall and precipitation fluxes. Both fluxes needed to be downscaled, this time on a grid with a resolution of 0.5° in latitude and longitude. Bilinear interpolation was used to regrid the values and it should be acknowledged that the data are not expected to represent the snow-fraction variation with altitude as well as it would if the original dataset was in higher resolution in the first place.

Median snow-fraction from the ensemble of climate models is shown in Figure 12. In order to follow the results of the 2022 study, only winter months from November to April were kept in the dataset, and snow-fraction was yearly averaged. Here, the map shows the median ensemble snow-fraction yearly averaged for each model between 1986 and 2014. Mean value for the whole country is 43%, with values ranging from 9 to 76%, and a pronounced south-north gradient. To a certain extent, the ensemble of models manages to account for the presence of the Highlands region, where the snow-fraction is increased, with a strong zonal gradient both to the east and west of the Highlands region. As expected however, is the lack of details in the zones of complex orography such as the East- and Westfjords, Snæfellsnes as well as the southern glaciers.

It should be noted that those snow-fraction values are lower than the ones obtained from the ICRA dataset in the eleven hydropower catchments. Indeed, in the 2022 study, while the focus also was on the snow-fraction decrease over the reanalysis time-period, yearly snow-fraction was between 50 and 90% for all the catchments, while here on Figure 12, some catchments are located in an area where the median snow-fraction is below 50%.

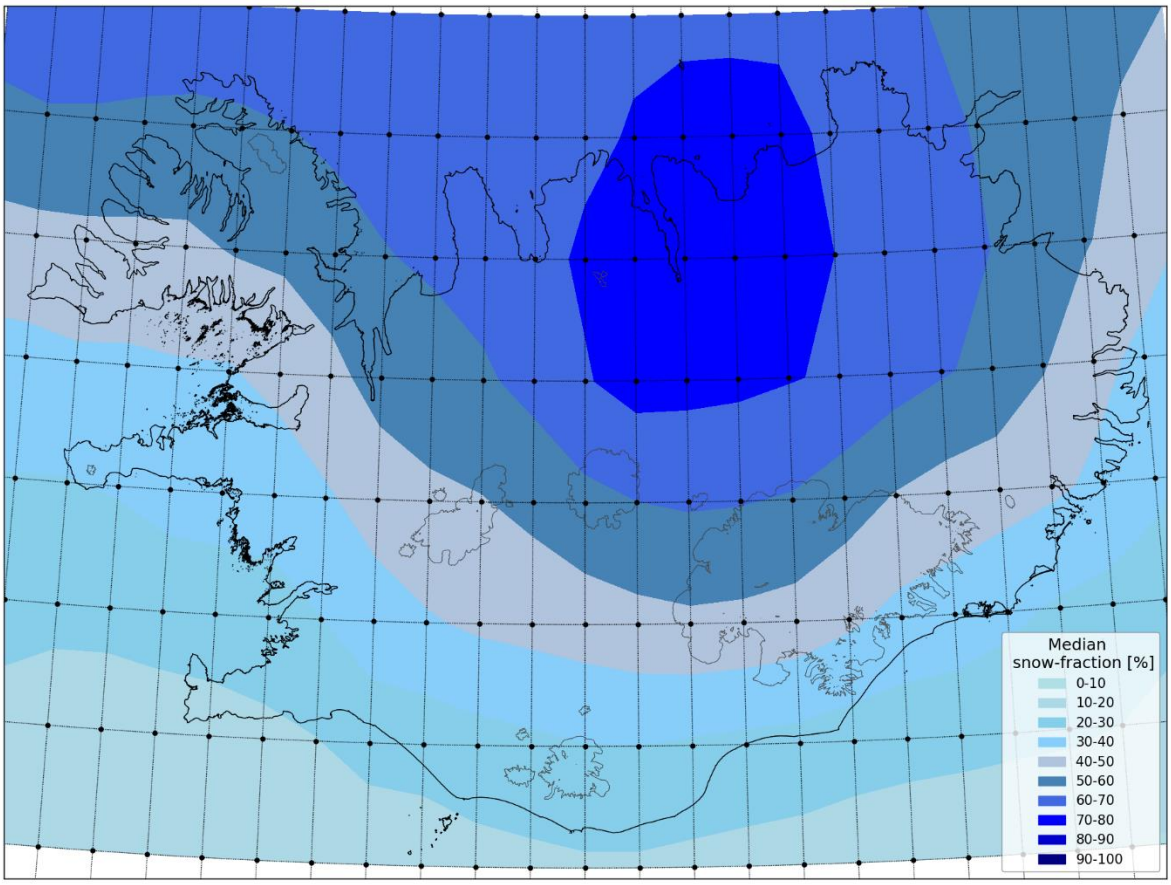

Figure 12 — Median snow-fraction values for each gridpoint yearly averaged over the winter months between 1986 – 2014 for the ensemble of climate models.

4.2 Change in snow-fraction in relation to CMIP6 climate scenarios

Median ensemble snow-fractions were consequently calculated yearly for the period 2015-2100 under the four SSP scenarios. Figure 13 shows the results in maps for each scenario, giving the median snow-fraction averaged over the period 2091-2100. As expected, the snow-fraction decreases gradually as the radiative forcing increases in the scenarios. Mean snow-fraction values averaged over all gridpoints are 40, 28, 23, and 17% for SSP126, SSP245, SSP370, and SSP585, respectively. Interestingly, the meridional gradient present in Figure 12 and in the SSP126 scenario becomes less pronounced as the scenarios become more critical and maximum values are found in zones of higher altitudes.

Figure 14 shows yearly snow-fraction timeseries between 1979 and 2100 for three catchments: Blöndulón, Sultartangi and Ufsarlón. Only values based on the SSP585 scenario are shown. For each catchment, a map is shown on the left with the outlines of the watershed in regard to the selected gridpoints. Because the catchments are rather small compared to the spacing between the gridpoints, each gridpoint close enough or included within the boundaries of the catchment is shown in colour, and the corresponding snow-fraction values over the years are shown in the same colour on the right figure. In

some instances, because of the vicinity of the catchments, the same gridpoint is used in several figures. This is the case for instance for Point 2 for Blöndulón, which is the same than Point 3 for Sultartangi. In order to reproduce the methodology used in the 2022 study, the percentage changes are calculated from the linear regression fitting the timeseries, by taking the difference between the value of the regression line in year 2100 and year 1979. On Figure 14, these percentage changes are given for individual gridpoints, and also as a median percentage over all the gridpoints considered for the catchment. Results for other catchments and SSPs are shown in Appendix V. Median percentage changes for all catchments and scenarios are given in Table 6.

Results show that in all cases and scenarios, snow-fraction decreases by the end of the century. The decrease ranges between -6% with SSP126 (for catchments Búðarháls, Kvíslaveita and Þórisvatn) and -15% with SSP585 (for catchment Hraunaveita). Overall, results are very similar for all catchments where the decrease for each scenario is within 5% range. Median snow-fraction values for scenario SSP370 show less decrease than for SSP245 in all catchments. This result, although counterintuitive, seems to reflect the weakening of the south-north gradient already discussed regarding Figure 13. Indeed, in the figure, focussing on the blue shade ranging from 50 to 60% snow-fraction, it can be noted that the contour of this area moves slightly southwards on the map for SSP370, which can then explain the less pronounced decrease when calculating the percentage changes. Another reason could come from the fact that the linear regression used to fit the data is sensitive to outliers.

An interesting result from the 2022 study showed a relation between the altitude of the catchment and the snow-fraction decrease, with largest changes observed for catchments at lower altitudes. Those results were obtained based on the ICRA dataset, with a 2.5-km resolution. Here, because of the coarser resolution of the climate models, it is however difficult to quantify the snow-fraction changes in relation to the catchment altitude.

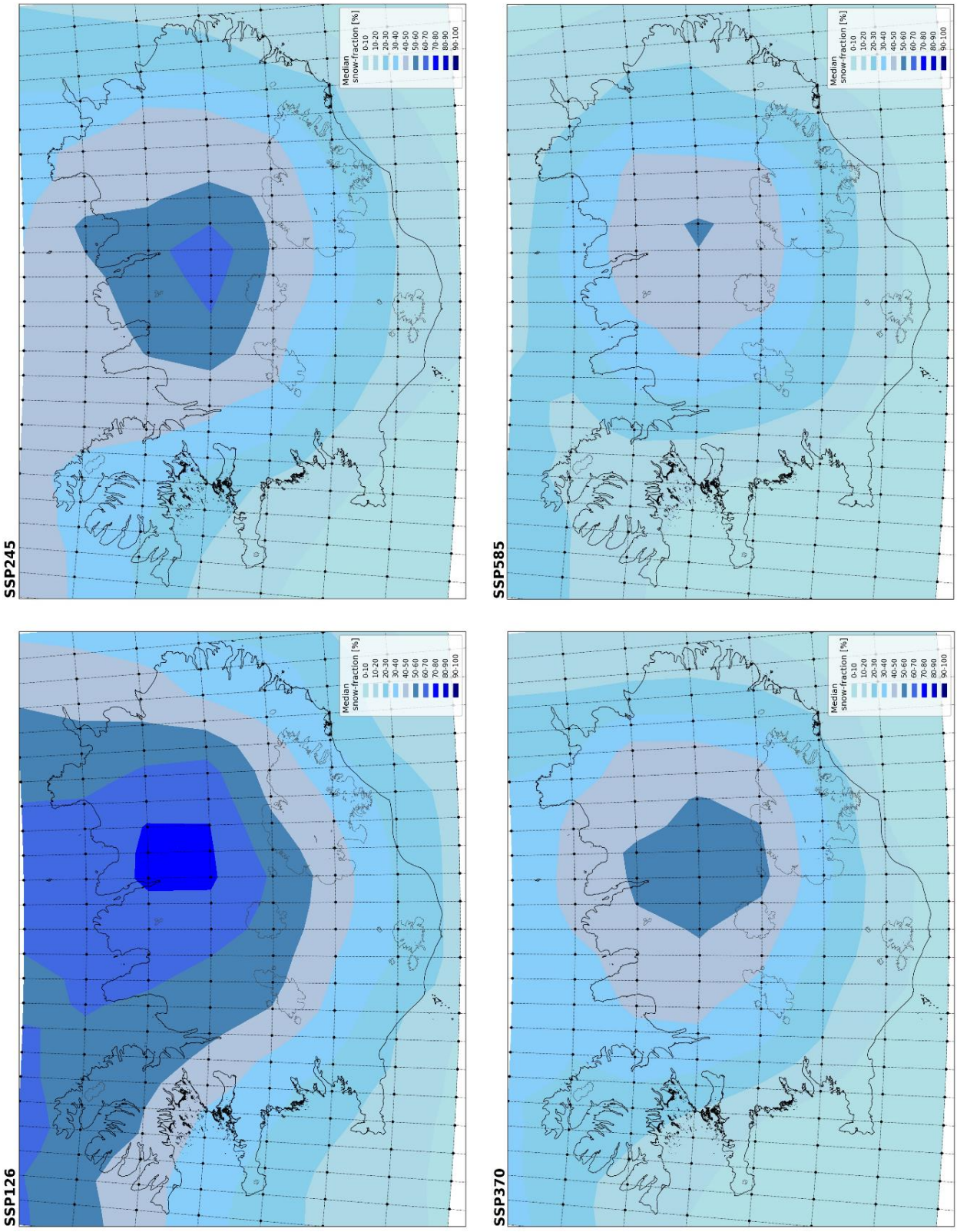

Figure 13 — Median snow-fraction for the period 2091 – 2100 for the four SSP scenarios.

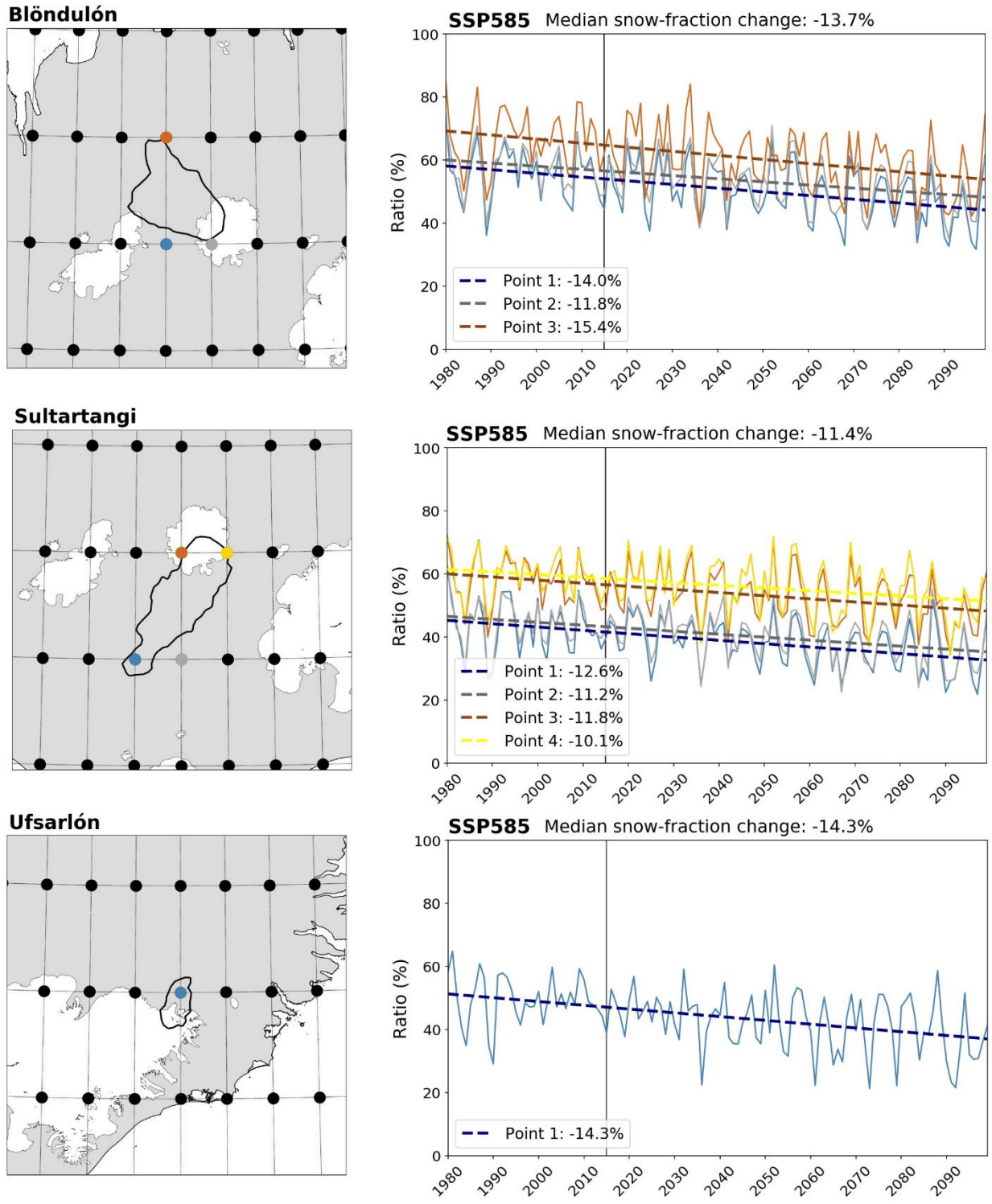

Figure 14 — (Left) Location of the gridpoints kept for the snow-fraction analysis. (Right) Evolution of the snow-fraction between 1979 and 2100 for catchments Blöndulón, Sultartangi, and Ufsarlón based on the SSP585 scenario. The colour of the timeseries matches the colour of the gridpoints.

Table 6 — Snow-fraction percentage change for the hydropower catchments based on the different SSP scenarios for the end of the century. Median values were calculated from the gridpoints within or close to the catchment outlines over the period 1979 – 2100.

	Median snow-fraction percentage change (%)			
	SSP126	*SSP245*	*SSP370*	*SSP585*
Blöndulón	-7.3	-12.3	-9.5	-13.7
Búðarháls	-6.2	-9.7	-7.7	-11.2
Hágöngulón	-6.5	-10.0	-7.5	-9.8
Hálslón	-8.5	-13.7	-9.2	-12.3
Hraunaveita	-9.0	-16.2	-9.7	-14.9
Kvíslaveita	-6.3	-9.8	-7.1	-10.1
Sultartangi	-6.7	-10.1	-7.9	-11.4
Tungnaá	-6.5	-9.7	-7.2	-10.4
Þingvallavatn	-7.8	-9.8	-7.3	-12.6
Þórisvatn	-6.2	-9.7	-7.7	-11.2
Ufsarlón	-9.0	-16.1	-9.7	-14.3

5 Summary

This research addressed two questions: First, how will precipitation return level be affected in Iceland, under the CMIP6 projections for different greenhouse gas concentration trajectories? Second, how will the snow-fraction be affected during the century, both for the whole of Iceland, and for the eleven hydropower catchments operated by Landsvirkjun?

In Section 3, daily and 5-day annual maximum precipitation amounts (RX1D and RX5D) from the CMIP6 dataset were retrieved for a historical period (1850 – 2014) and four SSP scenarios: SSP125, SSP245, SSP370, and SSP585 for the rest of the century (2015 – 2100). Because the initial spatial resolution differs in all models, the data were regridded over a box that covers Iceland between longitudes -13 and -19°, and latitudes 63 and 67°, with a horizontal resolution of 1°. Despite the coarseness of the dataset, the climate models still managed to capture the main features of the Icelandic precipitation patterns: enhanced precipitation in the southern half, with maximum values over the Vatnajökull region, and less precipitation in the N.E. quadrant, in the lowlands. In regions of complex orography such as the East- and Westfjords, values are higher than in areas of similar latitudes but more inland. This spatial distribution of precipitation was included in the EVA by calculating percentage changes between a control period (1986 – 2014) and an end-of-the-century period (2091 – 2100) for each quadrant and all SSPs.

Overall, percentage changes show a gradual increase as the projection scenarios imply an increased radiative forcing by the end of the century. Despite a few values obtained with the SSP126 scenario over the 10th percentile (indicating a decrease of the RX1D values at the end of the century), all percentage changes were positive, with an increase ranging from 0 to 25% in 2100, depending on the quadrant, percentile, and scenario considered. For RX5D, some negative values were found for other percentiles and scenarios, but most trends also indicate an increase in precipitation, up to 23% for the SSP585 scenario, based on the 90th percentile and for the N.W. quadrant.

These percentage changes were then incorporated to the ICRA dataset to create a new set of maps for various return periods, using the Block Maxima method. Results were shown in Figure 8, 9, and 11 for the whole of Iceland, as well as in Appendix IV. Maps were also created for individual catchments, as shown in Figure 10 and Appendix III.

In Section 4, snow-fraction was calculated as the ratio between the snowfall and precipitation fluxes from the CMIP6 dataset. Data were regridded with a resolution of 0.5° in both latitude and longitude and only winter months from November to April were kept in the analysis. Median values over the period 1986 – 2014 showed a yearly snow-fraction in Iceland ranging from 9 to 76%, with a pronounced meridional gradient, and a mean value over the whole country for the same period of 44%. These values were lower at the end of the century for all SSPs, with mean snow-fraction values averaged over Iceland of 40, 28, 23, and 17% for SSP126, SSP245, SSP370, and SSP585, respectively. Snow-fraction changes were also calculated at catchment-scale, as shown in Figure 14 and Appendix V. Because of the resolution of the dataset, results did not vary much from one catchment to the next, with results very similar for all catchments. Results showed a decrease in all

catchments for the period 1979 – 2100, ranging between -6% with SSP126 (for catchments Búðarháls, Kvíslaveita and Þórisvatn) and -15% with SSP585 (for catchment Hraunaveita).

To conclude, this study showed an increase in precipitation return levels, reaching a 25% for RX1D and 23% for RX5D, depending on the quadrant, scenario and percentile considered. Snow-fraction is expected to decrease, with a median value over the whole country of 44% for the historical period, versus 17% with SSP585.

References

Bengtsson, L., Andrae, U., Aspelien, T., Batrak, Y., Calvo, J., de Rooy, W. & Køltzow, M.Ø. (2017). The HARMONIE-AROME model configuration in the ALADIN-HIRLAM NWP system. *Mon. Wea. Rev*, 145, 1919–1935

Bintanja, R. (2018) The impact of Arctic warming on increased rainfall. *Scientific Reports*, 8, 16001. https://doi.org/10.1038/s41598-018-34450-3.

Björnsson, H., Sigurðsson, B. D., Davíðsdóttir, B., Ólafsson, J., Ástþórssson, Ó. S., Ólafsdóttir, S., Baldursson, T. & Jónsson, T. (2018). Loftslagsbreytingar og áhrif þeirra á Íslandi – Skýrsla vísindanefndar um loftslagsbreytingar 2018. *Veðurstofa Íslands*.

Crochet P., Johannesson T., Jonsson T., Sigurdsson O., Bjornsson H., Palsson F. & Barstad I. (2007). Estimating the spatial distribution of precipitation in Iceland using a linear model of orographic precipitation. *Journal of Hydrometeorology* 8, 1285–1306.

Eyring, V., S. Bony, G. A. Meehl, C. A. Senior, B. Stevens, R. J. Stouffer, and K. E. Taylor, 2016: Overview of the Coupled Model Intercomparison Project Phase 6 (CMIP6) experimental design and organization. Geoscientific Model Development, 9, 1937−1958.

Fjórða samantektarskýrsla vísindanefndar um loftslagsbreytingar. (2023). Umfang og afleiðingar hnattrænna loftslagsbrytinga á Íslandi. (https://cdn.loftslagsbreytingar.is/pdf/2023/10/skyrsla_visindanefndar.pdf)

IPCC (2021). Climate Change 2021: The Physical Science Basis. Contribution of Working Group I to the Sixth Assessment Report of the Intergovernmental Panel on Climate Change [Masson-Delmotte, V., P. Zhai, A. Pirani, S.L. Connors, C. Péan, S. Berger, N. Caud, Y. Chen, L. Goldfarb, M.I. Gomis, M. Huang, K. Leitzell, E. Lonnoy, J.B.R. Matthews, T.K. Maycock, T. Waterfield, O. Yelekçi, R. Yu, and B. Zhou (eds.)]. *Cambridge University Press.* In Press.

Krasting, J. P., Broccoli, A. J., Dixon, K. W., & Lanzante, J. R. (2013). Future changes in Northern Hemisphere snowfall. *Journal of Climate*, *26*(20), 7813-7828.

Li, Z., Chen, Y. & Li, Y. (2020). Declining snowfall fraction in the alpine regions, Central Asia. *Sci Rep* **10,** 3476.

Lin, W., Chen, H. (2022). Daily snowfall events on the Eurasian continent: CMIP6 models evaluation and projection. *International Journal of Climatology*.

Massad, A.-G. R., Petersen, G. N., Þórarinsdóttir, T., Roberts, M. J. (2020). Reassessment of return levels in Iceland. *Veðurstofa Íslands*. VÍ 2020-008.

Massad, A.-G. R., Petersen, G. N., Björnsson, H., Þórarinsdóttir, T., Roberts, M. J. (2022). Extreme precipitation in Iceland: Climate projections and historical changes in precipitation type. *Veðurstofa Íslands*. VÍ 2022-006.

Nawri, N., Pálmason, B., Petersen, G. N., Björnsson, H. & Þorsteinsson, S. (2017). The ICRA atmospheric reanalysis project for Iceland. *Veðurstofa Íslands*. VÍ 2017-005.

O'Gorman, P. (2014). Contrasting responses of mean and extreme snowfall to climate change. *Nature* **512**, 416–418.

O'Neill, B.C., Kriegler, E., Ebi, K. L., Kemp-Benedict, E., Riahi, K., Rothman, D. S., van Ruijven, B. J., van Vuuren, D. P., Birkmann, J., Kok, K., Levy, M., Solecki, W. (2017). The roads ahead: Narratives for shared socioeconomic pathways describing world futures in the 21st century. *Global Environmental Change*, Volume 42, Pages 169-180, ISSN 0959-3780

Appendix I. Annual Maximum Series

In this appendix, figures similar to Figure 5 from the report are presented.

Figure I.1 shows the ensemble median RX1D calculated for each quadrant by taking the mean value over all gridpoints within the region. Results are shown for both the historical period (1850 – 2014) and for the future (2015 – 2100), as covered by the four SSP scenarios. And plotted over time from 1850 to 2100 for each SSP projection. Figure I.2 shows results based on the ensemble median RX5D.

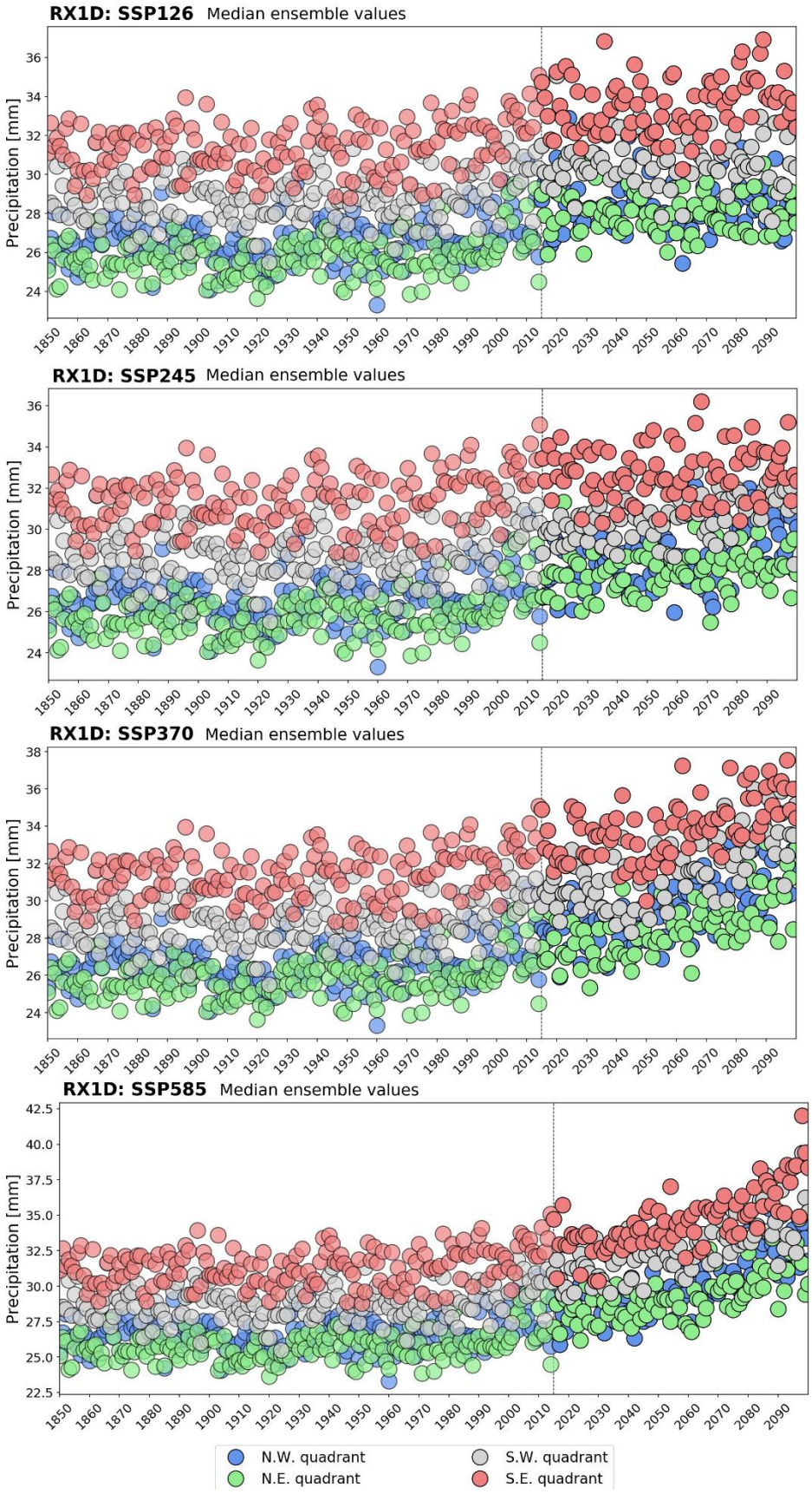

Figure I.1 — Median RX1D values for each quadrant calculated from the ensemble of climate models for a historical period (1985 – 2014, transparent dots) and various SSPs (2015 – 2100, opaque dots).

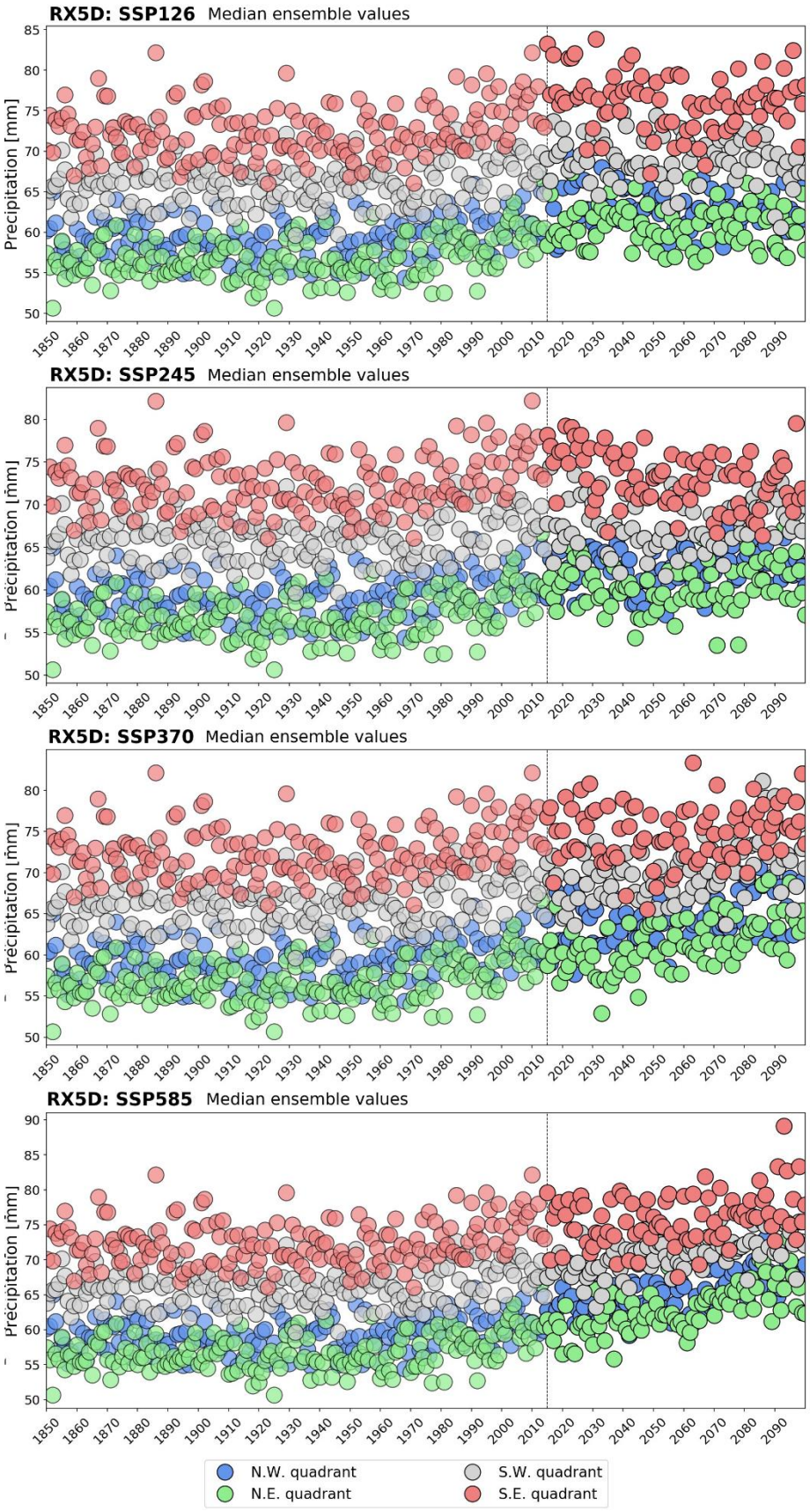

Figure I.2 — Median RX5D values for each quadrant calculated from the ensemble of climate models for a historical period (1985 – 2014, transparent dots) and various SSPs (2015 – 2100, opaque dots).

Appendix II. Precipitation percentage changes

In this appendix, figures similar to Figure 6 and 7 from the report are presented.

On each subplot, precipitation values for a specific quadrant were normalised by dividing each one of them by the median values over the control period (1986 – 2014). Values from the 19 models are shown with grey dots, while the yearly median and 10th-90th percentile range are shown in different colour for each quadrant. While the values are shown continuously for the entire period from 1986 to 2100, only the two periods used to calculate the percentage changes are shown with opaque colours. Percentage changes are indicated on the figures. They were calculated based on median values, as well as 10th and 90th percentiles from all data within each period.

Figure II.1 – 4 show results for RX1D for the scenarios SSP126, SSP245 and SSP370. Figures II.4 – 6 shows results for RX5D. Results for SSP585 are in the main text of the report.

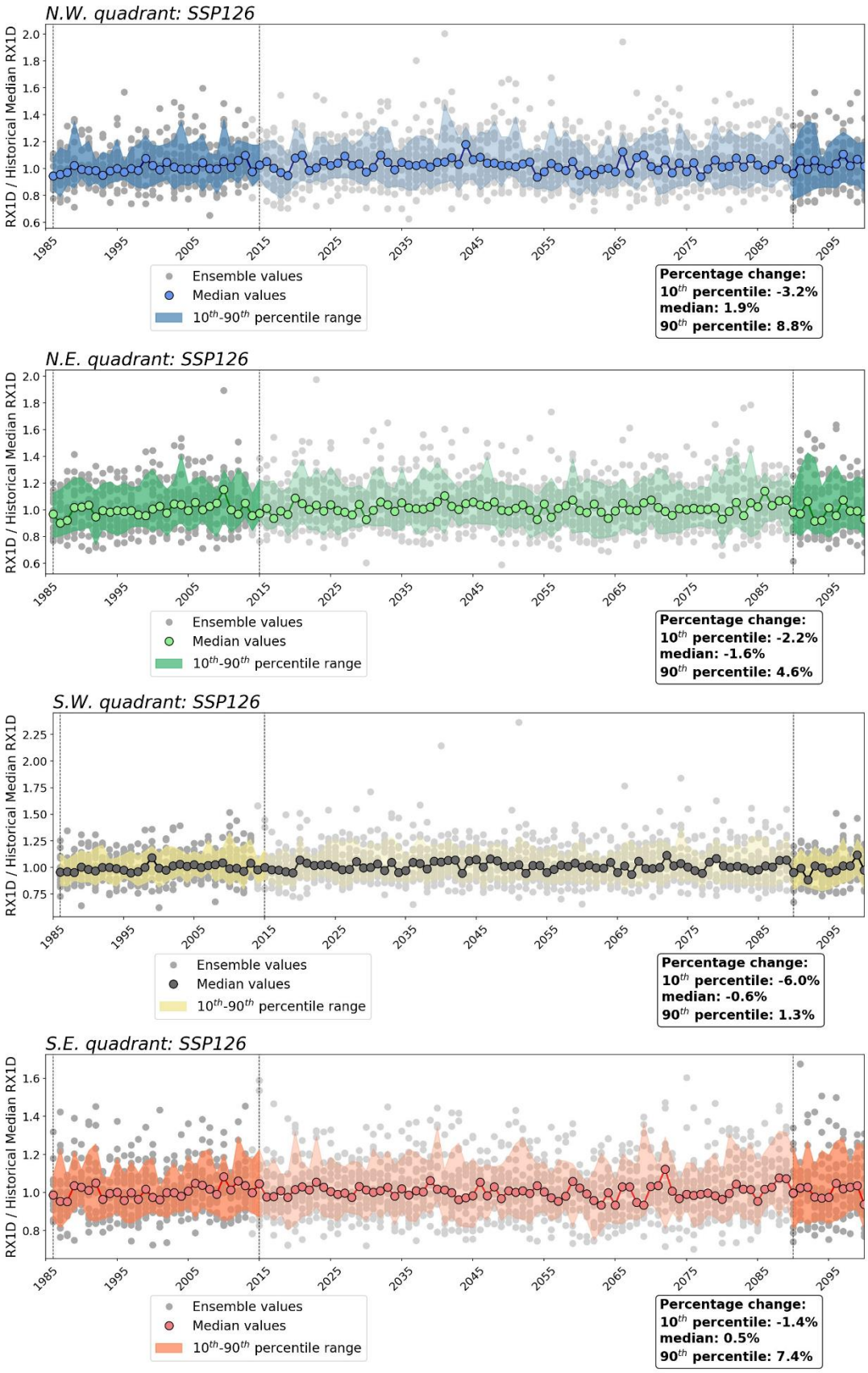

Figure II.1 — RX1D percentages changes by quadrant calculated from median, 10th and 90th percentile values of the ensemble of climate models for SSP126.

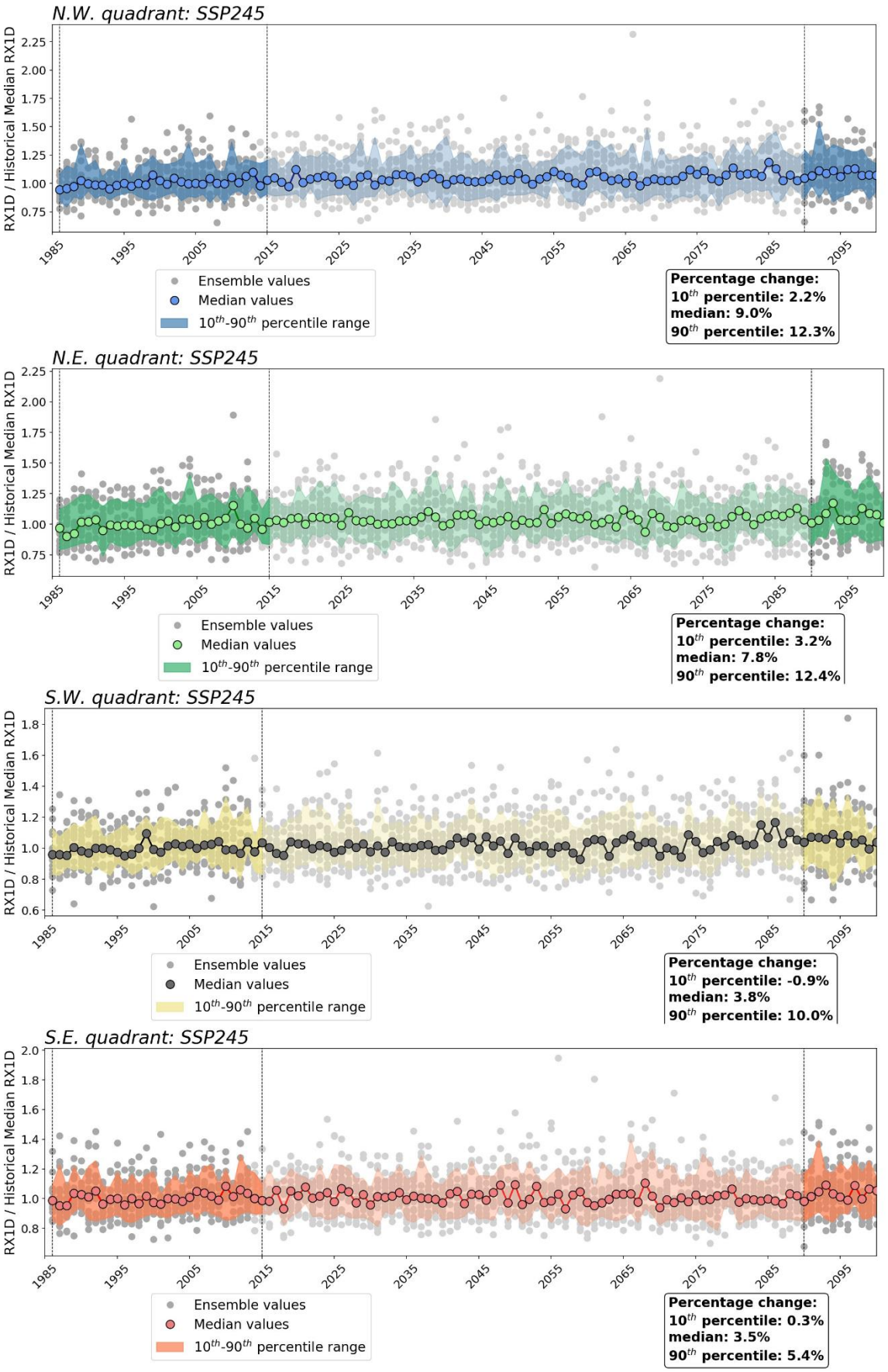

Figure II.2 — RX1D percentages changes by quadrant calculated from median, 10th and 90th percentile values of the ensemble of climate models for SSP245.

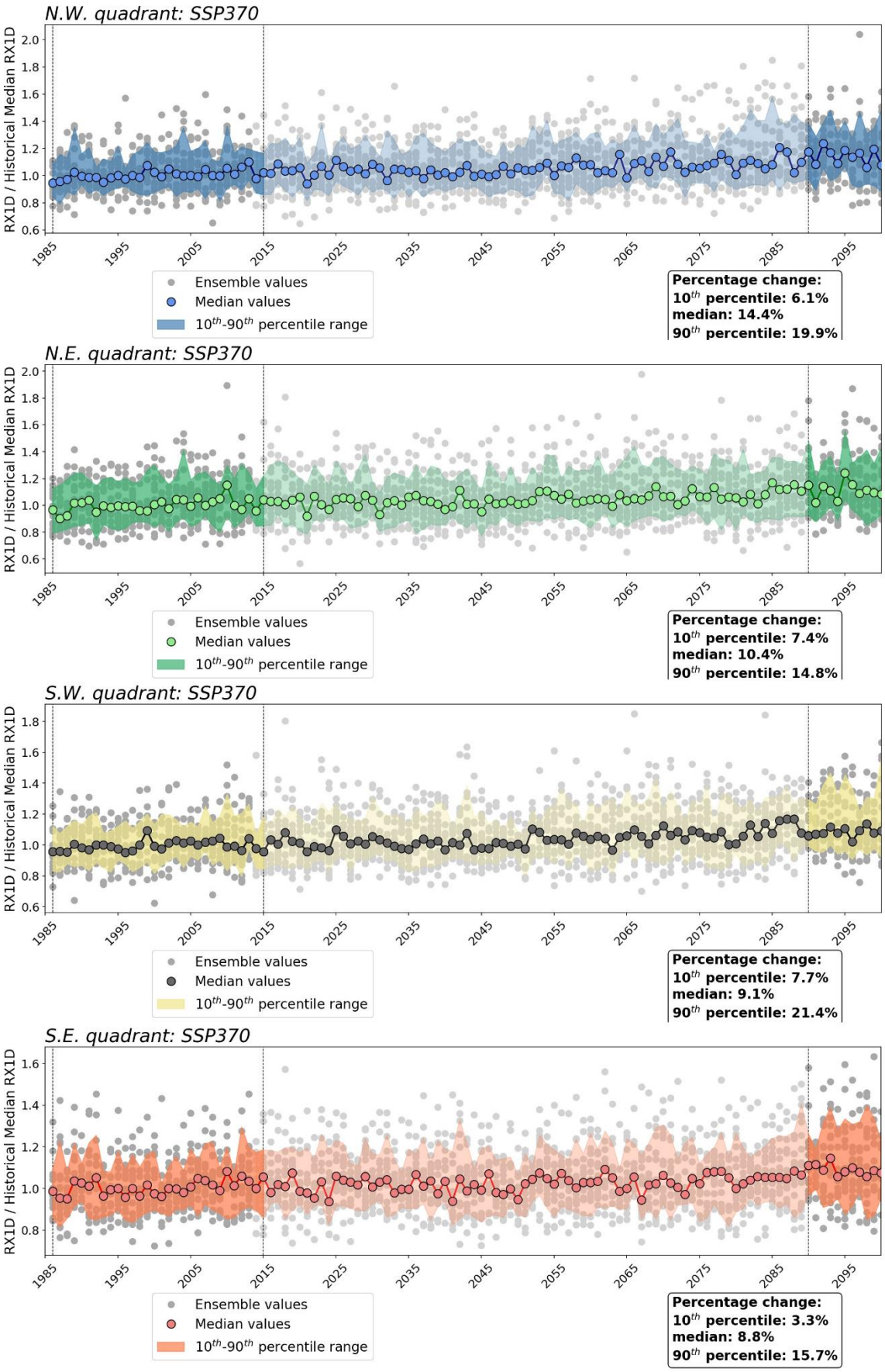

Figure II.3 — RX1D percentages changes by quadrant calculated from median, 10th and 90th percentile values of the ensemble of climate models for SSP370.

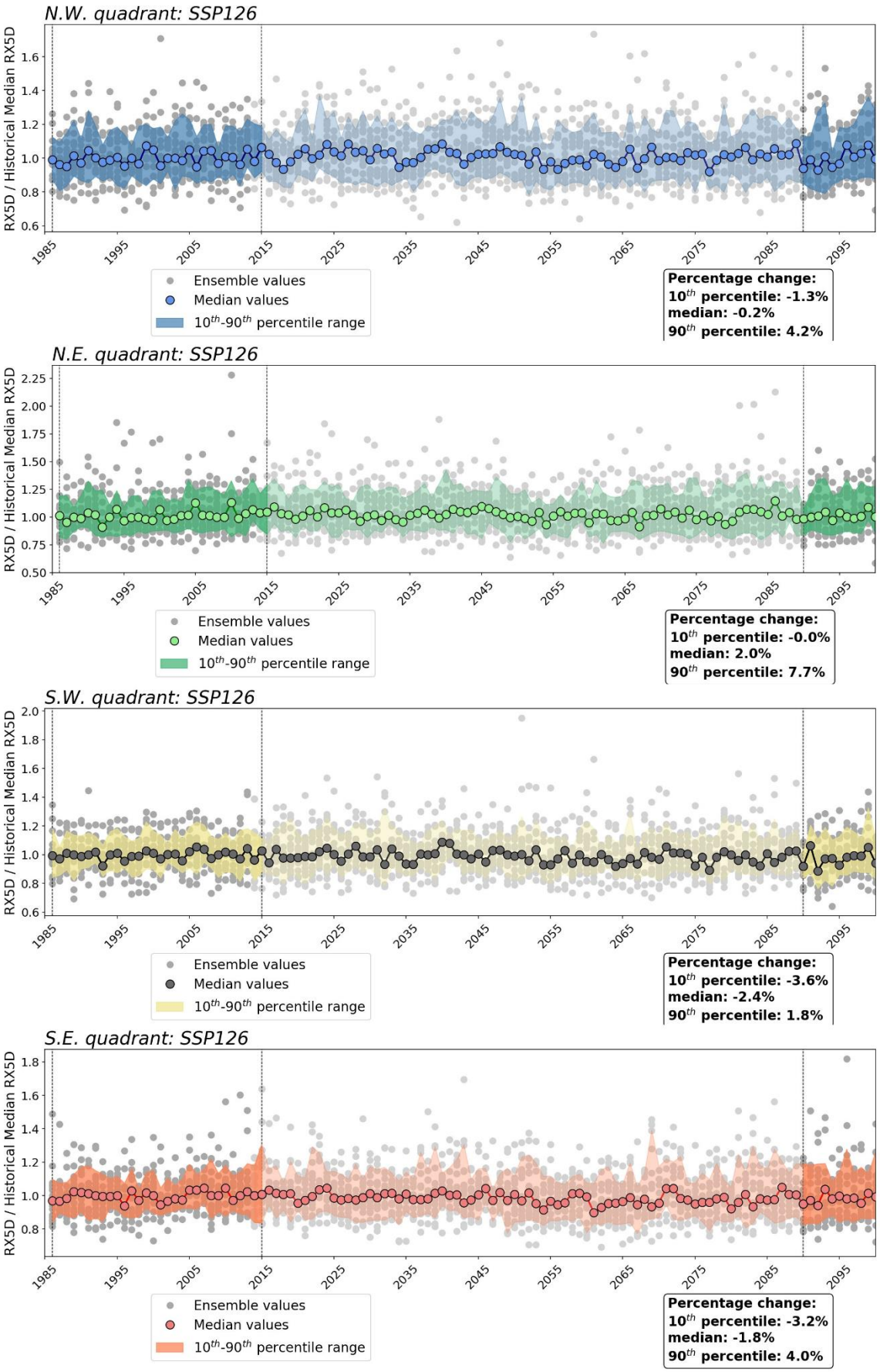

Figure II.4 — RX5D percentages changes by quadrant calculated from median, 10th and 90th percentile values of the ensemble of climate models for SSP126.

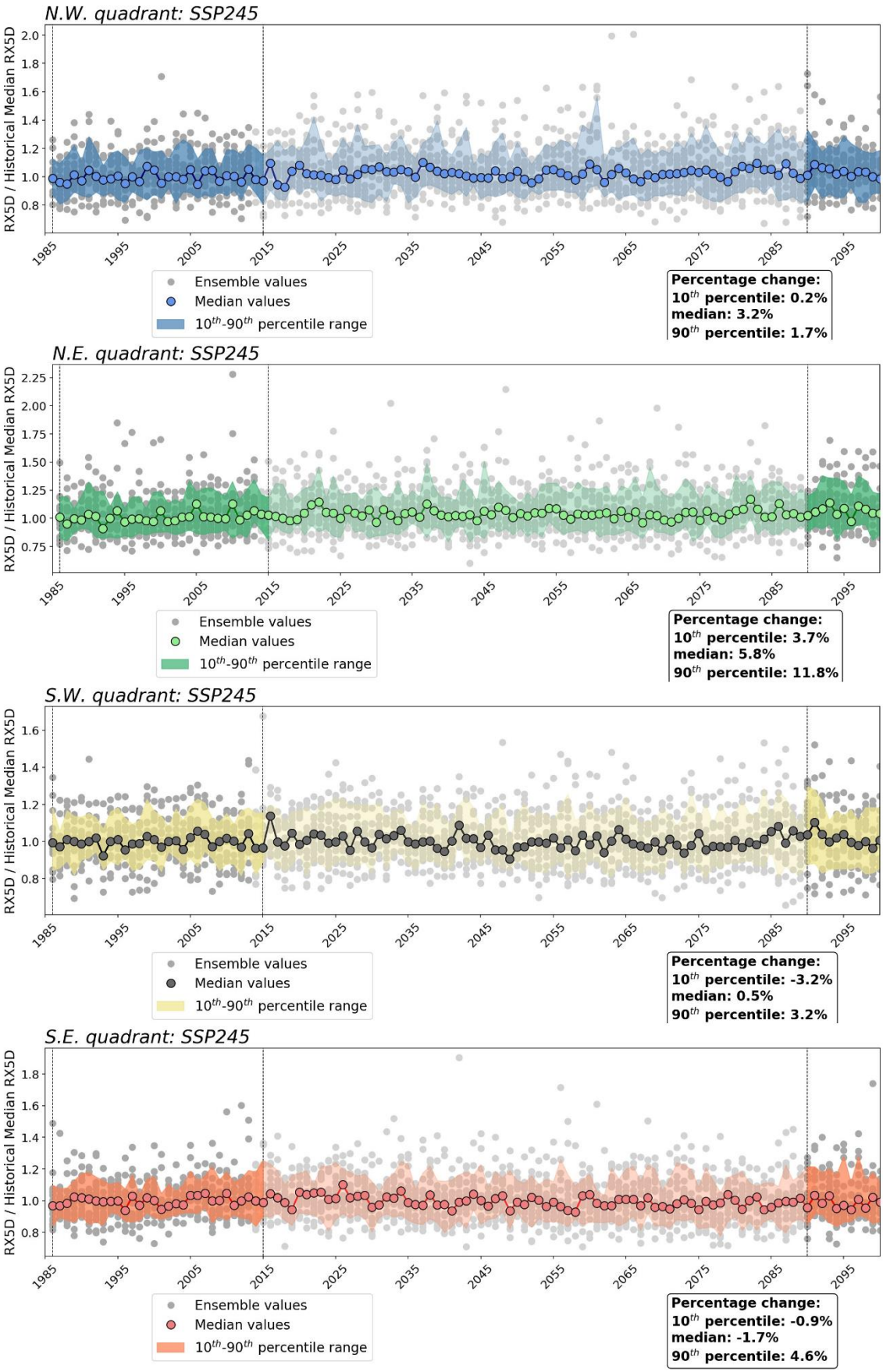

Figure II.5 — RX5D percentages changes by quadrant calculated from median, 10th and 90th percentile values of the ensemble of climate models for SSP245.

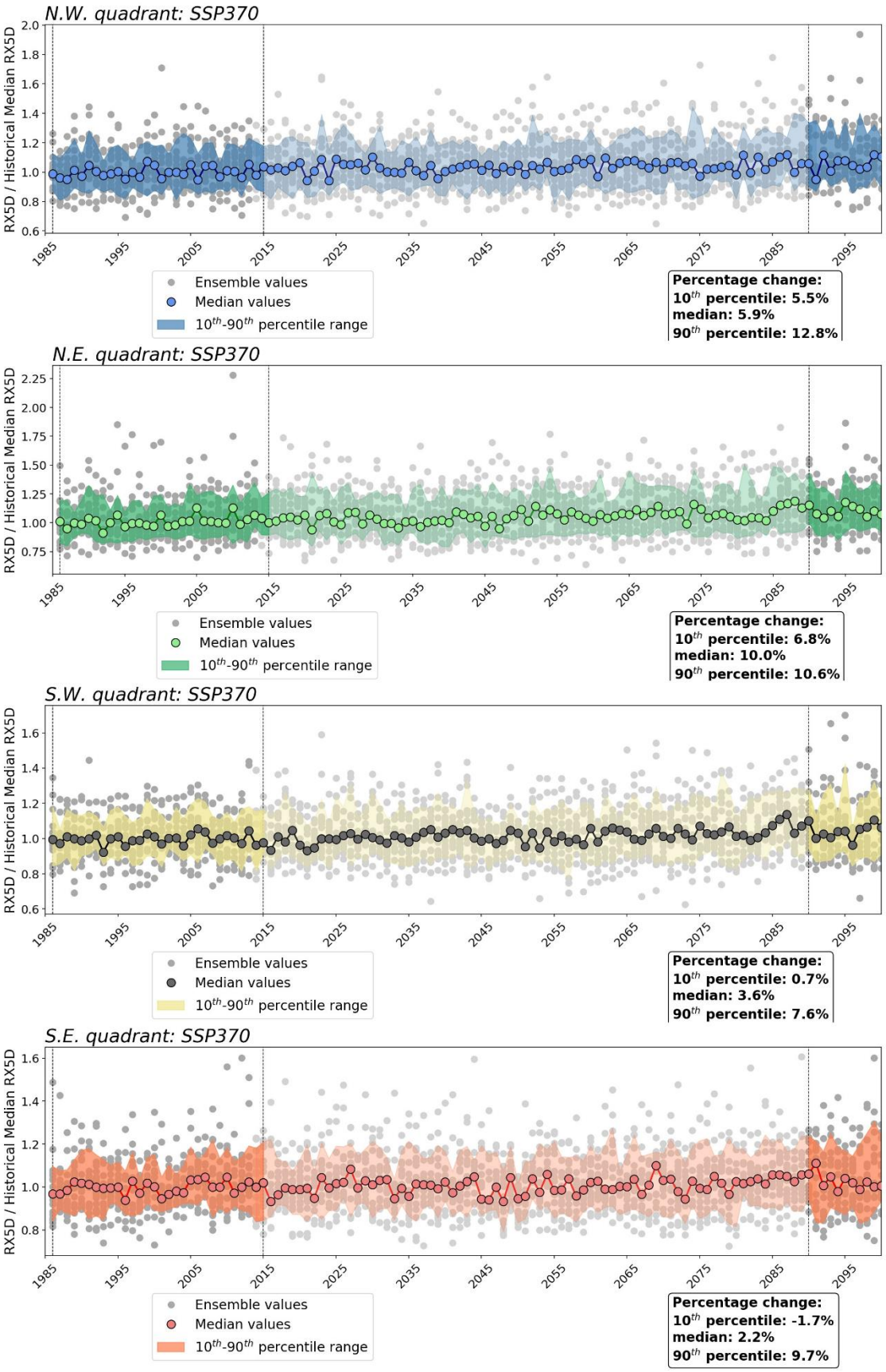

Figure II.6 — RX5D percentages changes by quadrant calculated from median, 10th and 90th percentile values of the ensemble of climate models for SSP370.

Appendix III. Catchment-scale 1M5 maps

In this appendix, figures similar to Figure 10 from the report are presented.

Figures III.1 – III.11 show individual 1M5 maps for all the catchment, with and without climate projections, as calculated using the Block Maxima method.

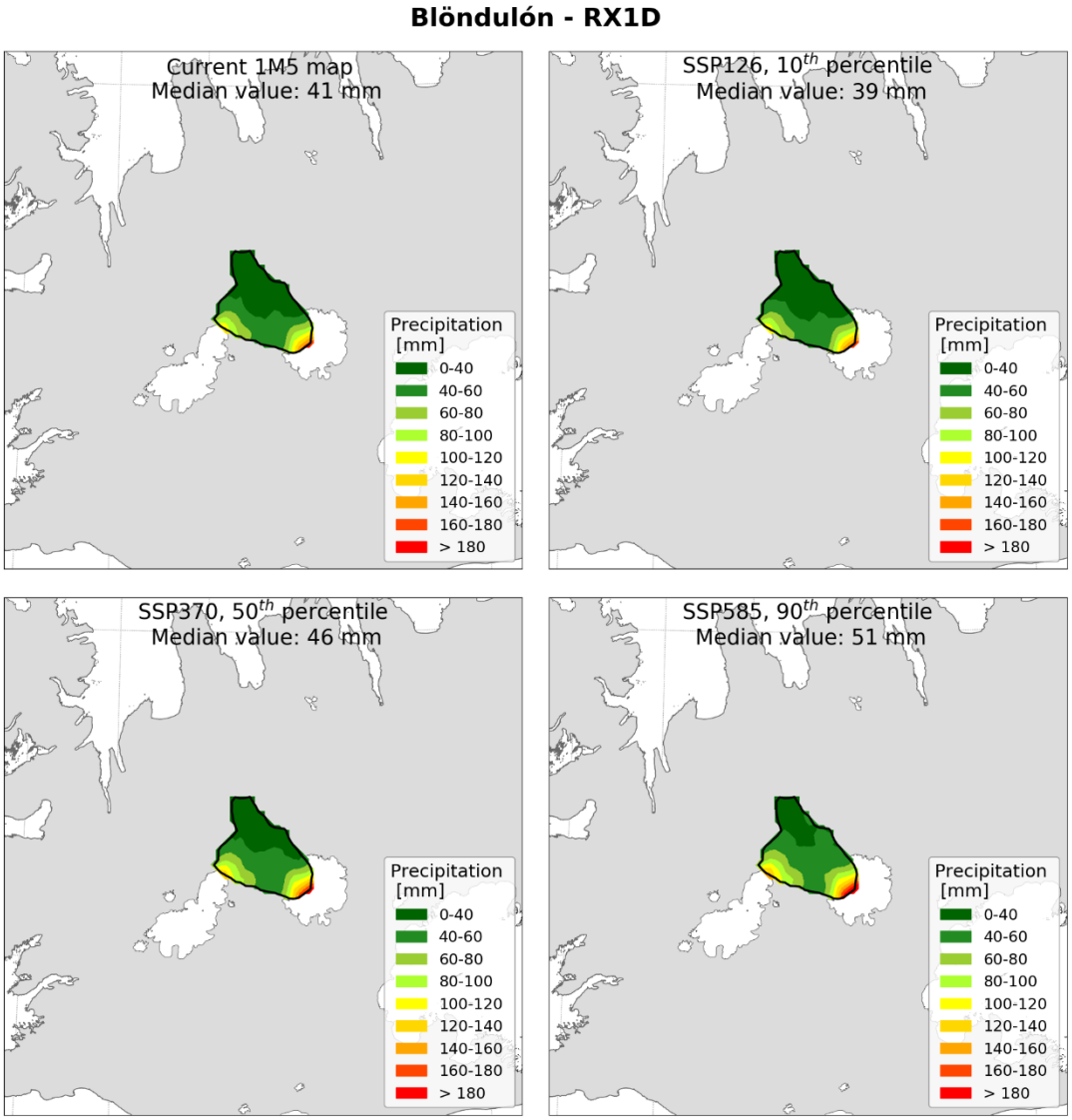

Figure III.1 — 1M5 maps for catchment Blóndulón based on the ICRA dataset without projection (top left), with SSP126 and 10th percentile percentage changes (top right), with SSP370 and median percentage changes (bottom left) and with SSP585 and 90th percentile percentage changes (bottom right).

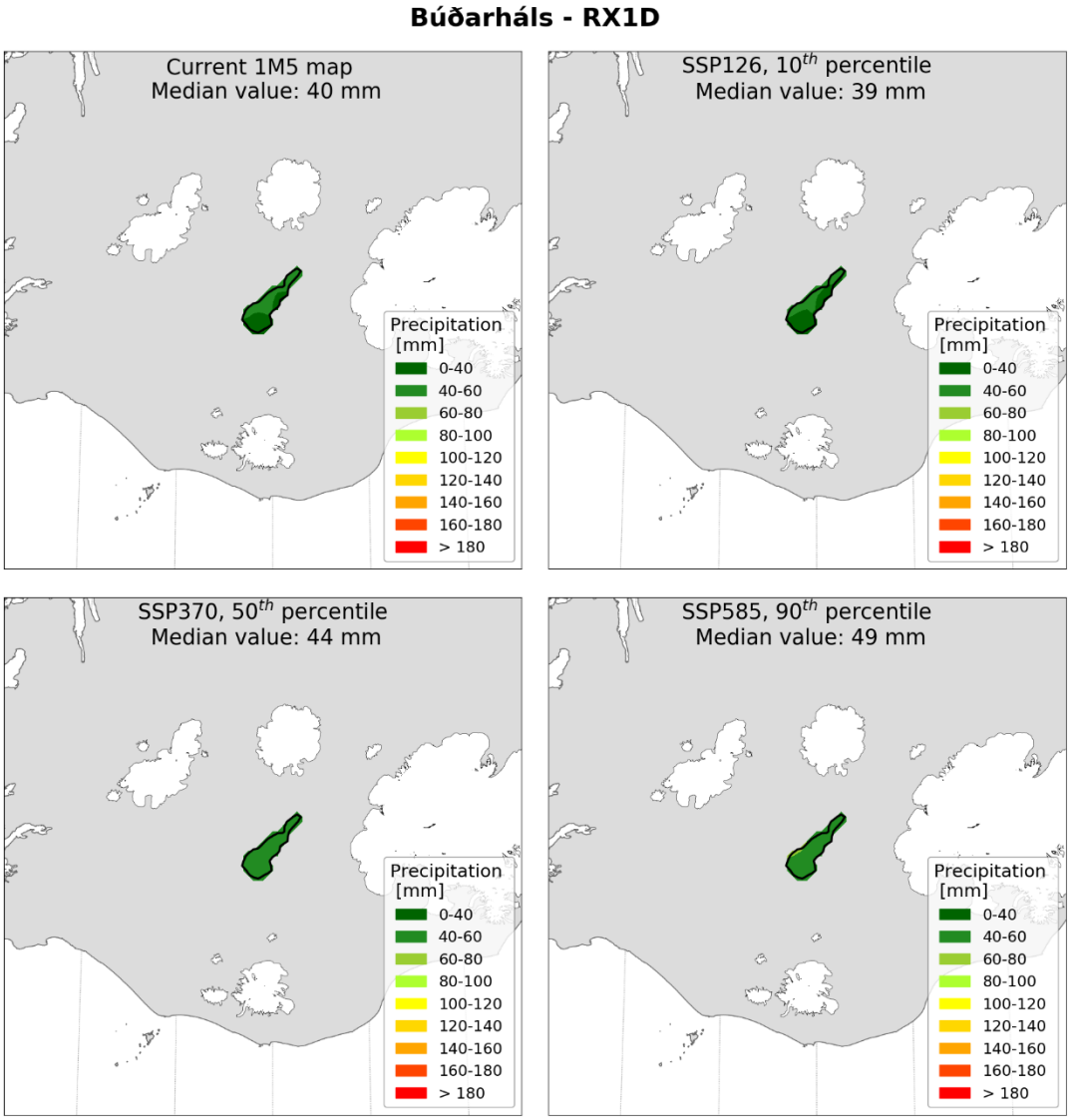

Figure III.2 — 1M5 maps for catchment Búðarháls based on the ICRA dataset without projection (top left), with SSP126 and 10th percentile percentage changes (top right), with SSP370 and median percentage changes (bottom left) and with SSP585 and 90th percentile percentage changes (bottom right).

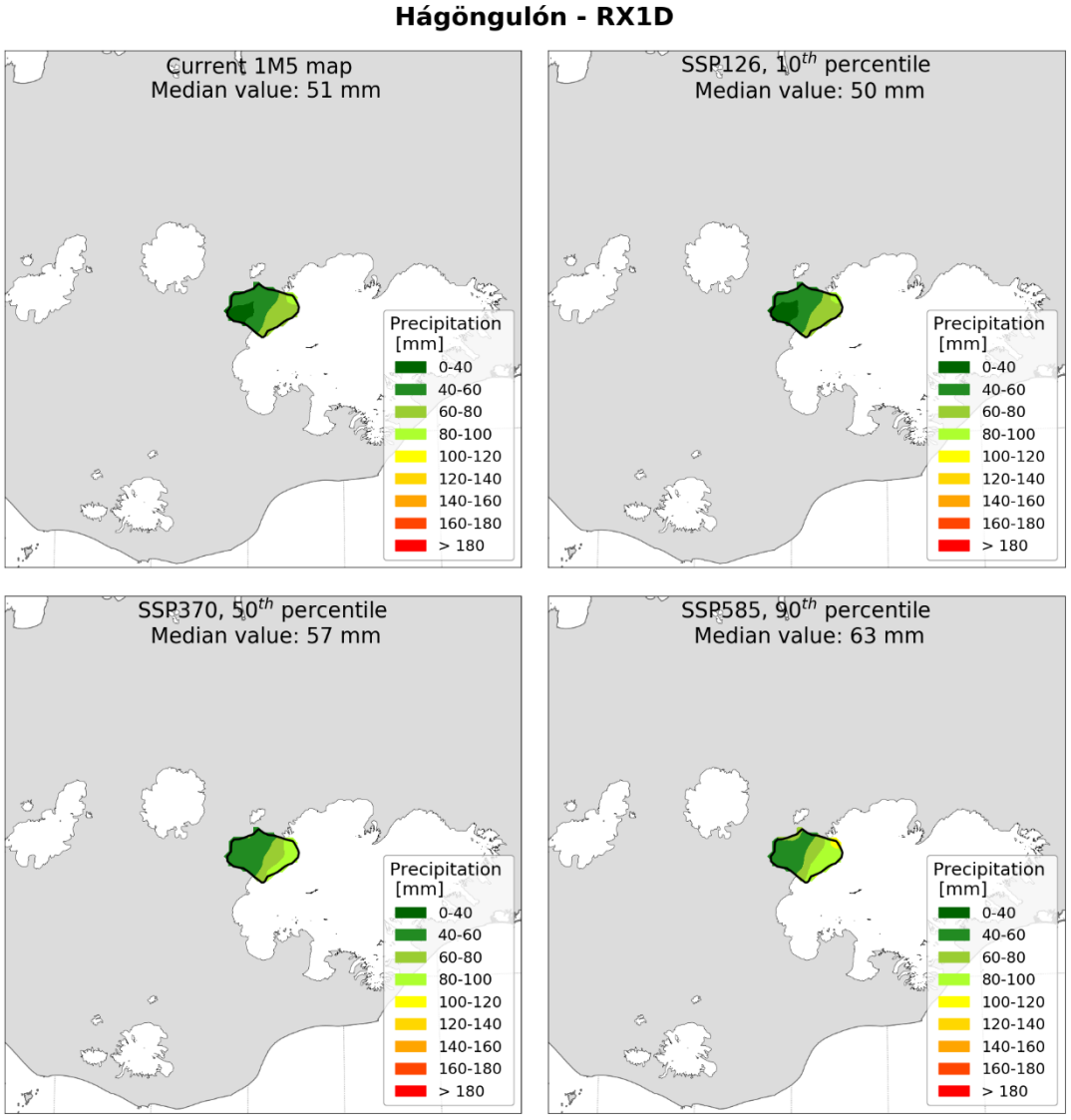

Figure III.3 — 1M5 maps for catchment Hágöngulón based on the ICRA dataset without projection (top left), with SSP126 and 10th percentile percentage changes (top right), with SSP370 and median percentage changes (bottom left) and with SSP585 and 90th percentile percentage changes (bottom right).

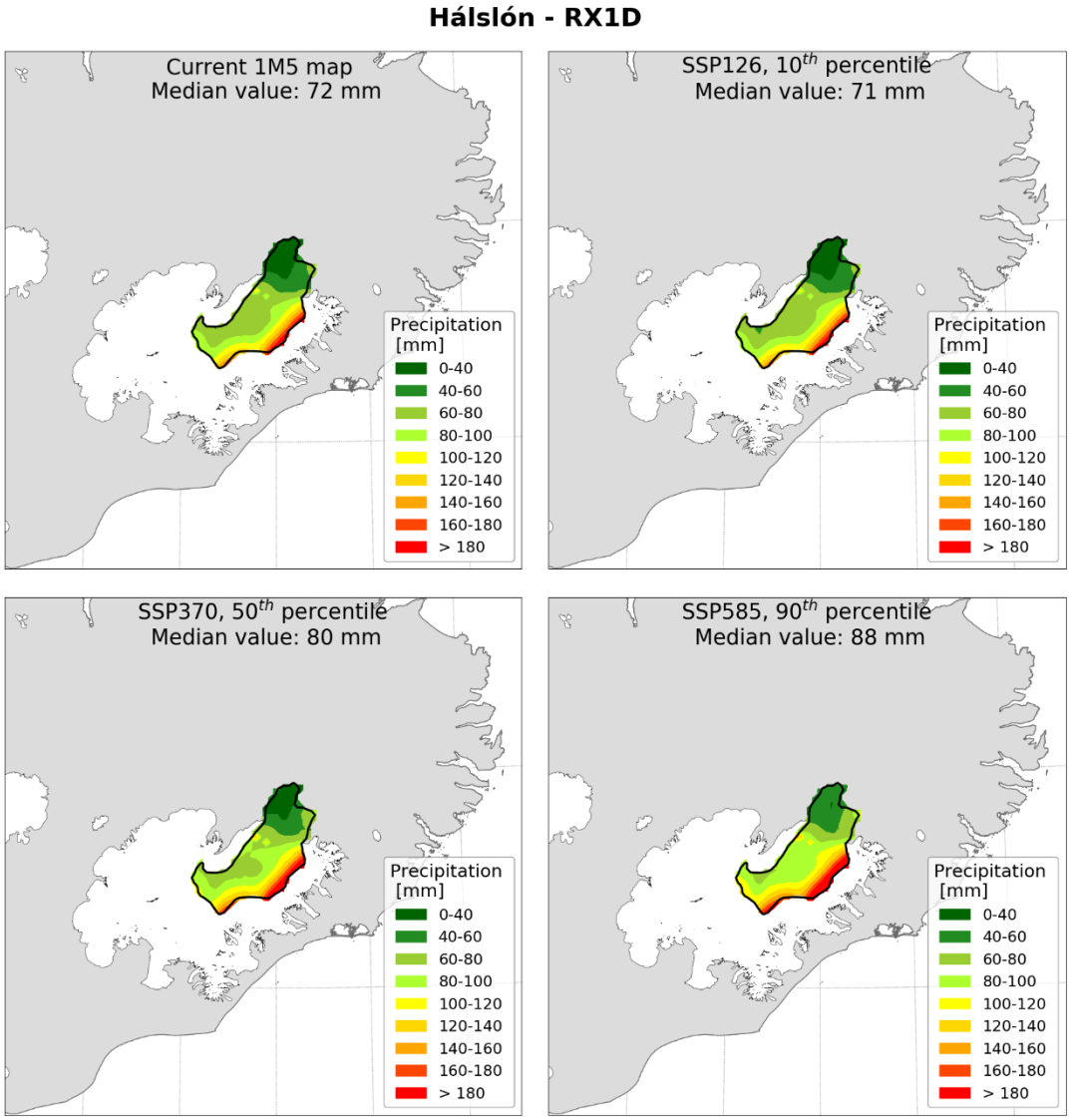

Figure III.4 — 1M5 maps for catchment Hálslón based on the ICRA dataset without projection (top left), with SSP126 and 10th percentile percentage changes (top right), with SSP370 and median percentage changes (bottom left) and with SSP585 and 90th percentile percentage changes (bottom right).

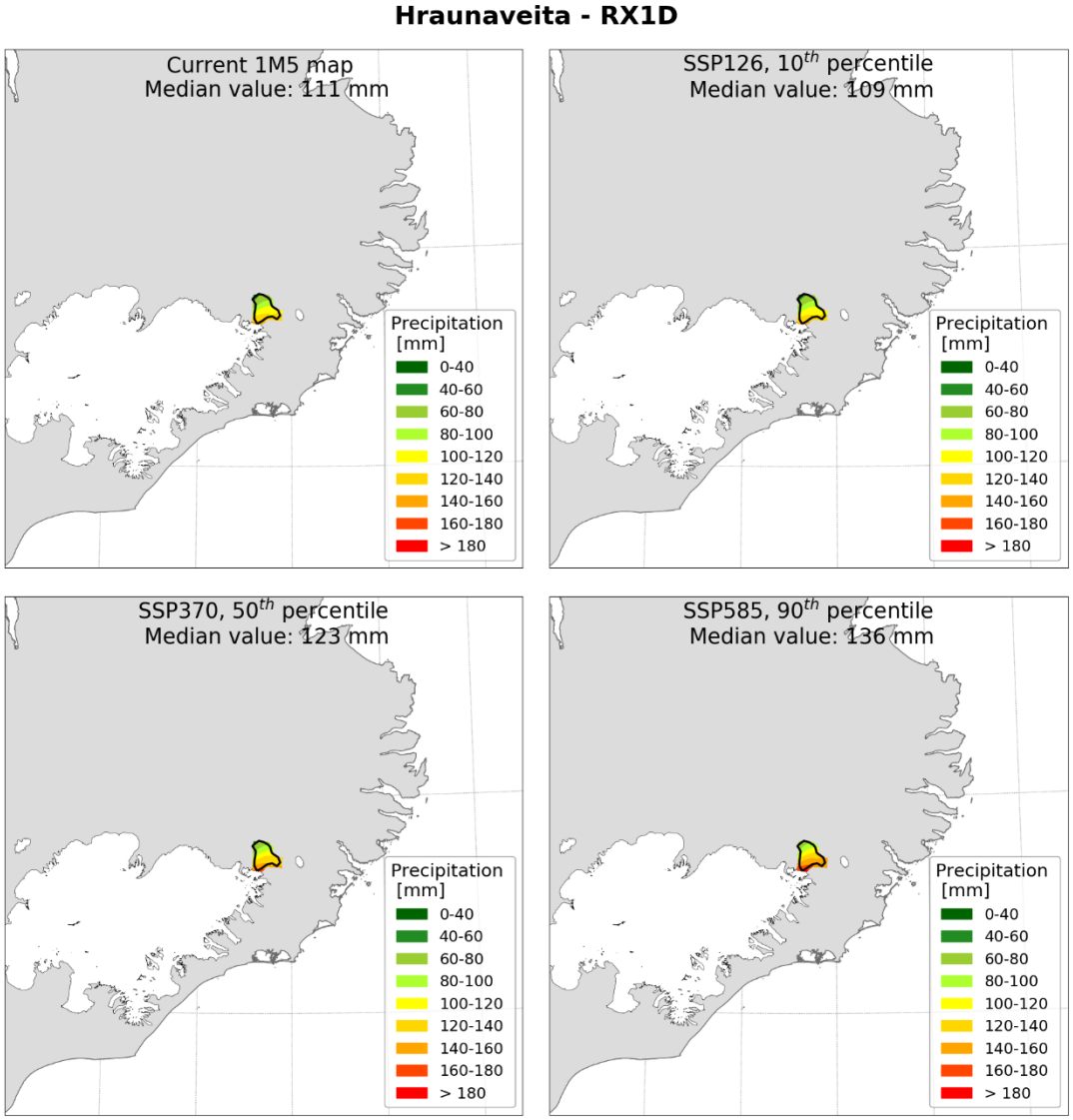

Figure III.5 — 1M5 maps for catchment Hraunaveita based on the ICRA dataset without projection (top left), with SSP126 and 10th percentile percentage changes (top right), with SSP370 and median percentage changes (bottom left) and with SSP585 and 90th percentile percentage changes (bottom right).

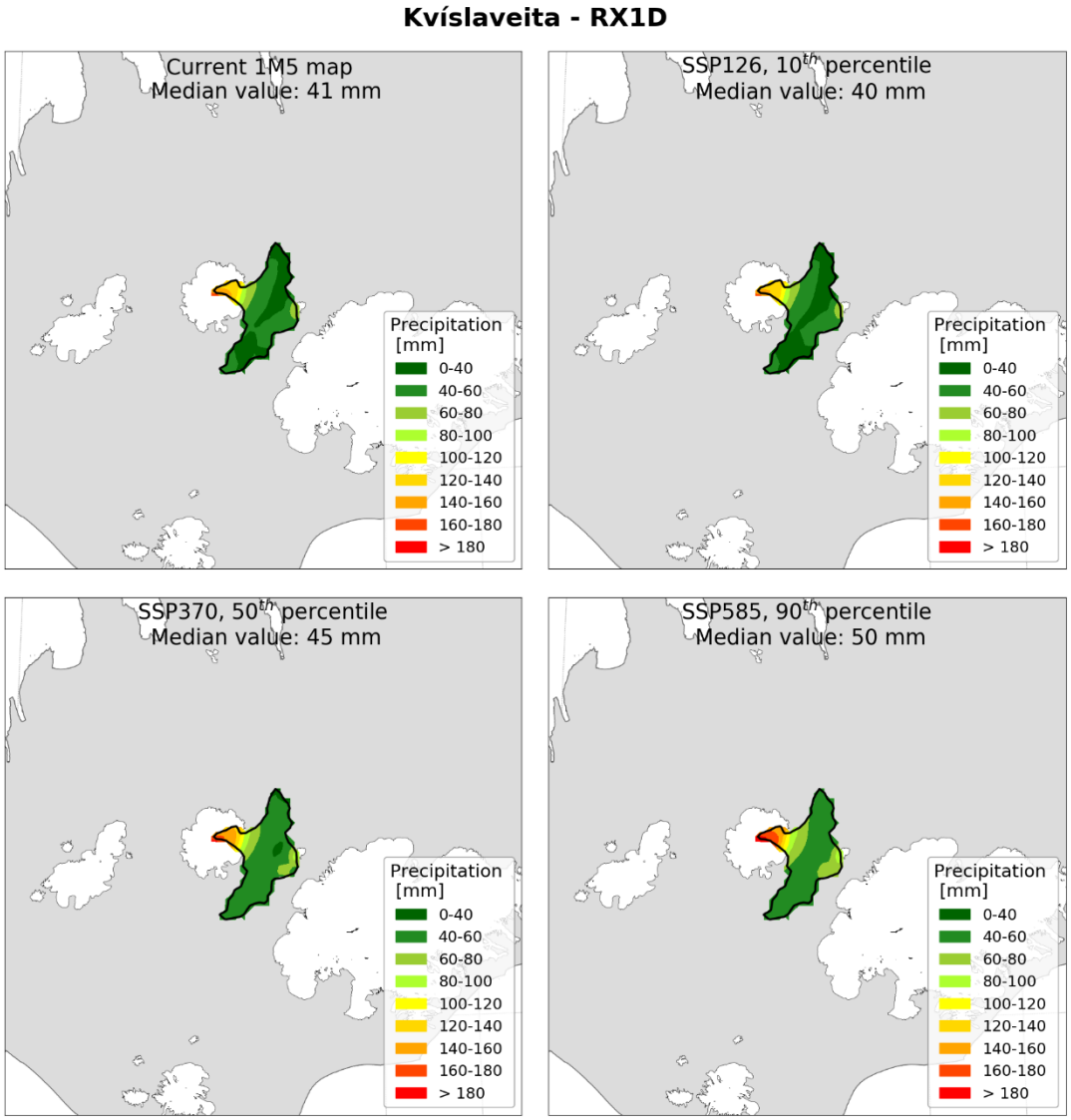

Figure III.6 — 1M5 maps for catchment Kvíslaveita based on the ICRA dataset without projection (top left), with SSP126 and 10th percentile percentage changes (top right), with SSP370 and median percentage changes (bottom left) and with SSP585 and 90th percentile percentage changes (bottom right).

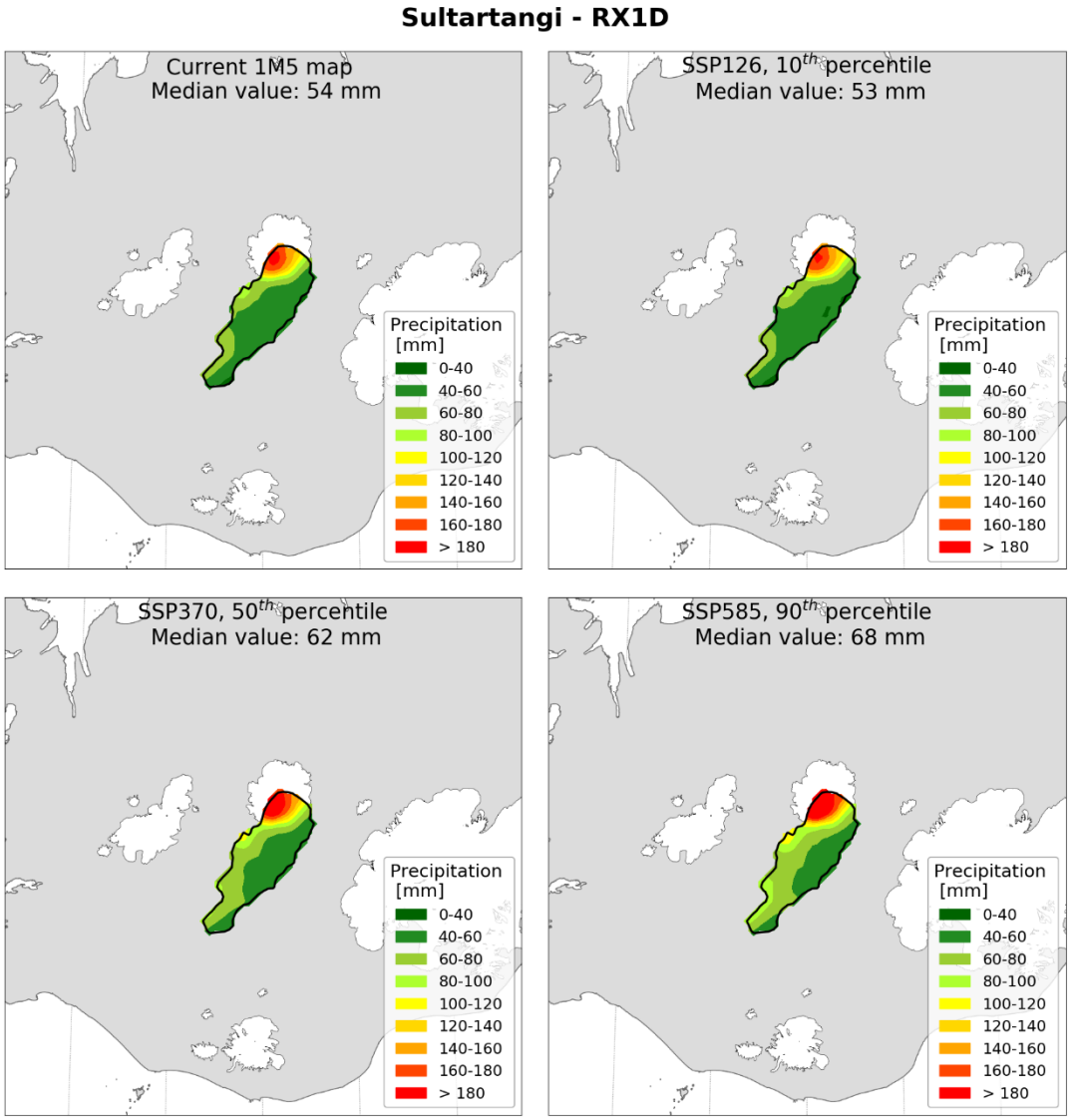

Figure III.7 — 1M5 maps for catchment Sultartangi based on the ICRA dataset without projection (top left), with SSP126 and 10th percentile percentage changes (top right), with SSP370 and median percentage changes (bottom left) and with SSP585 and 90th percentile percentage changes (bottom right).

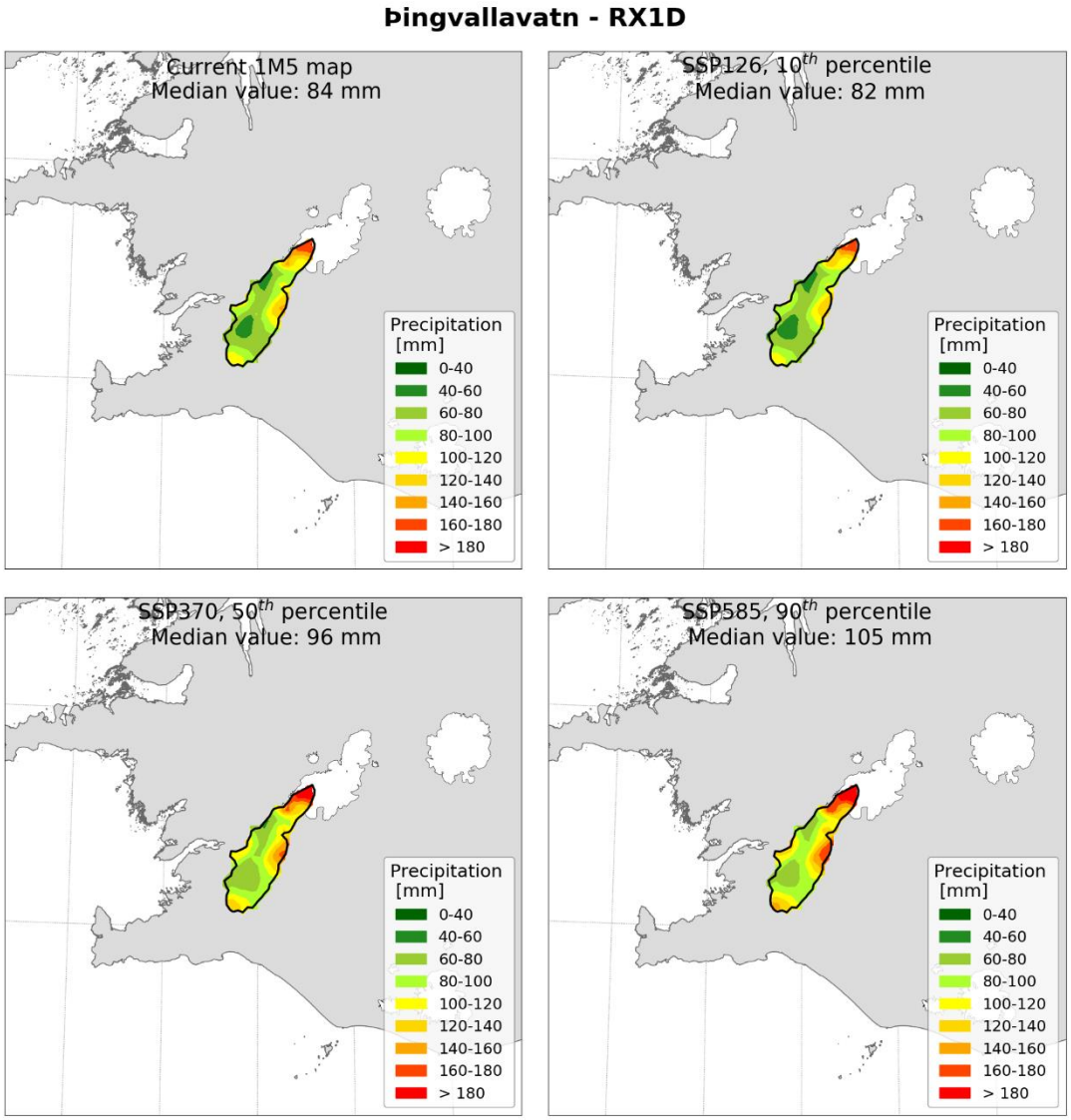

Figure III.8 — 1M5 maps for catchment Þingvallavatn based on the ICRA dataset without projection (top left), with SSP126 and 10th percentile percentage changes (top right), with SSP370 and median percentage changes (bottom left) and with SSP585 and 90th percentile percentage changes (bottom right).

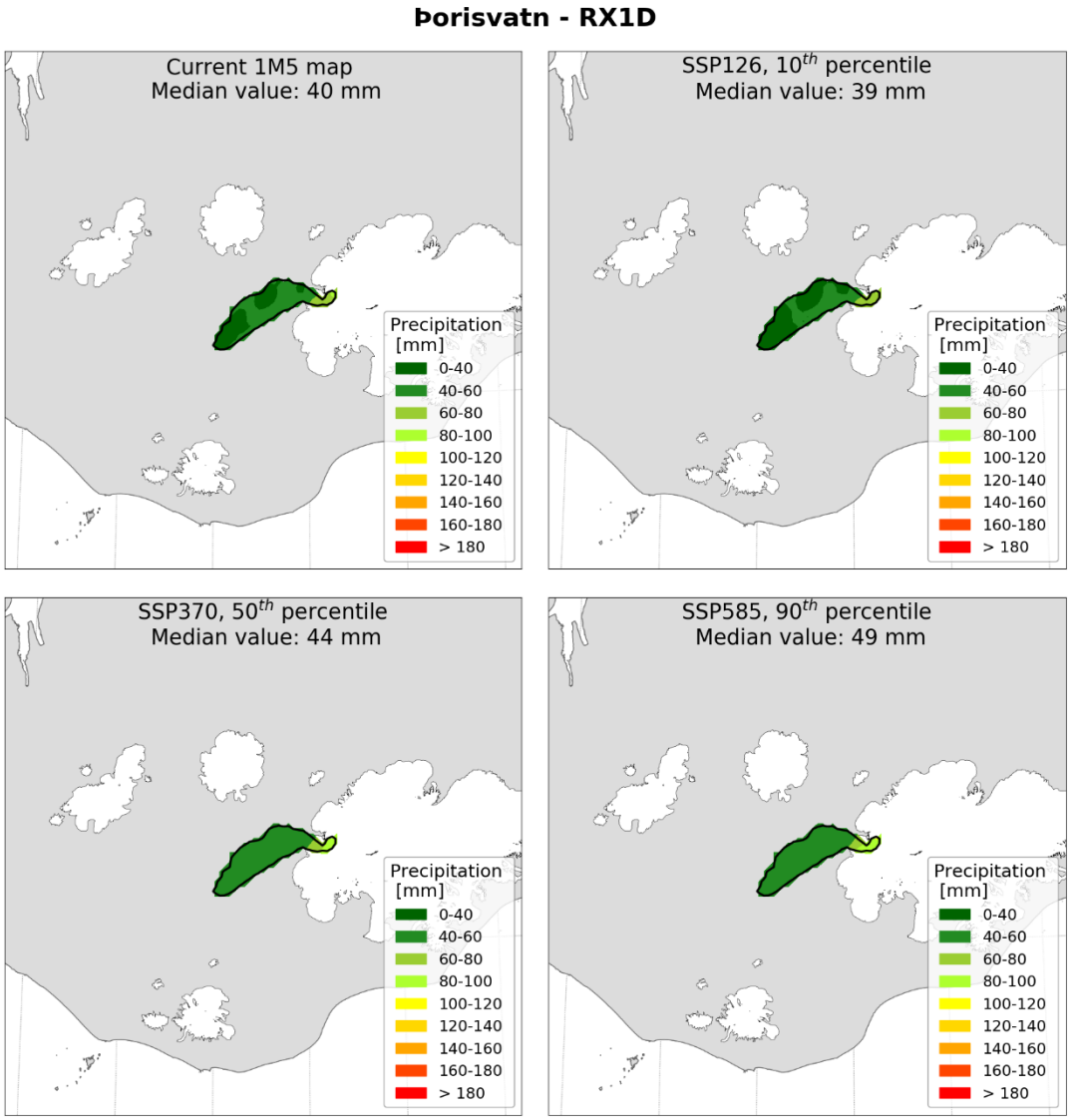

Figure III.9 — 1M5 maps for catchment Þorisvatn based on the ICRA dataset without projection (top left), with SSP126 and 10th percentile percentage changes (top right), with SSP370 and median percentage changes (bottom left) and with SSP585 and 90th percentile percentage changes (bottom right).

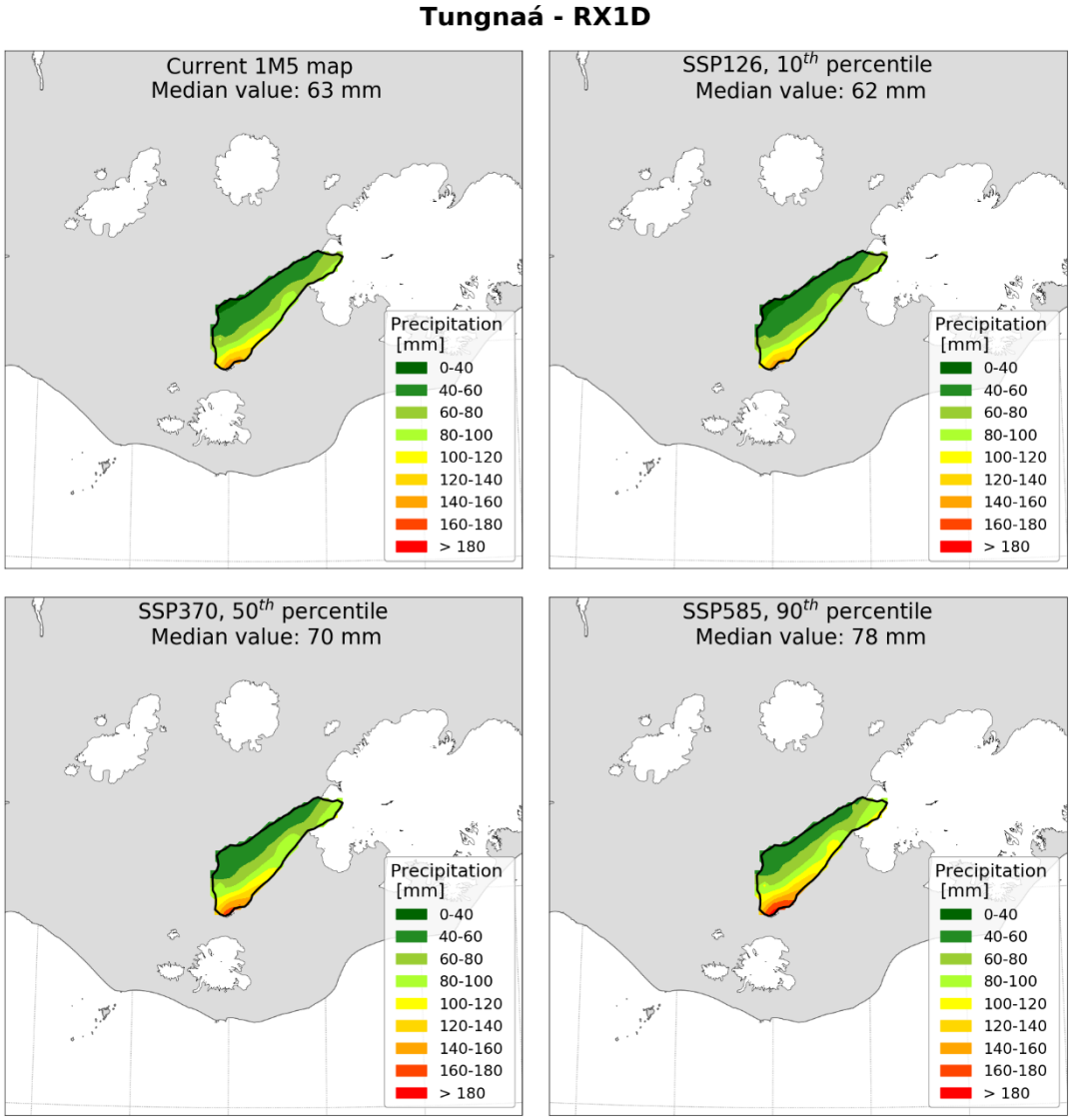

Figure III.10 — 1M5 maps for catchment Tungnaá based on the ICRA dataset without projection (top left), with SSP126 and 10th percentile percentage changes (top right), with SSP370 and median percentage changes (bottom left) and with SSP585 and 90th percentile percentage changes (bottom right).

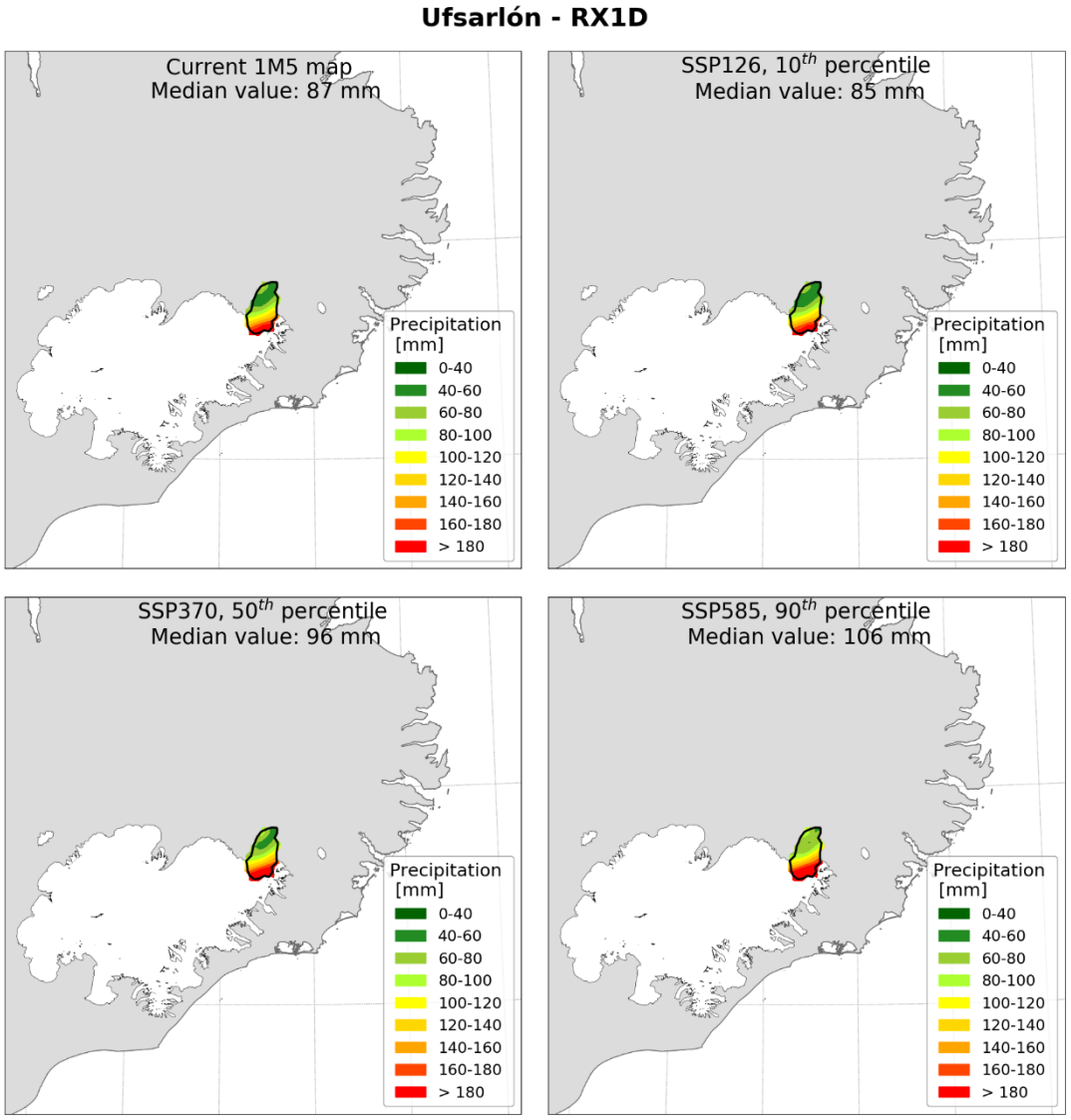

Figure III.11 — 1M5 maps for catchment Ufsarlón based on the ICRA dataset without projection (top left), with SSP126 and 10th percentile percentage changes (top right), with SSP370 and median percentage changes (bottom left) and with SSP585 and 90th percentile percentage changes (bottom right)

Appendix IV. Return level maps

In this appendix, figures similar to Figure 8,9 and 11 from the report are presented.

Figures IV.1 – IV.6 show daily return level maps with a 2-, 5-, 10-, 25-, 50- and 100-year return period for the each SSP scenario, based on percentage changes from Table 4 incorporated to the ICRA dataset, and calculated with the Block Maxima method with MLE.

Figures IV.7 – IV.12 shows maps for 5-day precipitation return levels with the same return periods.

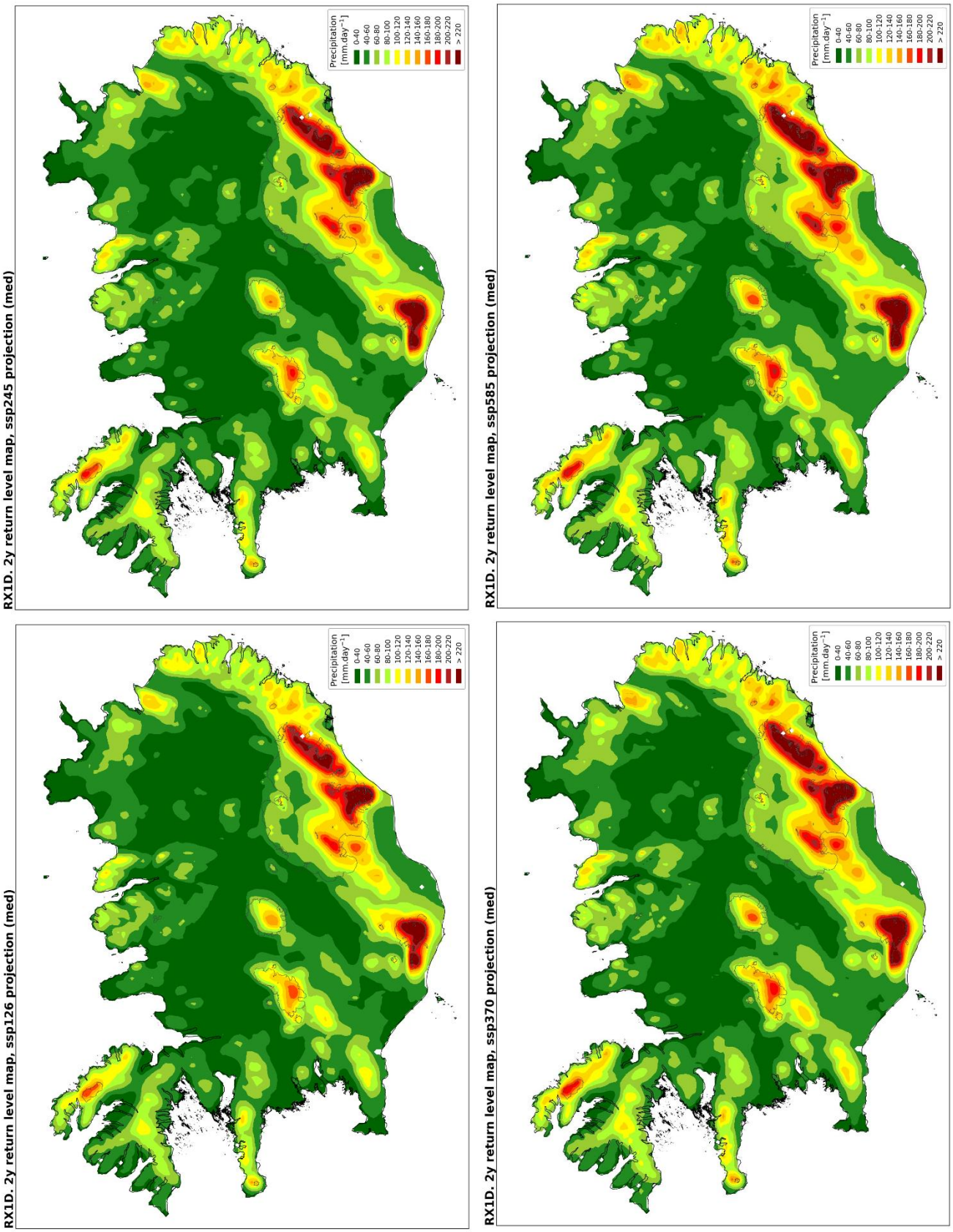

Figure IV.1 — Maps of daily precipitation with a 2-year return level, based on the ICRA dataset with percentage changes calculated from RX1D values for SSP126, SSP245, SSP370 and SSP585. EVA was carried using the Block Maxima method with MLE.

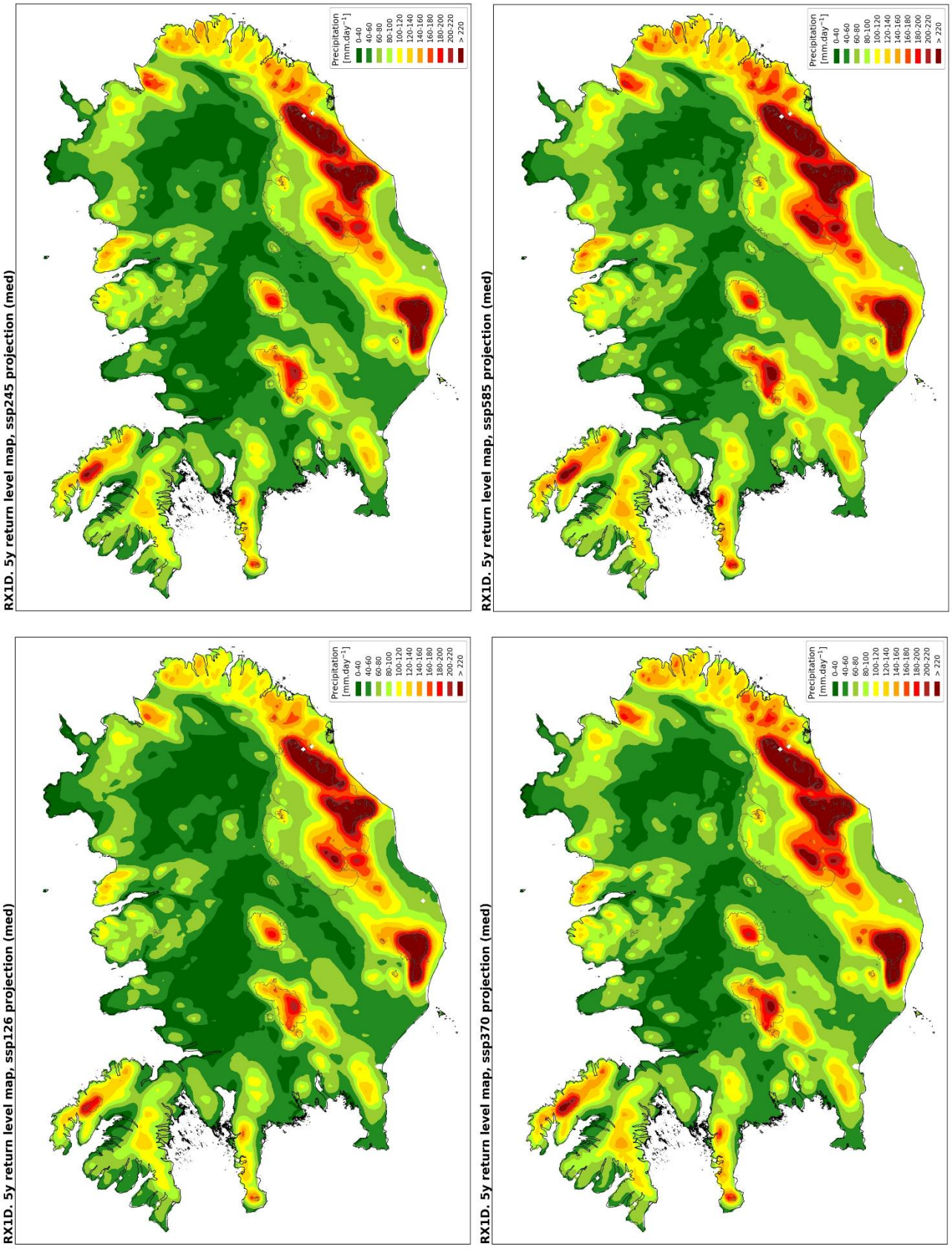

Figure IV.2 — Maps of daily precipitation with a 5-year return level, based on the ICRA dataset with percentage changes calculated from RX1D values for SSP126, SSP245, SSP370 and SSP585. EVA was carried using the Block Maxima method with MLE.

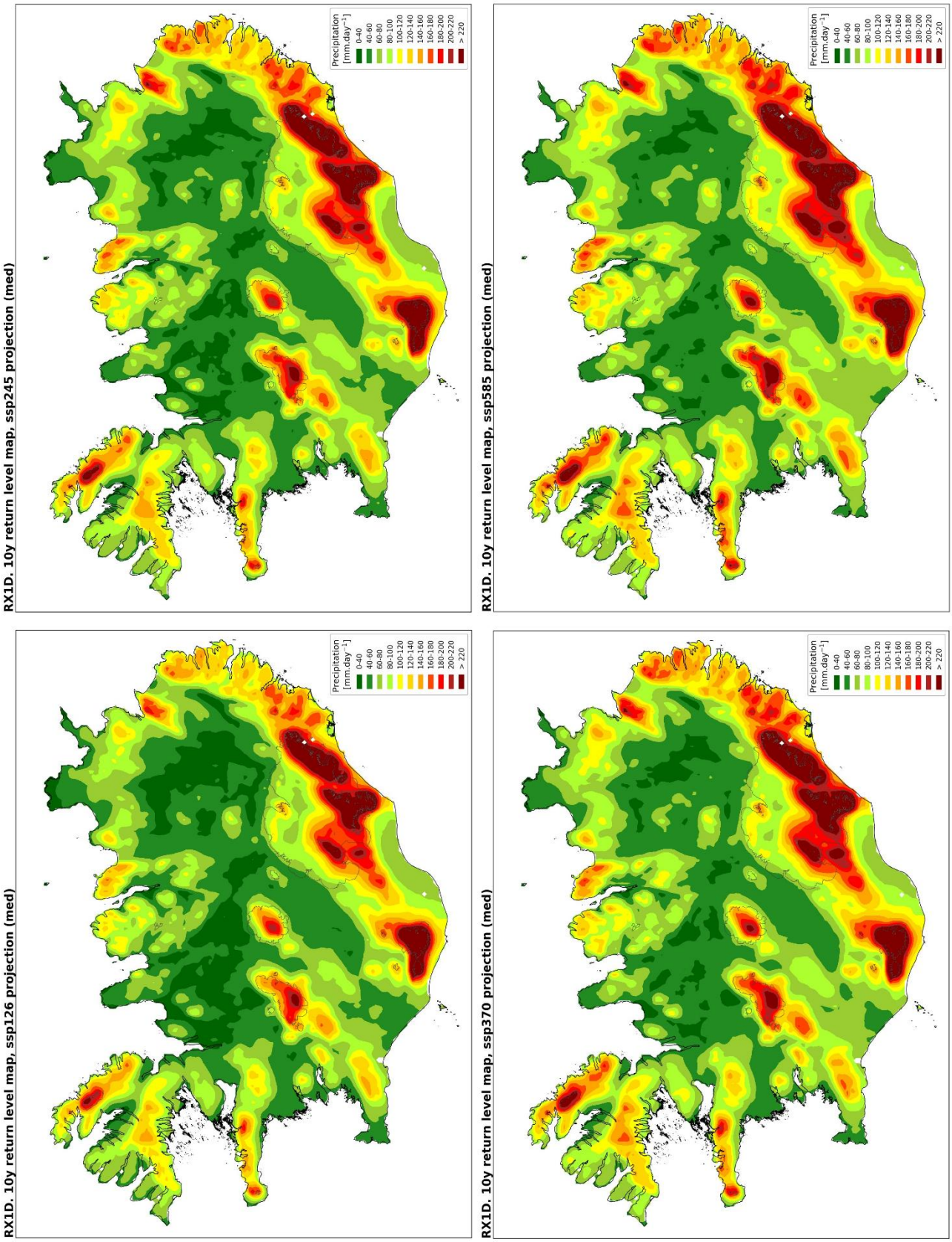

Figure IV.3 — Maps of daily precipitation with a 10-year return level, based on the ICRA dataset with percentage changes calculated from RX1D values for SSP126, SSP245, SSP370 and SSP585. EVA was carried using the Block Maxima method with MLE.

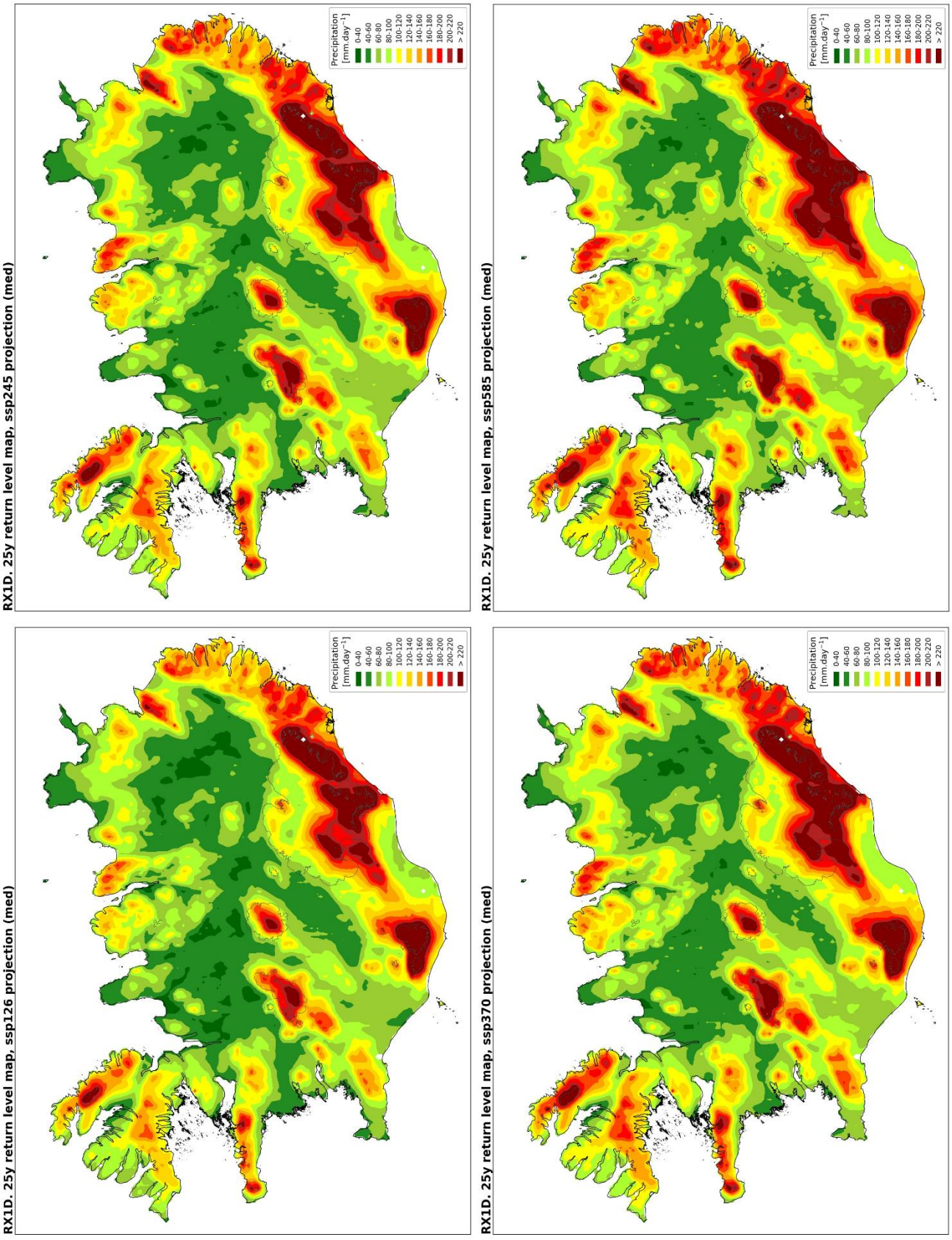

Figure IV.4 — Maps of daily precipitation with a 25-year return level, based on the ICRA dataset with percentage changes calculated from RX1D values for SSP126, SSP245, SSP370 and SSP585. EVA was carried using the Block Maxima method with MLE.

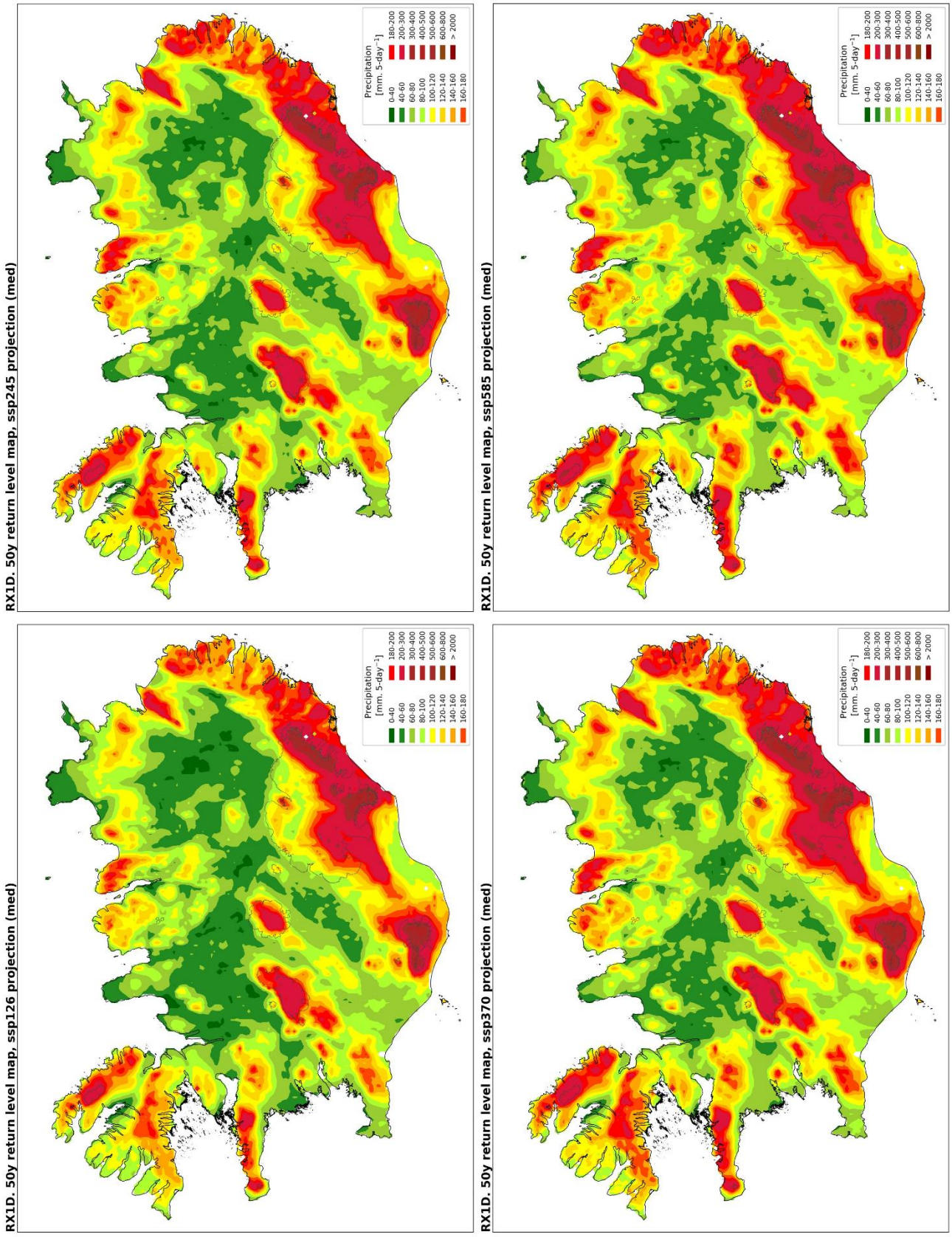

Figure IV.5 — Maps of daily precipitation with a 50-year return level, based on the ICRA dataset with percentage changes calculated from RX1D values for SSP126, SSP245, SSP370 and SSP585. EVA was carried using the Block Maxima method with MLE.

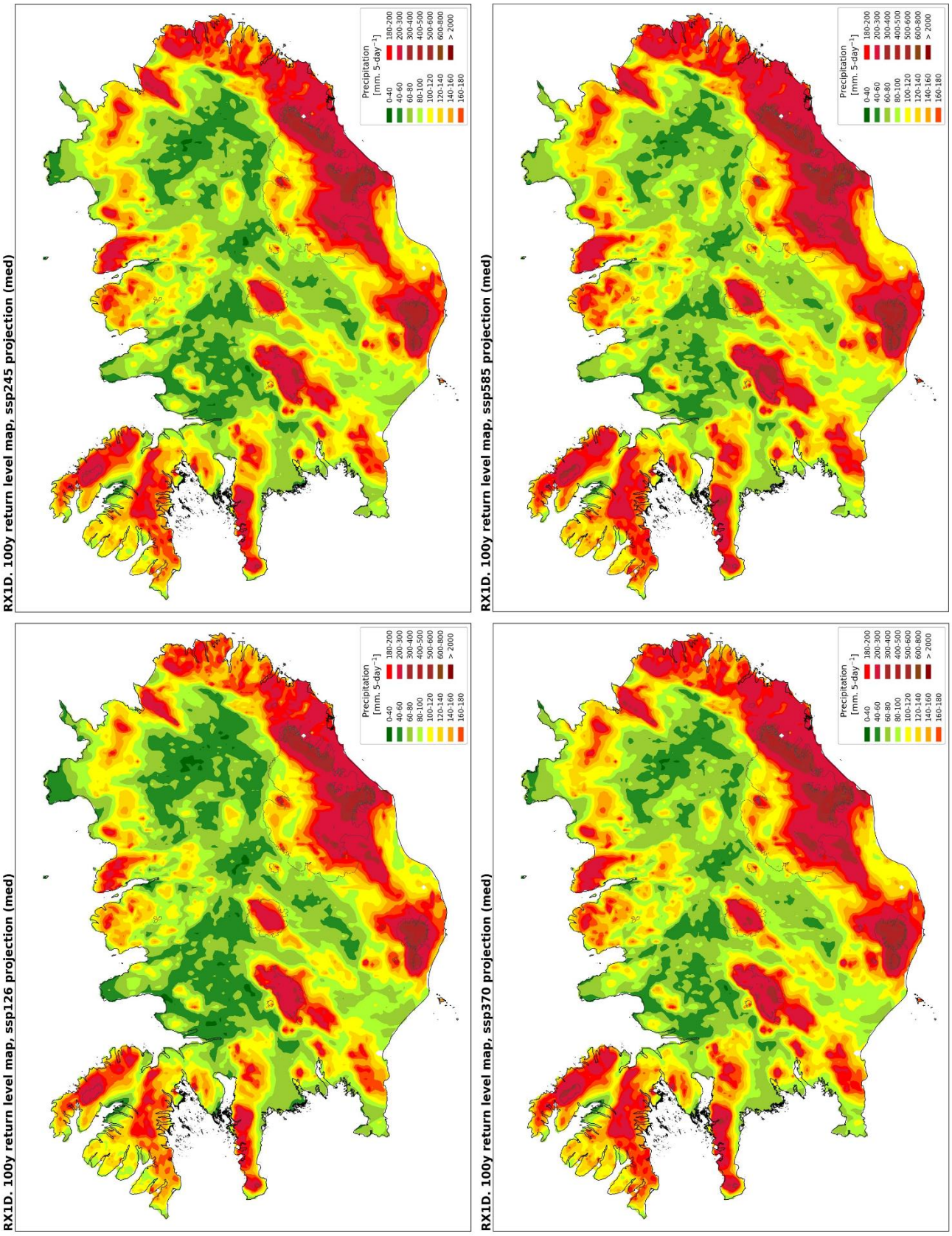

Figure IV.6 — Maps of daily precipitation with a 100-year return level, based on the ICRA dataset with percentage changes calculated from RX1D values for SSP126, SSP245, SSP370 and SSP585. EVA was carried using the Block Maxima method with MLE.

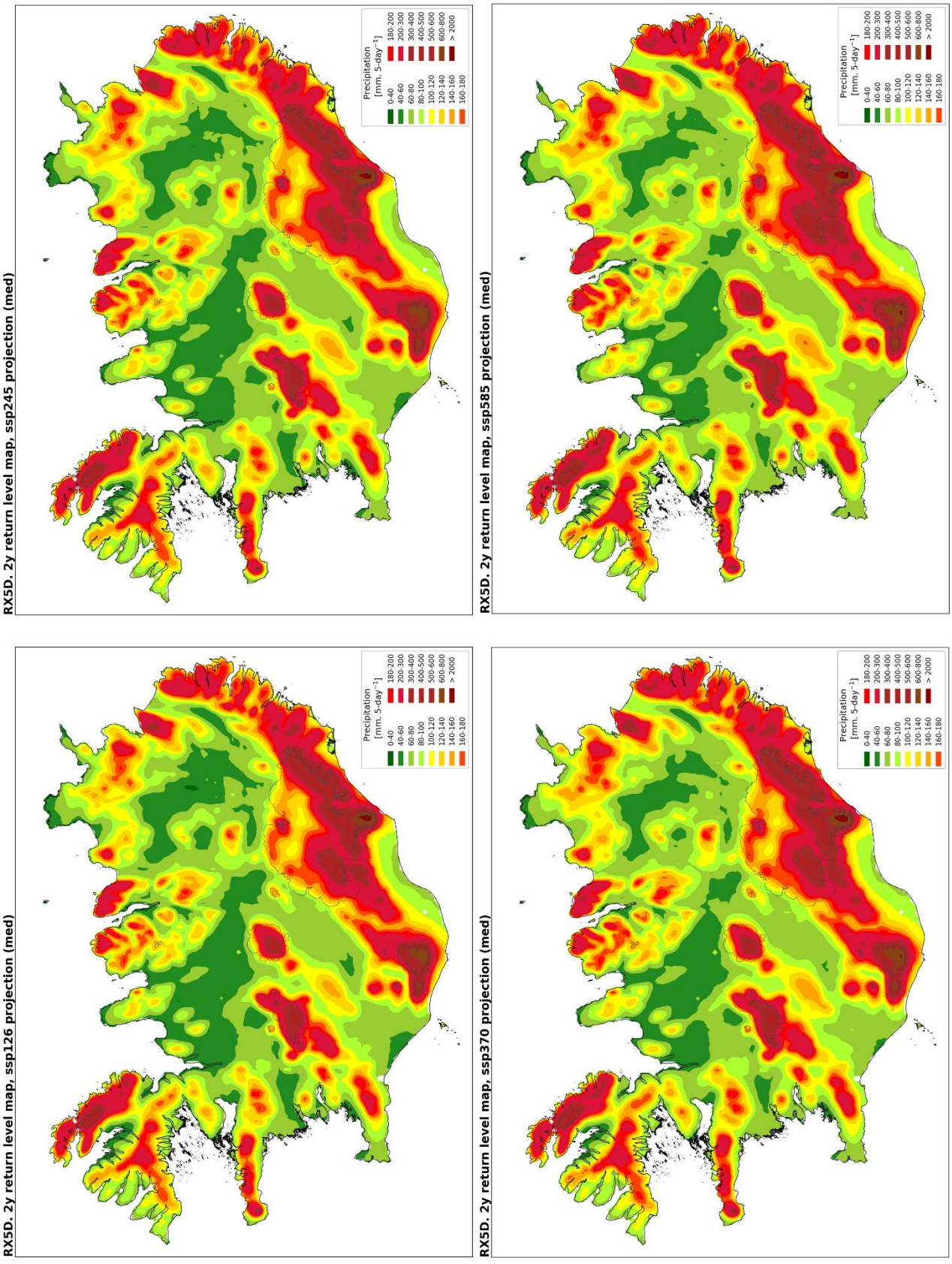

Figure IV.7 — Maps of 5-day precipitation with a 2-year return level, based on the ICRA dataset with percentage changes calculated from RX5D values for SSP126, SSP245, SSP370 and SSP585. EVA was carried using the Block Maxima method with MLE.

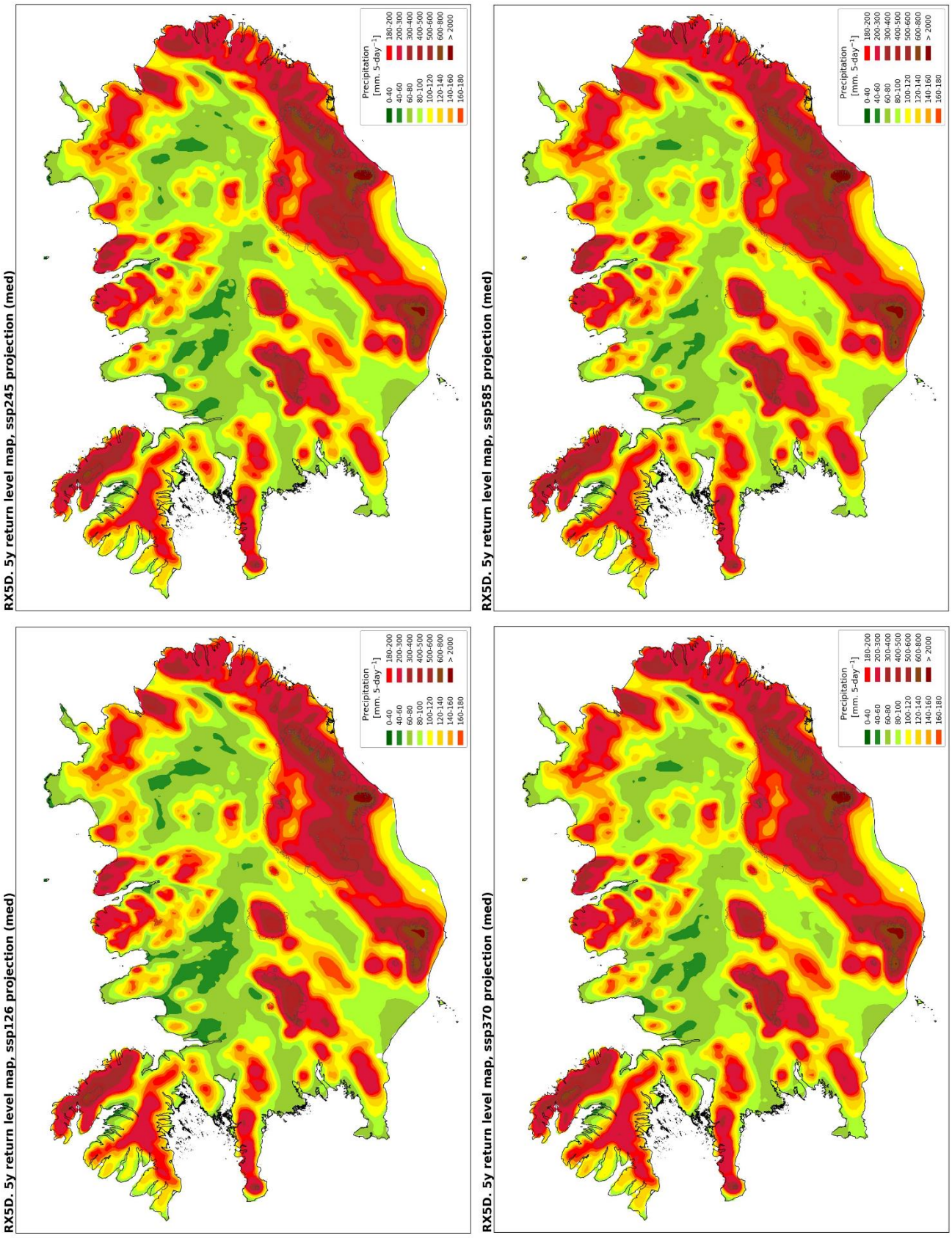

Figure IV.8 — Maps of 5-day precipitation with a 5-year return level, based on the ICRA dataset with percentage changes calculated from RX5D values for SSP126, SSP245, SSP370 and SSP585. EVA was carried using the Block Maxima method with MLE.

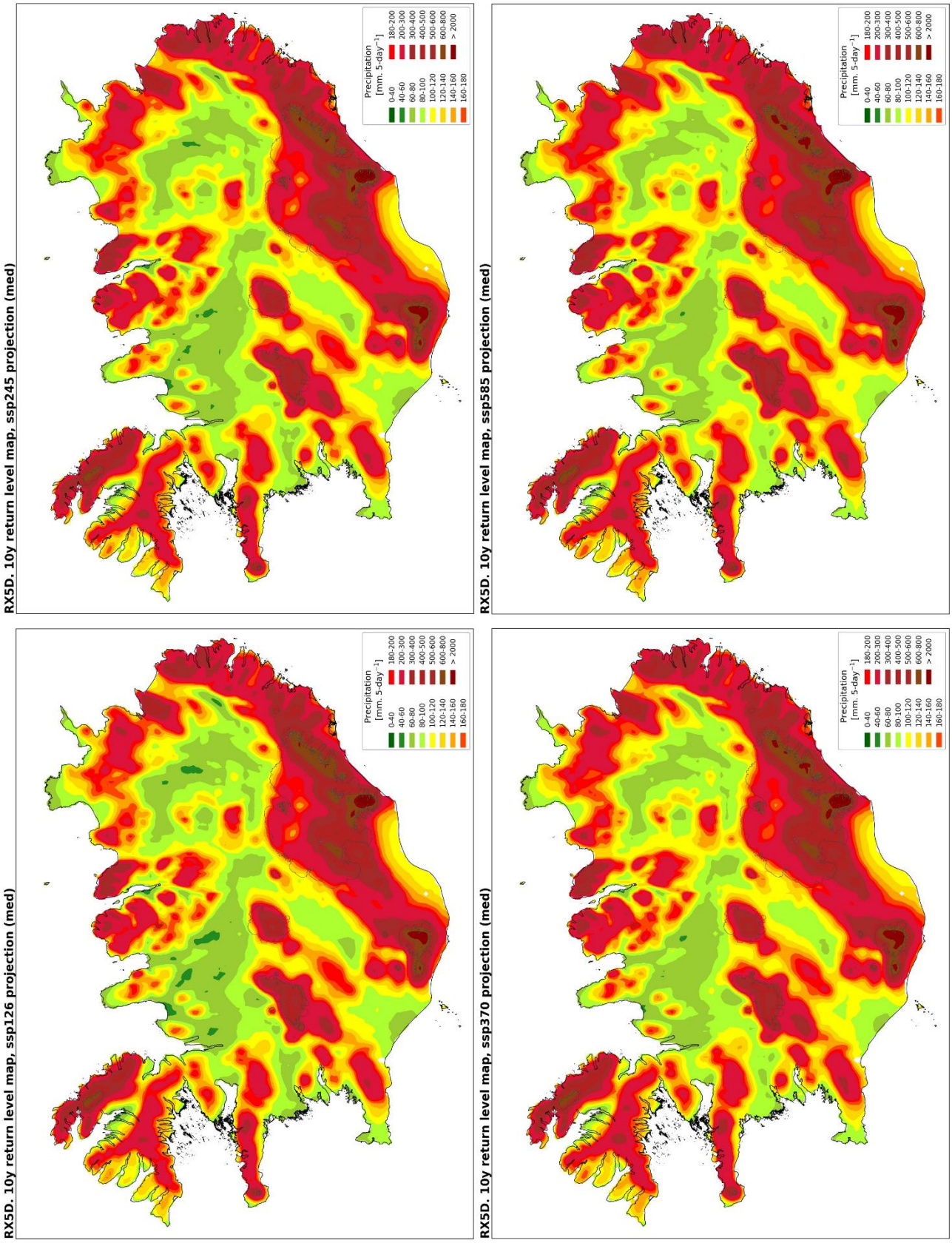

Figure IV.9 — Maps of 5-day precipitation with a 10-year return level, based on the ICRA dataset with percentage changes calculated from RX5D values for SSP126, SSP245, SSP370 and SSP585. EVA was carried using the Block Maxima method with MLE.

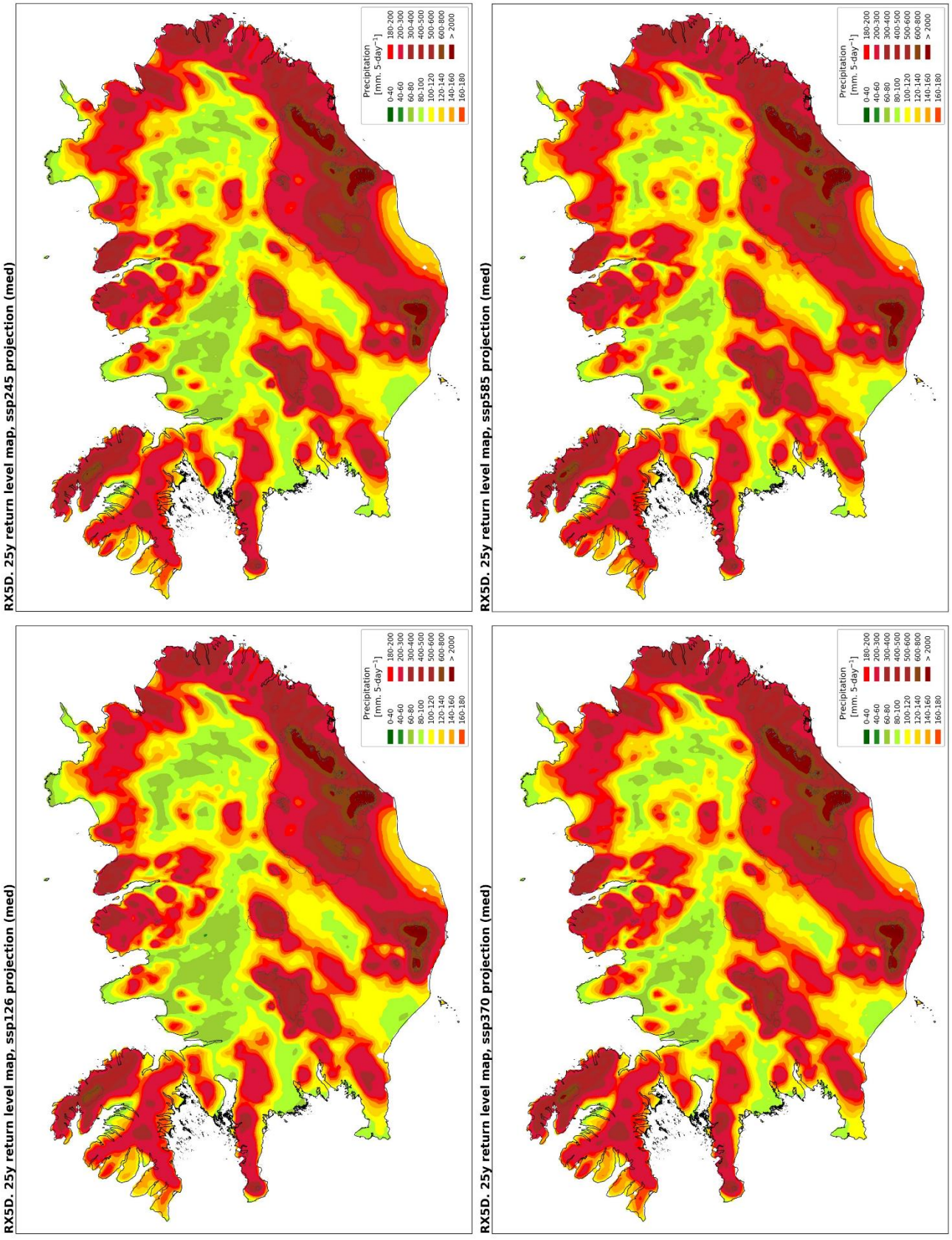

Figure IV.9 — Maps of 5-day precipitation with a 25-year return level, based on the ICRA dataset with percentage changes calculated from RX5D values for SSP126, SSP245, SSP370 and SSP585. EVA was carried using the Block Maxima method with MLE.

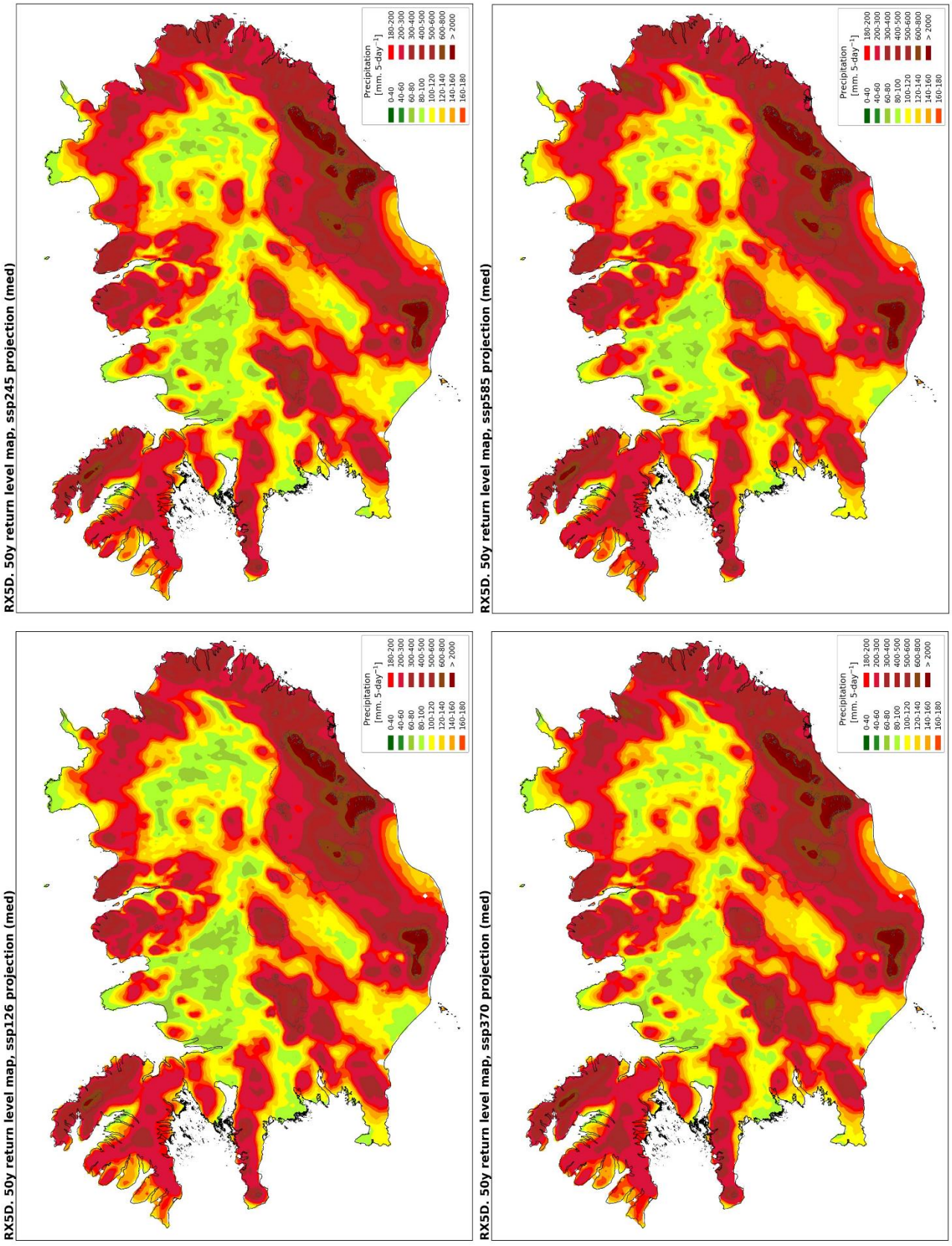

Figure IV.10 — Maps of 5-day precipitation with a 50-year return level, based on the ICRA dataset with percentage changes calculated from RX5D values for SSP126, SSP245, SSP370 and SSP585. EVA was carried using the Block Maxima method with MLE.

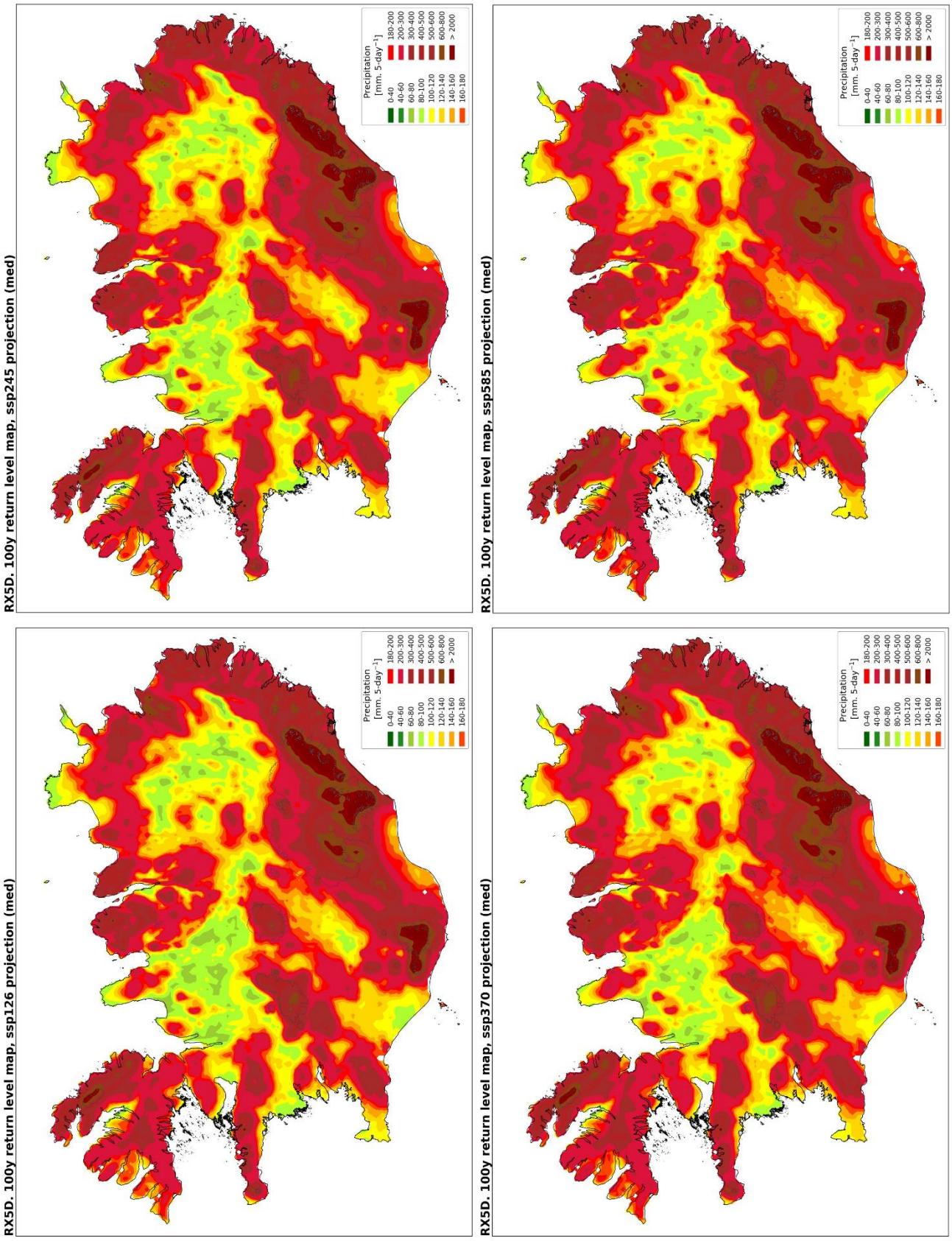

Figure IV.11 — Maps of 5-day precipitation with a 100-year return level, based on the ICRA dataset with percentage changes calculated from RX5D values for SSP126, SSP245, SSP370 and SSP585. EVA was carried using the Block Maxima method with MLE.

Appendix V. Snow-fraction change

In this appendix, figures similar to Figure 14 from the report are presented.

On each figure, the top panel shows the catchment outlines in regard to the gridpoints location. Gridpoints used for the analysis are coloured to match the timeseries in the four subplots. On those figures, the snow-fraction change over the period 1979 – 2100 is shown for each gridpoint and scenario, with the median percentage change over the period calculated from the linear regression line.

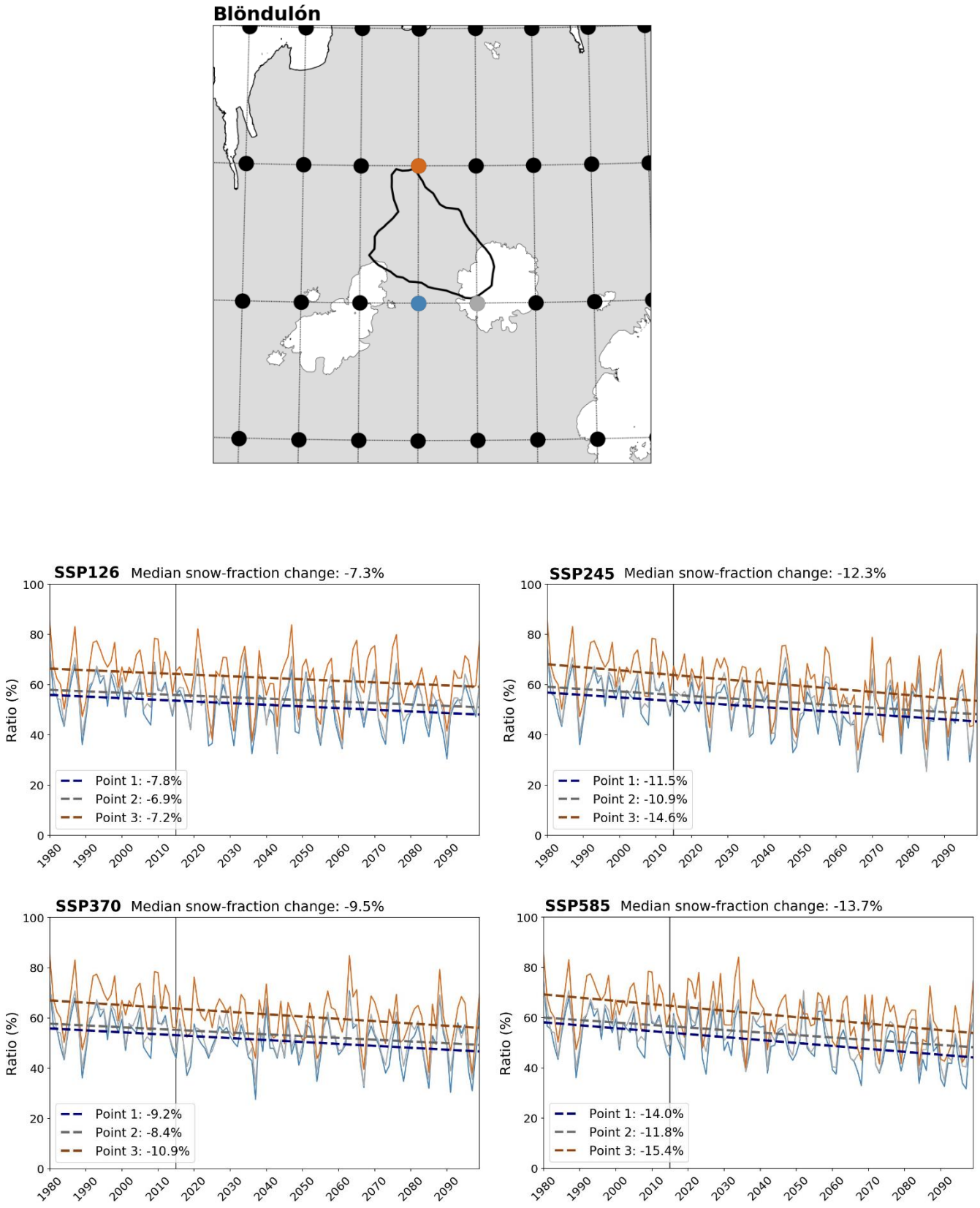

Figure V.1 — Evolution of the snow-fraction between 1979 and 2100 for catchment Blöndulón. The colour of the timeseries matches the colour of the gridpoints.

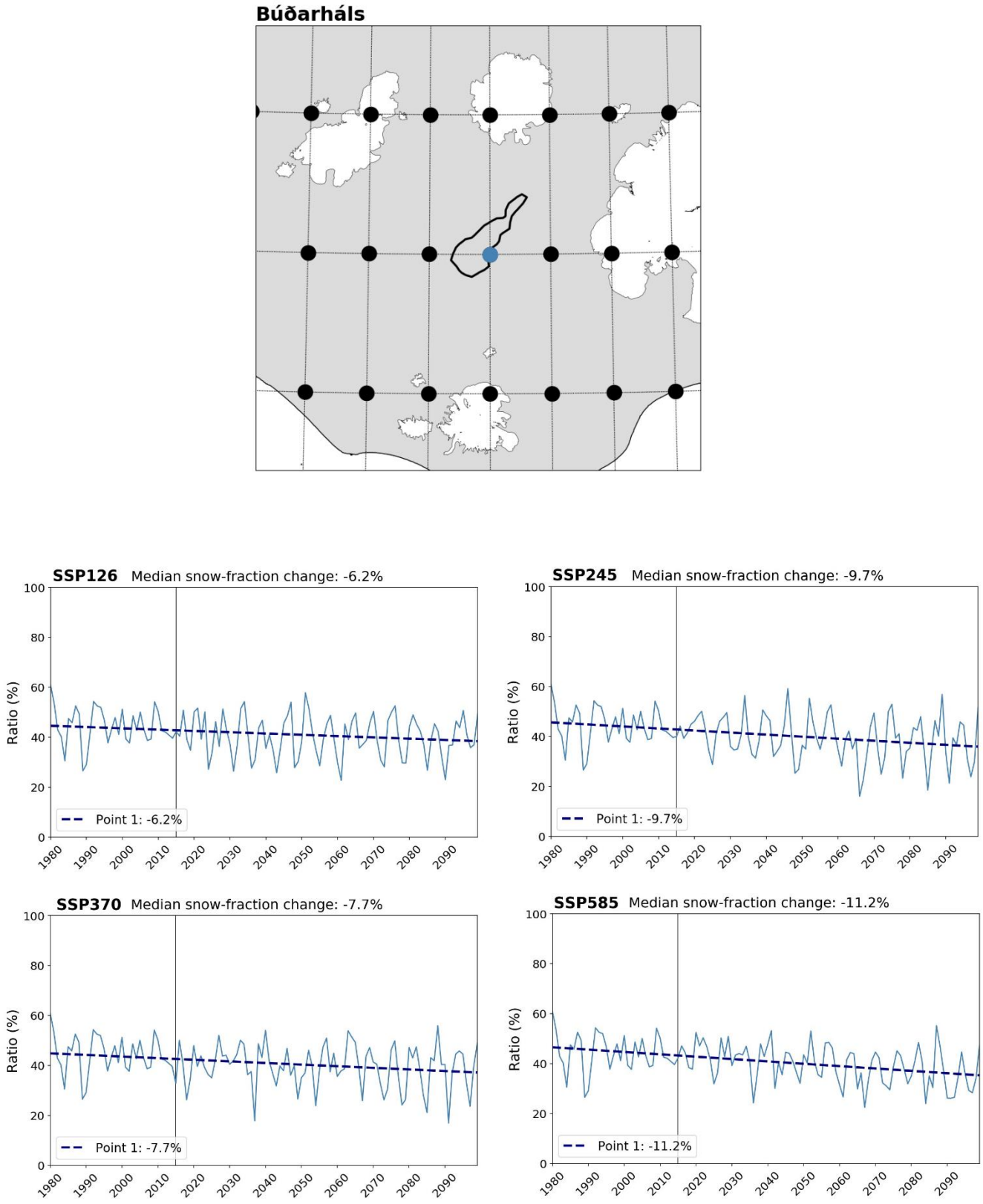

Figure V.2 — Evolution of the snow-fraction between 1979 and 2100 for catchment Búðarháls. The colour of the timeseries matches the colour of the gridpoints.

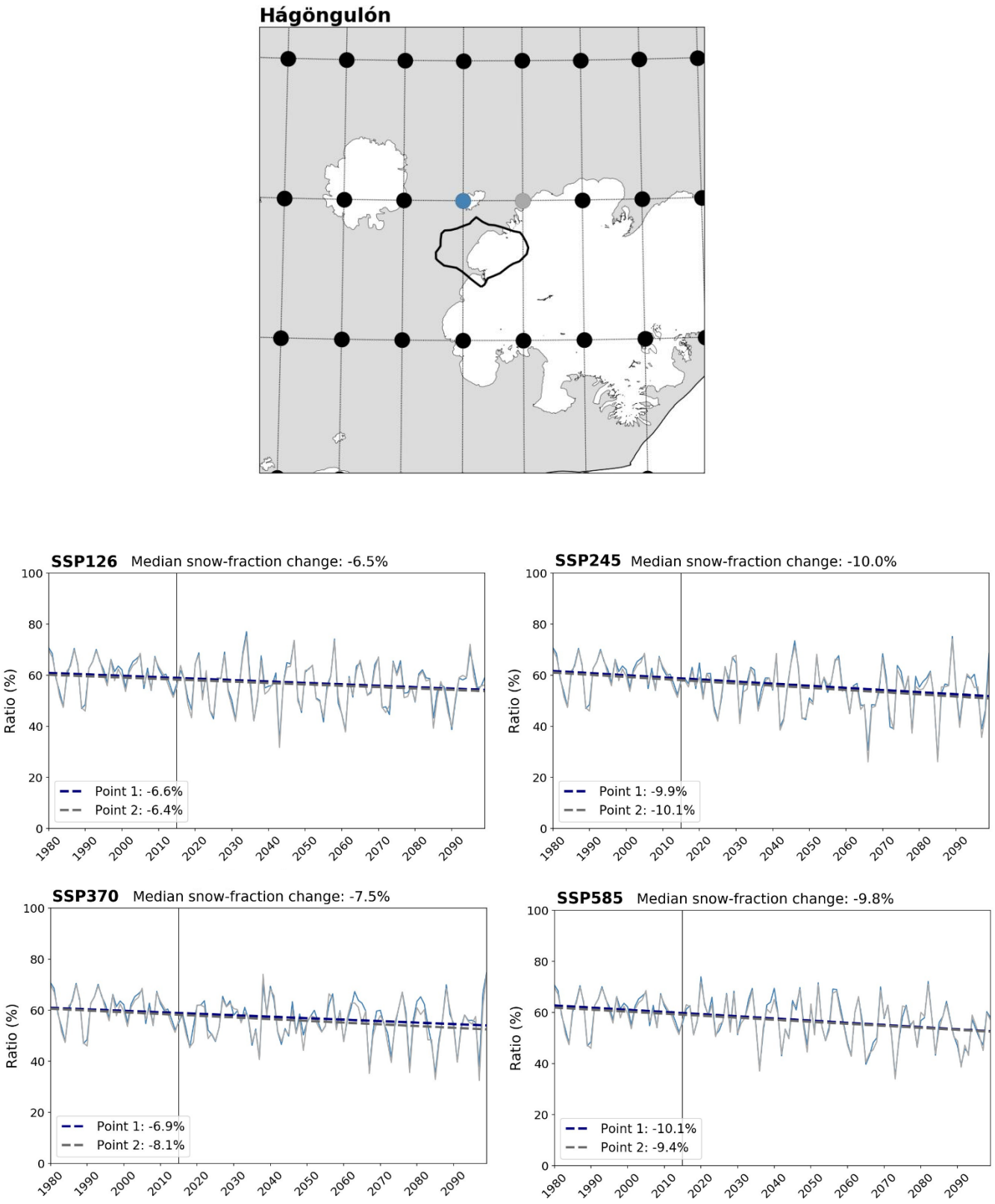

Figure V.3 — Evolution of the snow-fraction between 1979 and 2100 for catchment Hágöngulón. The colour of the timeseries matches the colour of the gridpoints.

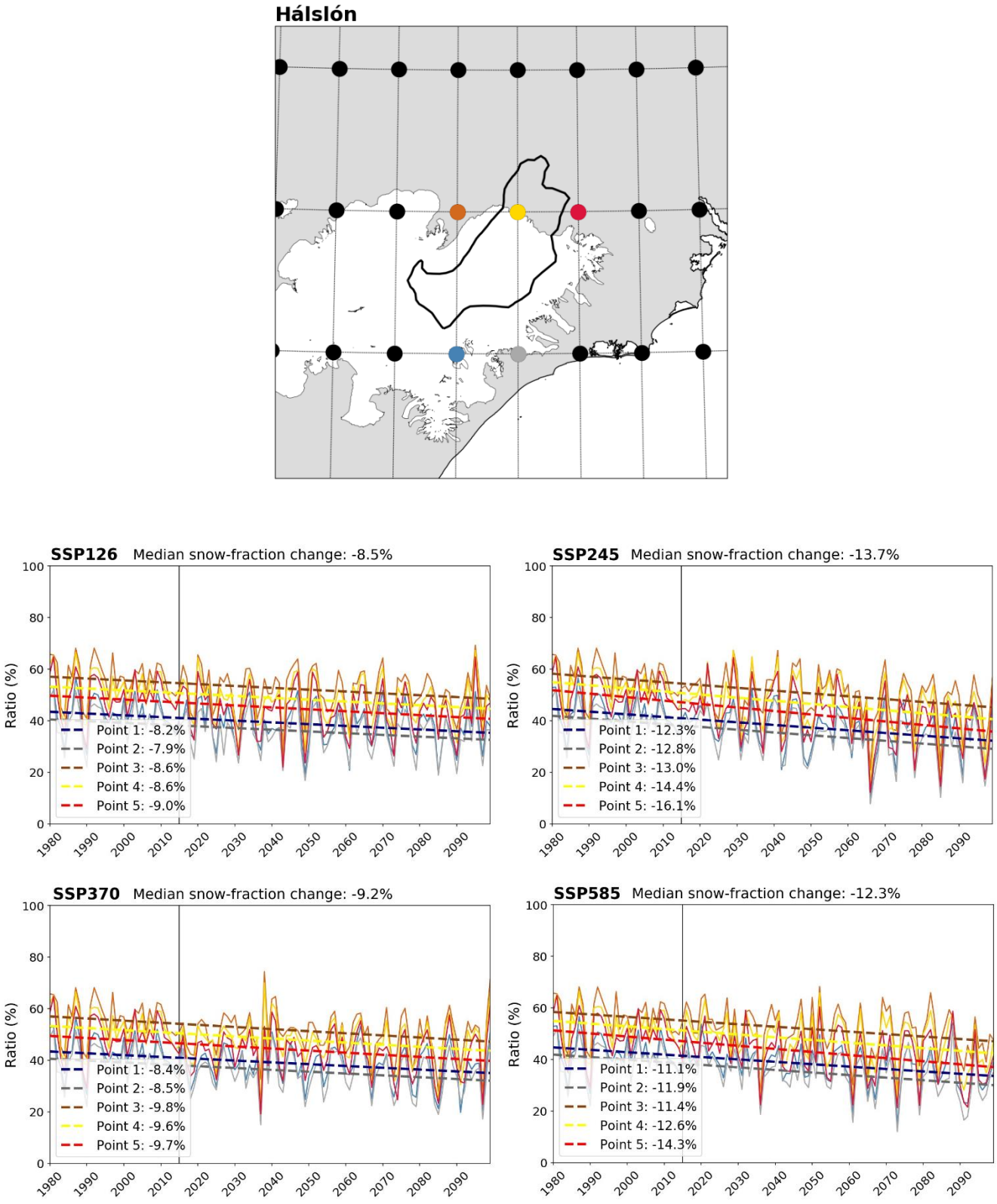

Figure V.4 — Evolution of the snow-fraction between 1979 and 2100 for catchment Hálslón. The colour of the timeseries matches the colour of the gridpoints.

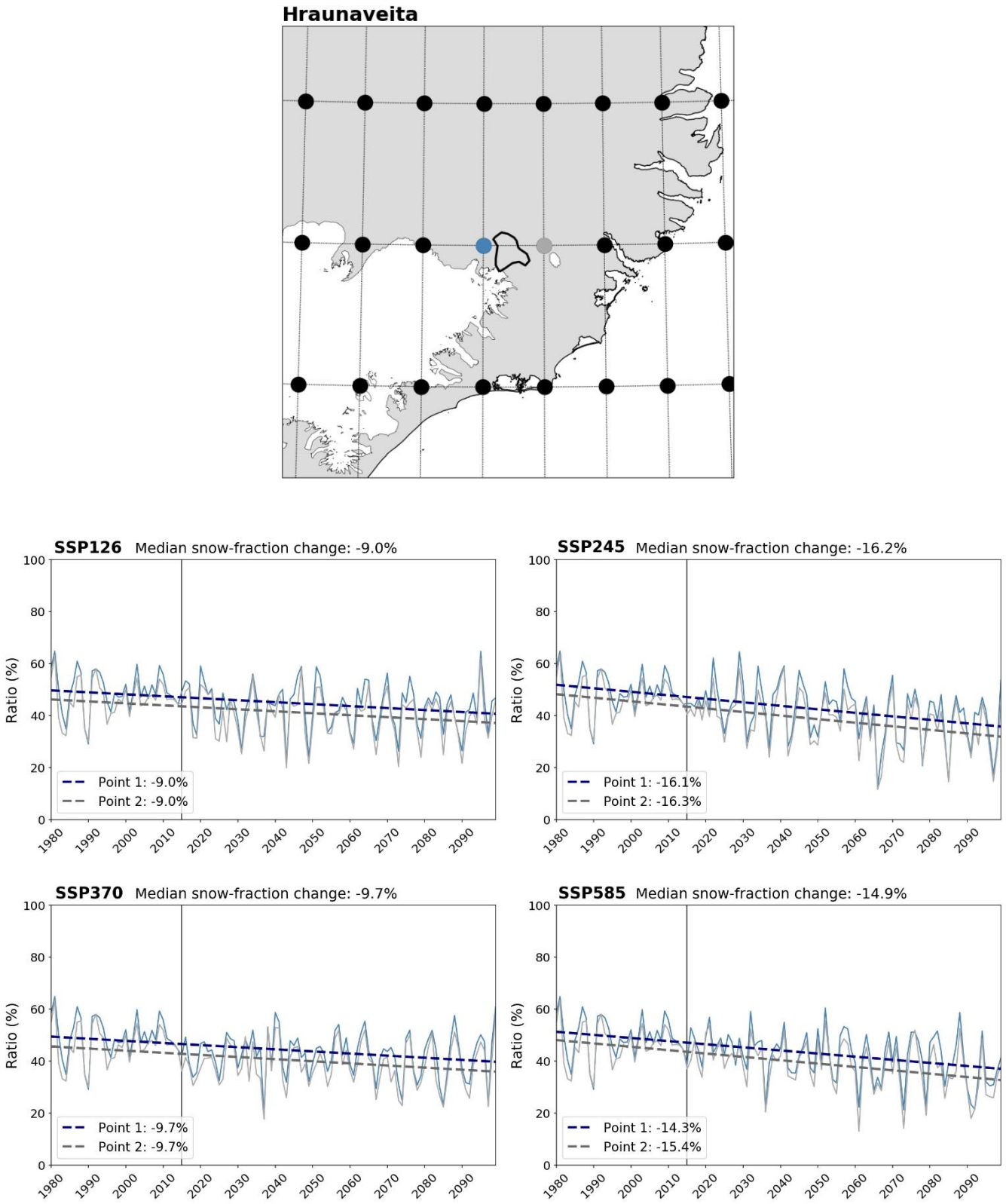

Figure V.5 — Evolution of the snow-fraction between 1979 and 2100 for catchment Hraunaveita. The colour of the timeseries matches the colour of the gridpoints.

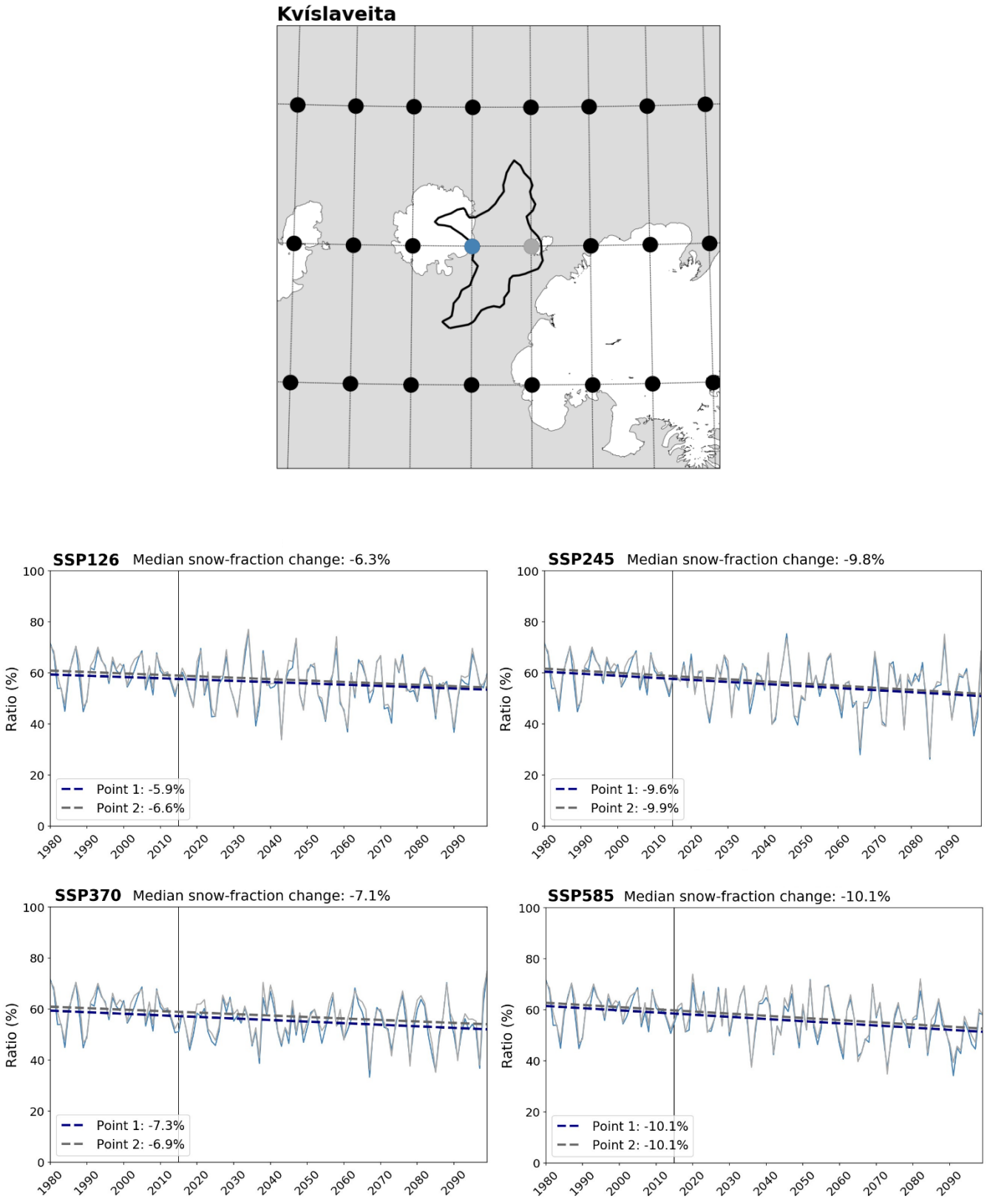

Figure V.6 — Evolution of the snow-fraction between 1979 and 2100 for catchment Kvíslaveita. The colour of the timeseries matches the colour of the gridpoints.

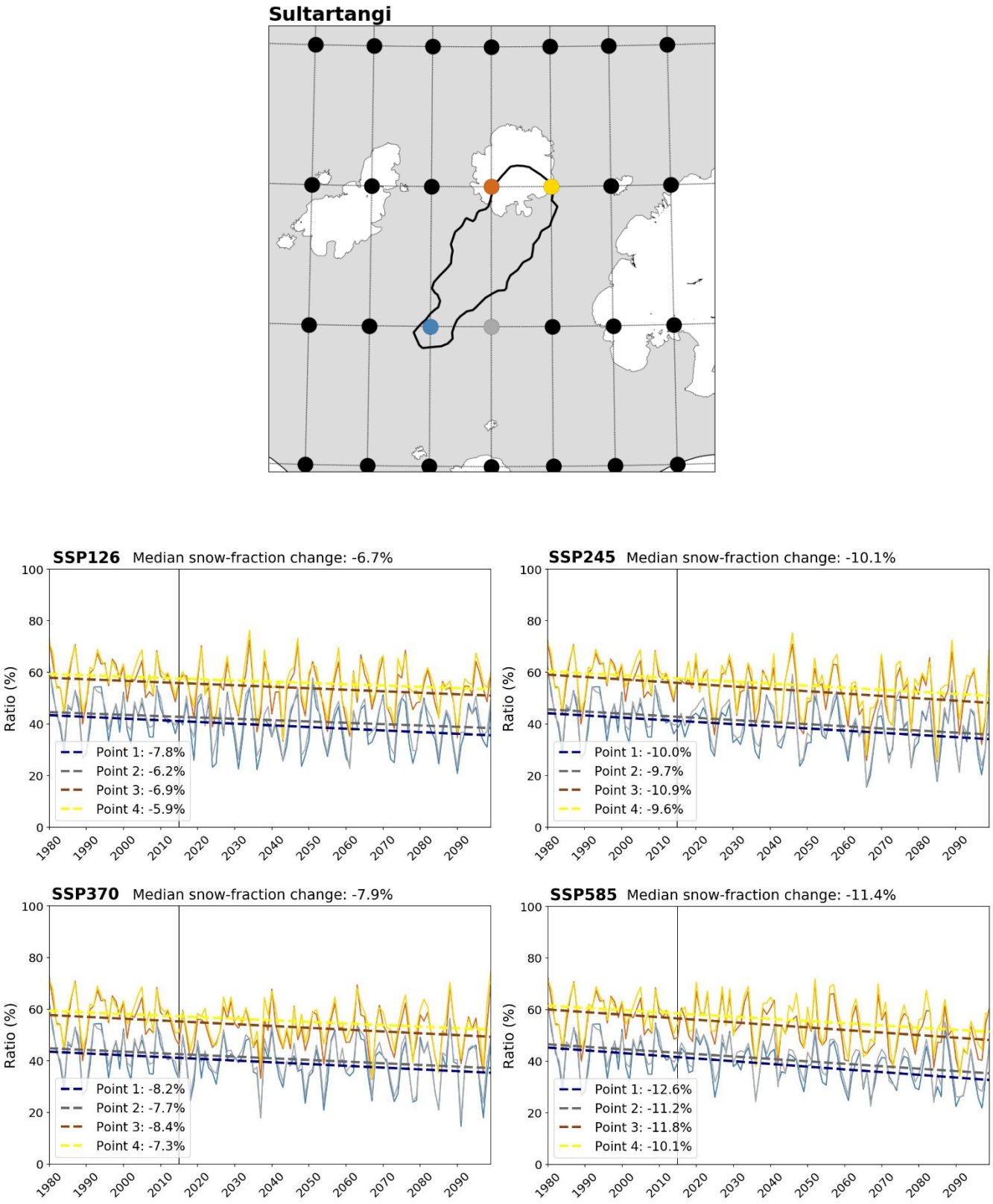

Figure V.7 — Evolution of the snow-fraction between 1979 and 2100 for catchment Sultartangi. The colour of the timeseries matches the colour of the gridpoints.

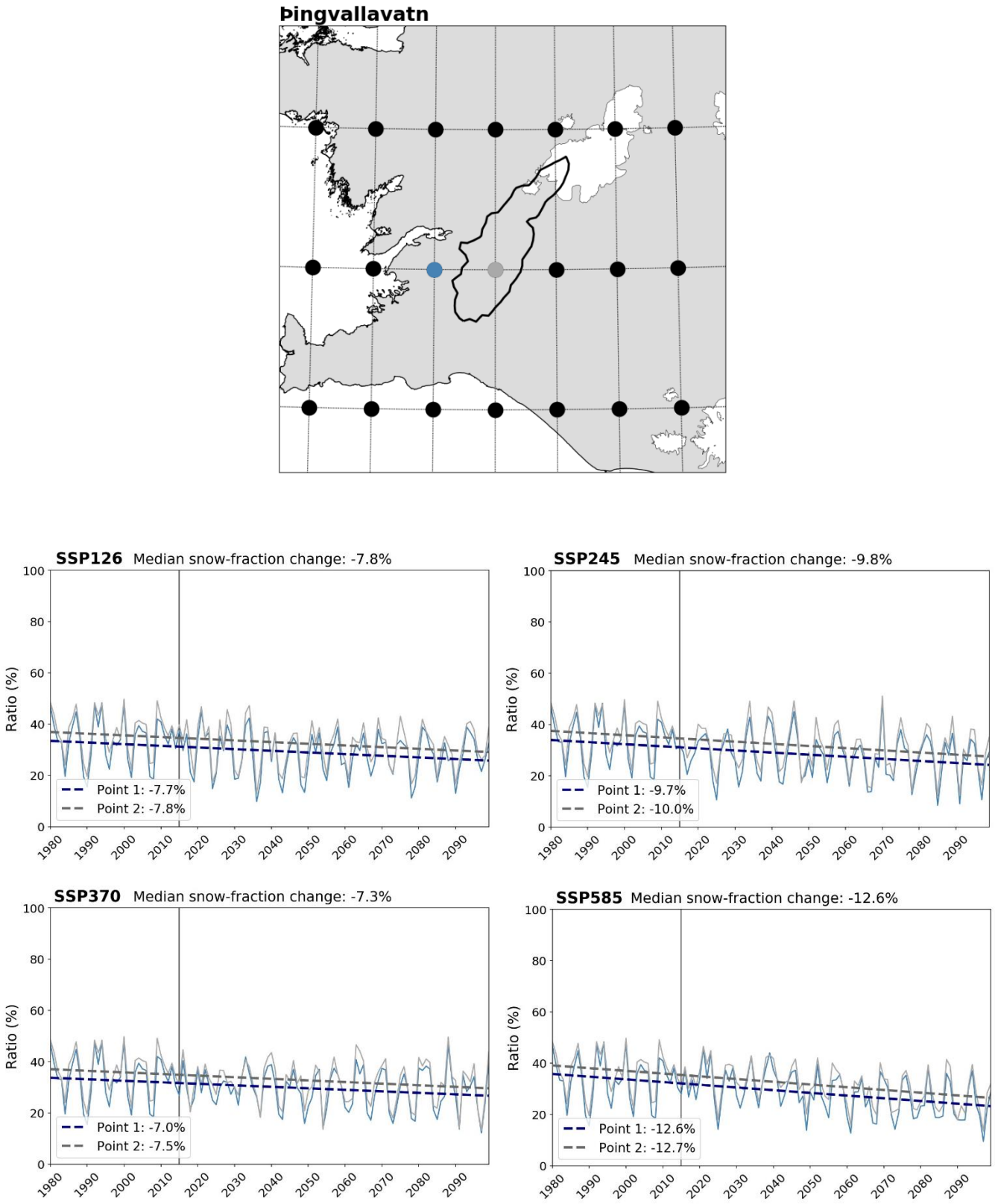

Figure V.8 — Evolution of the snow-fraction between 1979 and 2100 for catchment Þingvallavatn. The colour of the timeseries matches the colour of the gridpoints.

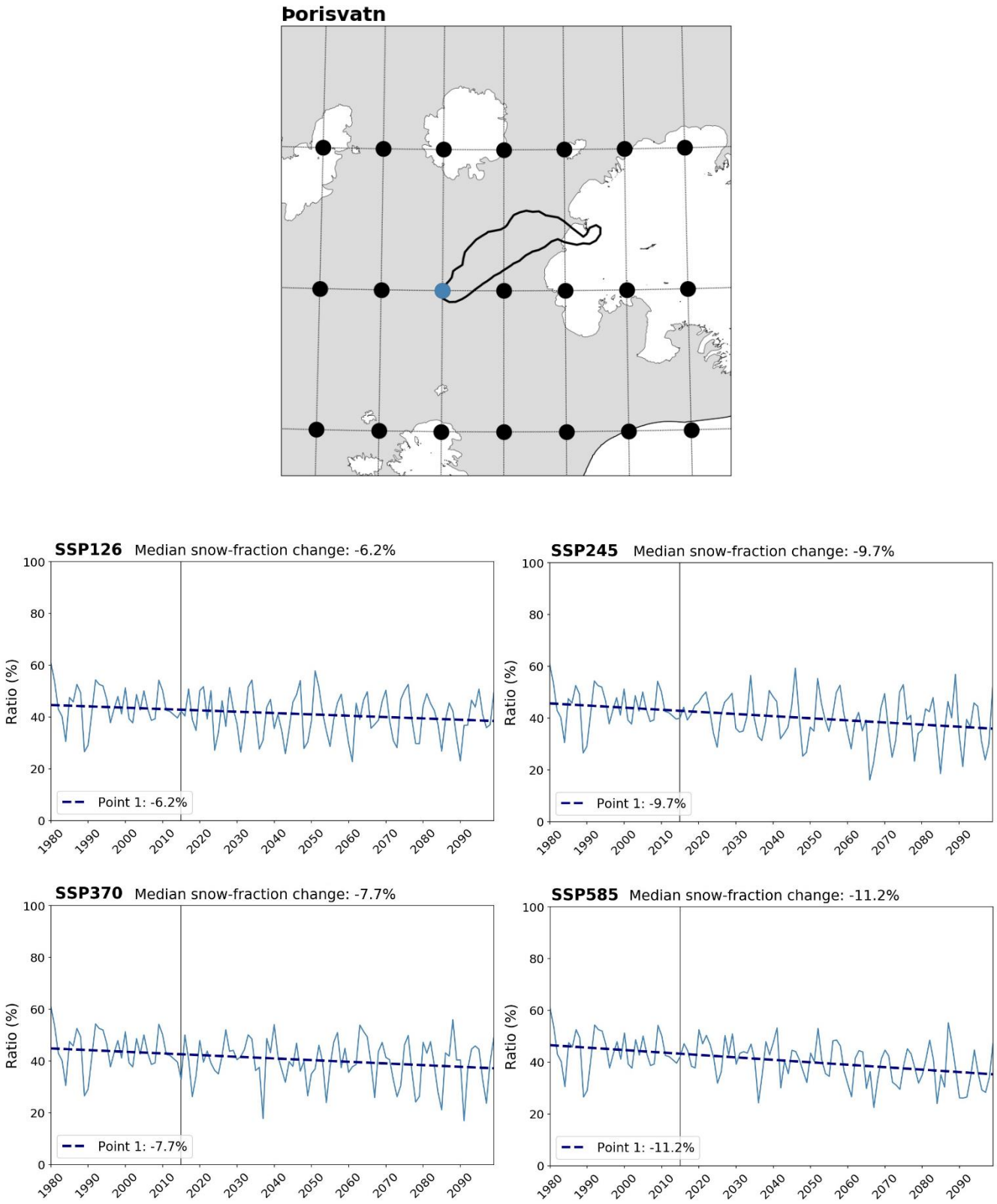

Figure V.9 — Evolution of the snow-fraction between 1979 and 2100 for catchment Þorisvatn. The colour of the timeseries matches the colour of the gridpoints.

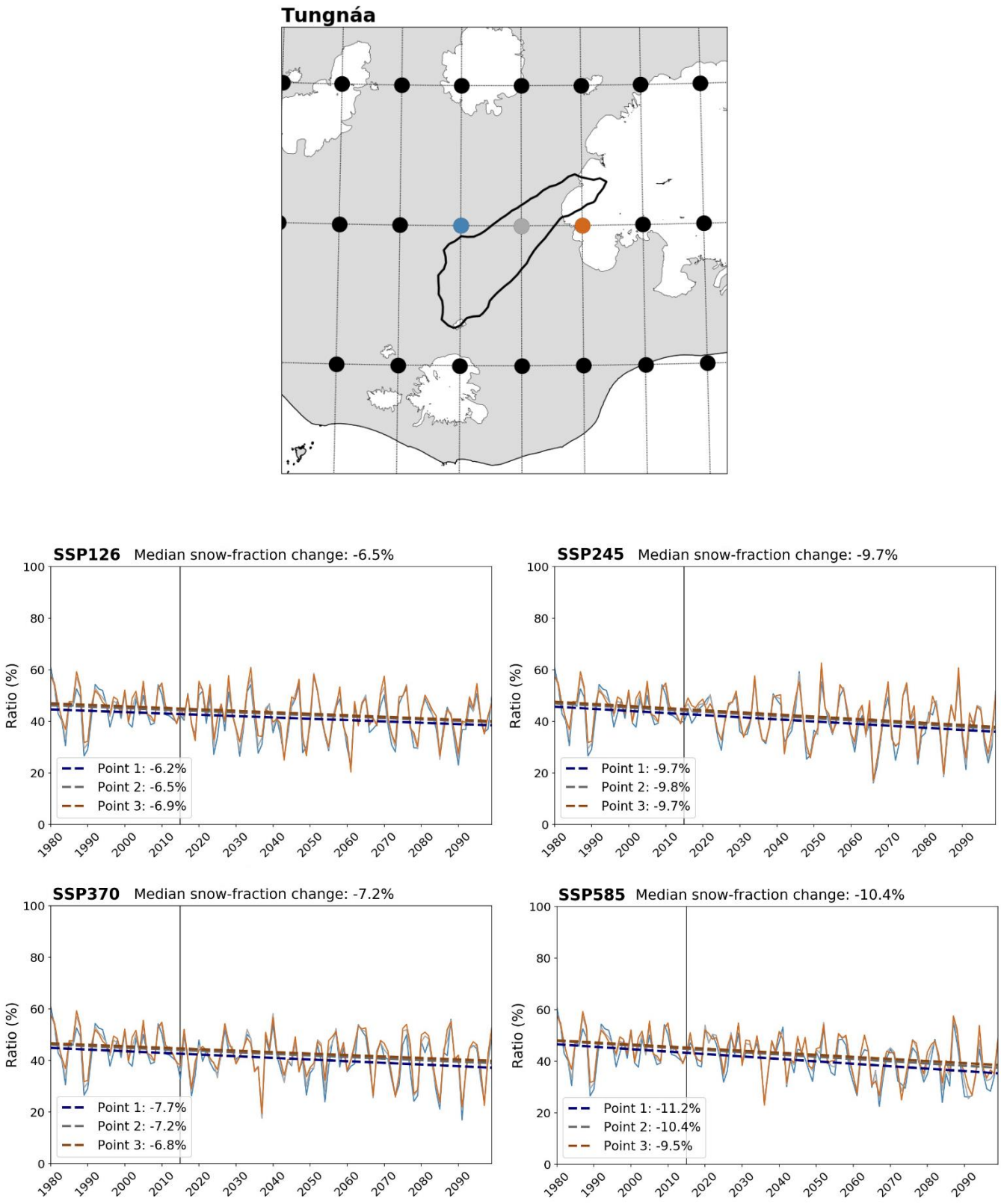

Figure V.10 — Evolution of the snow-fraction between 1979 and 2100 for catchment Tungnaá. The colour of the timeseries matches the colour of the gridpoints.

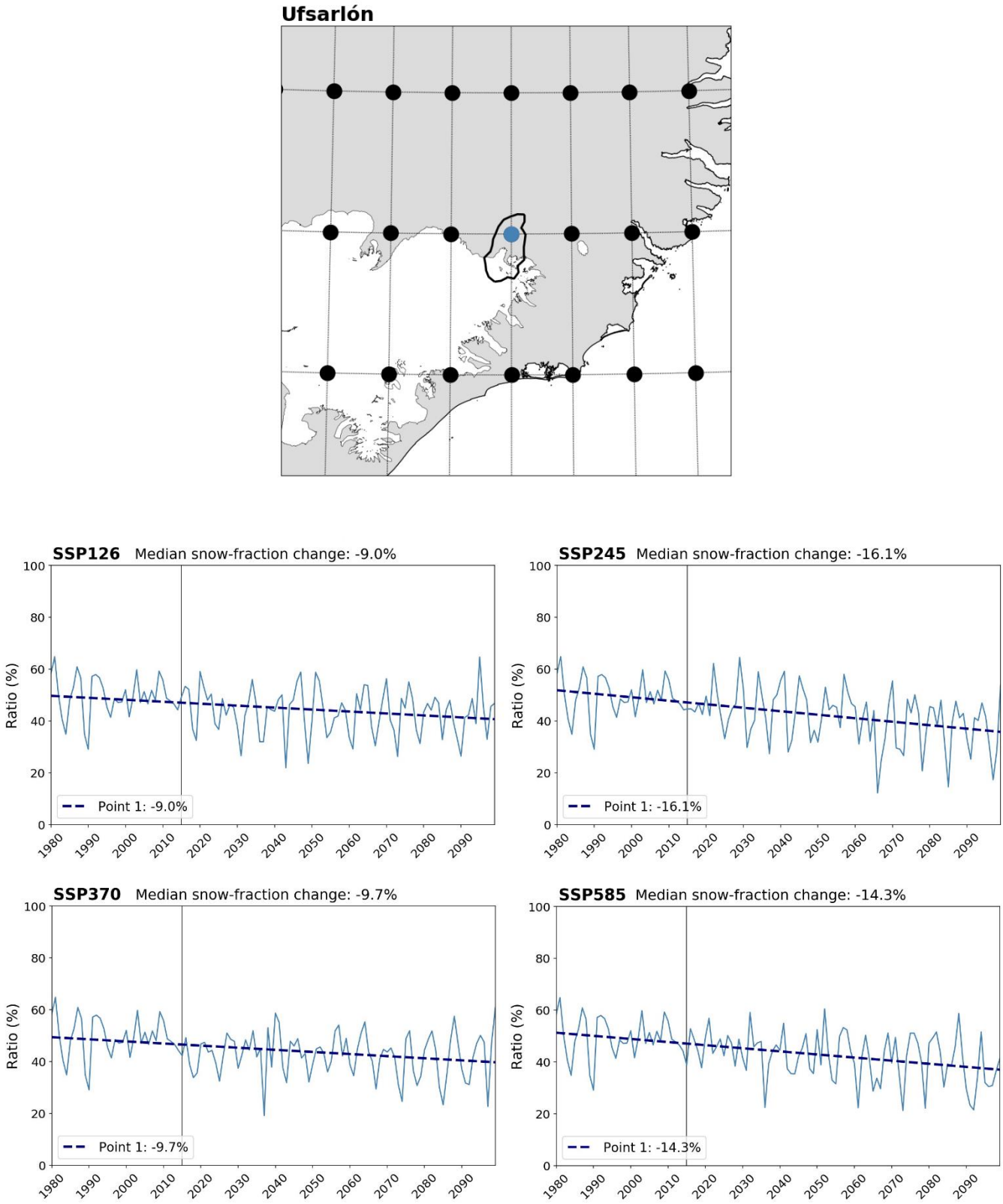

Figure V.11 — Evolution of the snow-fraction between 1979 and 2100 for catchment Ufsarlón. The colour of the timeseries matches the colour of the gridpoints.